Table 1. Host response to nucleic acids and other DAMPs

PAMP/DAMP	Receptors
Microbial nucleic acids(PAMP)	
cytosolic long dsRNA	MDA5
cytosolic 5'-PPP-RNA	RIG-I
endosomal >140 bp dsRNA	TLR3
nonmethylated CpG DNA	TLR9
cytosolic dsDNA	DNA sensors*
Self molecular patterns(DAMP)	
HMGB1	RAGE, TLR2/4
Uric acid	CD14, TLR2/4
HSPs	CD14, TLR2/4,**
S100 proteins	RAGE
Self nucleic acids (DAMP)	
Self DNA	DNA sensors*
Self mRNA	TLR3

*See **Table 2**; ** D40, CD91, Scavenger receptors etc.

Table 2. RNA·DNA recognition molecules in vertebrates

Receptors	Adaptors	Ligands	Induction of Type I IFN
		TLR family	
TLR3	TICAM-1	dsRNA, stem RNA	+
TLR7/8	MyD88	ssRNA	+
TLR22	TICAM-1	dsRNA	+
PKR	?	dsRNA	-
		RLR family	
RIG-I	MAVS	5'-PPP RNA, dsRNA	+
MDA5	MAVS	dsRNA (long)	+
		NLR family	
NALP3	ASC	dsRNA	+
NOD2	MAVS	ssRNA	+
		DDX family	
DDX1	TICAM-1	dsRNA	+
DDX21	TICAM-1	dsRNA	+
DHX36	TICAM-1	dsRNA	+
		DNA sensors	
TLR9	MyD88	CpG DNA	+
DAI	TBK1	dsDNA	+
Pol3/RIG-I	MAVS	dsDNA	+
IFI16	TBK1	dsDNA	+
DDX41	STING	dsDNA	+
DHX9	MyD88	dsDNA	+
DDX36	MyD88	dsDNA	+
ZAPS	?	dsDNA	+

constituents that are liberated from damaged or necrotic cells.[10] Thus, innate pattern-recognition is not only a mechanism for discriminating pathogens from the host, but also a means for inspecting cellular homeostasis. Molecules that, upon release from damaged/necrotic cells, activate the immune system are called damage-associated molecular patterns (DAMPs).[11] The most popular TLR adaptor MYD88 is known to contain death domains, and some reports have suggested that TLR signaling may be involved in cell death secondary to PAMP/DAMP-stimulation. Necroptotic or damaged cells may thus represent a result of TLR death signaling, and generate a functional complex consisting of sources of DAMPs as well as of the phagocytic response.[11,12]

DAMPs refer to intracellular molecules that acquire inflammation-inducing capacities when released from cells. DAMPs do not belong to the cytokine family but rather resemble PAMP in their functional properties, in particular with regard to mDC and macrophages. The functions of DAMPs may be associated with responses including regeneration and tumorigenesis. During the past 5 years, necroptotic cell death has been closely connected with innate immune responses involving pattern-sensing.[12,13] DAMPs include a large number of cytosolic or nuclear molecules (**Table 1**), as well as, surprisingly, self nucleic acids.[14] This implies that, like viral DNA and RNA, autologous nucleic acids can evoke inflammation. Here, we discuss the importance of the immune modulation induced by nucleic acids and necroptotic host cells.

Necroptosis: Programmed Necrosis Induced by TNFα

TNFα has been reported to induce two different types of cell death, apoptosis and necrosis, in a cell type-specific manner.[15,16] Through TNFR1, TNFα is implicated in NFκB activation and contributes to cell growth in many cancer cell lines. In parallel TNFα-induced hemorrhagic necrosis has been observed in several cancer cell lines, but the molecular mechanisms underlying these differential responses to TNFα remain poorly understood. Recently, several reports have suggested that the formation of a supracomplex containing the receptor-interacting protein kinase 1 (RIP1) and its homolog RIP3 (which has been named "necrosome") is responsible for the switch from apoptosis to necroptosis.[17,18] RIP1 and RIP3 can assemble only in the absence of functional caspase-8, indicating that this enzyme acts as a key protease for blocking the formation of the necrosome.[5,19] Many viral factors, as well as the genomic instability that frequently characterizes tumor cells, can compromise caspase-8 function, thereby facilitating the induction of necroptosis. Hence, TNFα can promote cell death by signaling through its receptors, including TNRF1 and downstream via RIP1/RIP3, although the output of TNFα signaling is ultimately determined by cell type.

Virus-Mediated Necroptosis

It is notable that a necrotic phenotype has been observed in polyI:C-stimulated bone marrow-derived murine macrophages and other cell lines.[13] TICAM-1 and RIP3 are involved in this process, suggesting the implication of the necrosome pathway in dsRNA-mediated cell death.[12,13] It has been reported that viral dsRNA frequently induces apoptosis in infected cells, a process that in general is known as cytopathic effect.[20] TICAM-1 and RIPs, mainly RIP1, may also be involved in virus-derived necrotic cell death.[5,13] This is relatively rare compared with apoptosis since it occurs only when the viral genome encodes caspase-8 inhibitors.[19] Furthermore, this process requires viral dsRNA to be delivered from the cytosol to the endosomes (where TLR3 is situated) of infected cells. This may happen if the dsRNA is engulfed by autophagosomes, which ensure its transfer to endosomes. The possible involvement of another PRR that sense viral RNA, RIG-I/MDA5, in cell death as induced by viral infection cannot be always ruled out. TNFα can be produced downstream of the TLR3- and RIG-I-mediated RNA-sensing pathways and may induce necrotic cell death. Many RNA viruses trigger cell death,[20] but the factors determining the induction of necroptosis in virus-infected cells remain to be clarified.

DNA viruses can induce necroptosis via another mechanism, which involves the DNA-dependent activator of IFN-regulatory factors (DAI, also known as DLM-1/ZBP1).[21] DAI is a DNA sensor[22] and directly activates RIP3 in the absence of Type I IFN induction.[21] This said, the sensing of DNA in the cytoplasm of virus-infected cells is complex, and it may be that DAI is not the only molecule linked to such a necroptotic response. It is unknown whether RIP3-mediated necroptosis can be induced even if caspase-8 is blocked upon the recognition of viral DNA by DAI or via other mechanisms.[20] In fact, this type of virus-derived necrosis has been reported with DNA viruses that encode caspase inhibitors including vaccinia virus (VV), which encodes B13R/Spi2, poxvirus, encoding CrmA, the Kaposi sarcoma-associated herpesvirus (KSHV), encoding K13 and the molluscum contagiosum virus (MCV), which encodes MC159.[20,23] Generally speaking, the mode of cell death secondary to virus infection differ as a function of viral species. The physiological role of TLR3- and DAI-mediated necroptosis should therefore be analyzed in a virus-specific fashion.

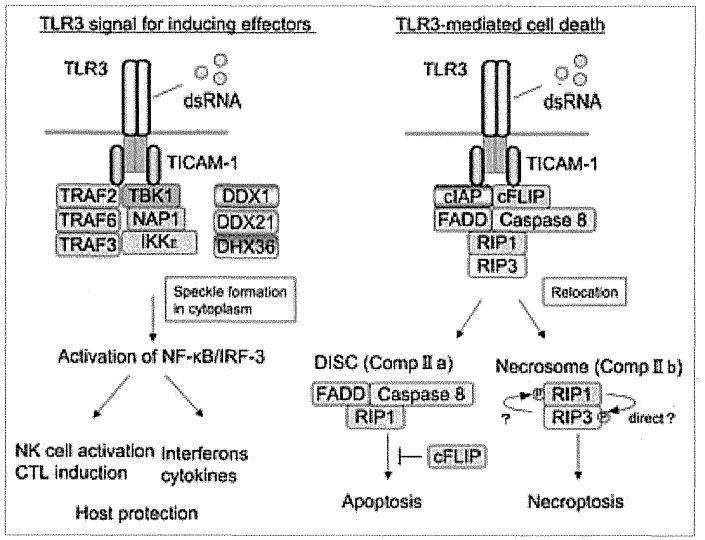

Figure 1. TLR3 signals inducing cell death or effector functions in myeloid cells. Cell survival (left panel) and cell death (right panel) signals are schematically depicted. TICAM-1 assembles in a supramolecular complex around oligomerized Toll-like receptor 3 (TLR3) in the endosome. The complex (named Speckle) then dissociates from TLR3, tranlocating to the cytoplasm. IRF-3 and NFκB are activated by Speckle, leading to their nuclear translocation and induction of Type I interferon (IFN) and inflammatory cytokines, respectively. In dendritic cells (DCs), natural killer (NK) cell-activating ligands and factors for cross-presentation are induced downstream of IRF-3/7 (left panel). In contrast, cell death signaling culminates in apoptosis and/or necrosis depending on downstream signal transducers (right panel). TLR3-dependent apoptosis has been reported in several cancer cell lines,[4] while TLR3-dependent necroptosis has been observed in mouse bone marrow-derived macrophages.[13] These events rely on RIP1/RIP3 activation, similar to those elicited upon ligation of the tumor necrosis factor α receptor 1 (TNFR1). Whether or not the translocation of the TICAM-1 complex is required for the cell death signaling, as well as the mechanisms determining either cytokine secretion or cell death, remain unknown.

Necroptosis in Inflammation

Apoptosis plays a major role in physiological contexts, while necrosis is very common under pathological conditions.[1] Necroptosis differs from accidental necrosis in its programmed nature, and differs from apoptosis in that necroptosis often stimulates inflammation. When virus-infected cells undergo apoptosis, they are removed by phagocytosis. Viral genomes, be they either

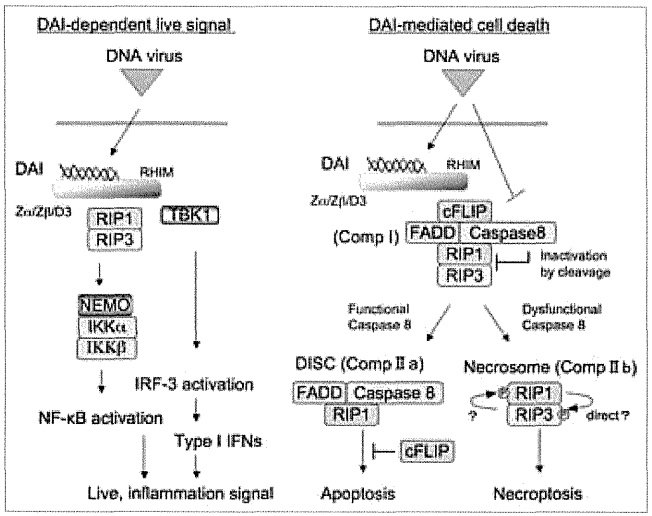

Figure 2. Necroptosis induced by the DAI pathway. Cell survival (left panel) and cell death (right panel) signals transmitted by the DNA-dependent activator of IFN-regulatory factors (DAI) are schematically depicted. Pro-survival signaling involves the activation of IRF-3 and NFκB to support antiviral responses (left panel). Type I IFNs and inflammatory cytokines are the main effectors induced by IRF-3/NFκB activation. In contrast, DAI activates RIP3 to induce necroptosis during viral infection, provided that caspases are inhibited. When viruses express caspase inhibitors, the RIP1/RIP3 necrosome plays a dominant role in the activation of cell death via necroptosis (right panel). If caspase-8 is active, RIP3 should get inactivated and apoptosis should be the dominant phenotype, though this scheme has not yet been experimentally confirmed. The mechanisms determining the choice between these two signaling pathways are unknown.

DNA- or RNA-based, are degraded in infected cells, thus being able neither to stimulate phagocytes including macrophages and DCs, nor to favor the liberation of DAMPs. In contrast, non-apoptotic cell death is accompanied by the release of DAMPs and viral products, resulting in the activation of macrophages,[13] as it occurs during chronic infection, in which viruses produce caspase inhibitors or render infected cells resistant to apoptosis.[24] A typical model of necroptosis evokes two effectors, namely, viral nucleic acids and DAMPs, to modulate immune and bystander cells of the host. In the context of necroptosis, these effectors allow for the amplification of inflammatory responses by myeloid phagocytes (mDCs and macrophages). These cells accumulate in inflammation as induced by persistent viral infection, and mediate the secondary release of cytokines and other biologically active molecules. In addition, viral factors can result in incipient inflammation, as observed in chronic infections by the hepatitis B or C virus.[24] This, in conjunction with viral nucleic acids and DAMPs, may modify the features of the infectious milieu. Further studies are needed to clarify the importance of viral nucleic acids and DAMPs in the context of virus-dependent chronic inflammation, as it may facilitate tumor progression.

Necroptosis and Oncogenesis

Accumulating evidence indicates that pro-inflammatory signals, including those following the activation of NFκB, are crucial for oncogenesis. Moreover, DAMPs have been associated with tumorigenesis as well as with antitumor immune responses.[25,26] Tumor progression is not always accompanied by viral infections, and it remains unclear whether DAMPs released from non-infected tumor cells are sufficient to support tumor growth. It has been reported that self mRNA acts as a TLR3 ligand[14] and that self DNA can stimulate host cell sensors.[22,27] Due to the uncomplete identification and functional characterization of DNA sensors and their signaling pathways, however, it is unknown whether host nucleic acids are potent inducers of inflammation as compared with viral RNA or unmethylated CpG DNA of bacterial origin. Moreover, the role of RNA sensors in the tumor microenvironment has not yet been clarified (**Table 2**).

DAMPs have recently been characterized at the molecular level[11] and representative DAMPs (**Table 1**) include HMGB1,[28] uric acid crystal,[10] S100 proteins,[29] naked actin[30,31] and heat-shock proteins (HSPs).[32] The functional features of DAMPs and the mechanisms whereby they provoke inflammation have been delineated,[11,28,29] and these studies have introduced the concept of "inflammasome" in the field of innate immunity.[33] Caspase-1 is activated upon the administration of NOD-like receptor (NLR) ligands, which include some DAMPs as well as inorganic PAMPs. Active caspase-1, together with the upregulation of the immature variants of IL-1 family proteins that ensues TLR stimulation, accelerates the robust release of IL-1β, IL-18 and IL-33.[34] There are many kinds of NLRs as well as TLRs, and the common pathways (including those centered around the adaptor ASC) can be activated by a variety of cytoplasmic DAMPs and PAMPs.[33,34] The cytoplasmic immature forms of the abovementioned cytokines are activated by limited caspase-1-mediated proteolysis, and then are secreted into the extracellular microenvironment.[34] Hence, IL-1 family proteins require two DAMPs/PAMP signals for their upregulation and activation.[35] Of note, the tumorigenic properties of asbestos and silica are in part attributable to the activation of the inflammasome, leading to the secreton of IL-1 family proteins. However, not all DAMPs operate as inflammasome activators, even in the broad sense of this term.

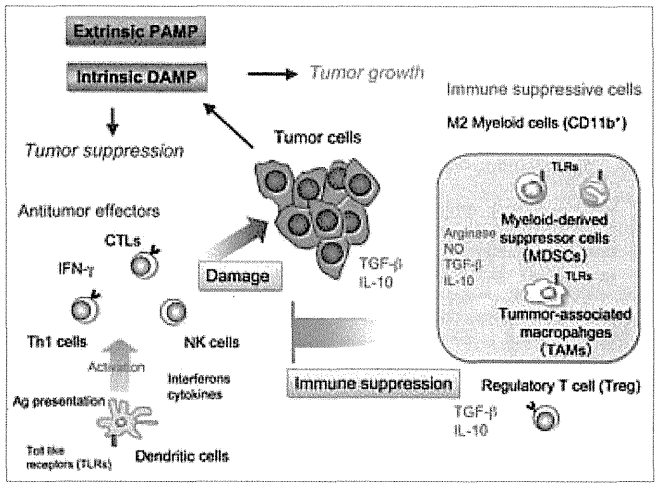

Figure 3. Inflammation provides the microenvironment for infection-related cancer. Immune cells infiltrating the tumor mass may modulate the local microenvironment upon the recognition of pathogen- or damage-associated molecular patterns (PAMP/DAMPs). Cancer cells undergoing necrosis liberate DAMPs and debris containing nucleic acids, which recruit immune cells stimulating an inflammatory response. In some cases, tumors benefit from the inflammatory response, while in other cases they regress following inflammation. The mechanisms determining this switch remain to be clarified.

Immune Response Elicited by the Phagocytosis of Dead Cells

Phagocytosis of dead cells involves not only cell clearance but also the initiation of an immune response. Dead cell antigens are rapidly presented on MHC Class II molecules after internalization by DCs, driving the recruitment and activation of various CD4+ T cell subsets, including Th1, Th2, Th17 and regulatory T cells (Tregs) (**Fig. 1**). In the presence of a second co-stimulatory signal provided by TLRs, working as an adjuvant, DCs cross-present antigens on MHC Class I molecules to induce the proliferation of CD8+ cytotoxic T lymphocytes (CTLs).[36] The presentation of exogenous antigens by DCs is therefore dependent on the presence of PAMPs/DAMPs.[36] Accordingly, necrotic debris appears to result in CTL cross-priming more efficiently than apoptotic bodies. Cross-presentation is enhanced by molecules such as Type I IFN and CD40, and by immune cells including CD4+ T, NK and NKT cells. Hence, the use of adjuvants to affect many cell types of the immune system other than antigen-presenting cells, and a precise evaluation of the total cross-priming activity appear to be indispensable for the development of efficient adjuvant therapies.

The TLR3/TICAM-1 axis is best known as an inducer of cross-presentation in vivo.[37] The cross-presentation activity of the TLR3 ligands polyI:C and viral dsRNA was first described by Schulz et al. in 2005.[38] While the potency of polyI:C as an adjuvant has been reported by Steinman and colleagues,[37,39] the precise identity of the DAMPs participating in cross-presentation and possessing latent cross-priming (CTL-inducing) capacities has not yet been determined.

It is known that phagocytosis induces functional changes in mDCs and macrophages (**Fig. 2**): phagocytes are skewed toward a regulatory phenotype accompanied by the production of IL-10 and TGFβ during the phagocytosis of apoptotic cell debris, even in the presence of PAMP.[40,41] This suggests that material that cannot be taken up exerts different effects on mDCs than internalizable material during their phagocytic interactions. Phagocytes undergo cytoskeletal rearrangement when they take up cell debris, involving cell adhesion molecules that accelerate the interaction between the phagocyte membrane and cell debris. The opsonization of dead cells further enhances phagocytosis as well as the induction of an immune outcome.[42] Complement-mediated opsonization of dead cells strongly alters the functional properties of mDCs and macrophages.[43] Yet, it has been impossible to discriminate apoptotic and necroptotic cells based on this.[44] Thus, the mechanisms whereby necroptotic cells initiate an immune response upon phagocytosis by mDCs and macrophages, compared with apoptotic cells, remain largely uncharacterized. Elucidating the role of necroptotic cells and DAMPs as adjuvants for NK-cell activation and antigen presentation is highly relevant for antitumor therapy. Since the phagocytosis of dead cells by mDCs usually leads to the generation of tolerogenic mDCs, additional adjuvants appear to be required for mDCs to present tumor antigens in an immunogenic fashion, leading to the induction of an effective immune response against cancer.

Termination of Inflammation

Inflammation often drives tissue repair and regeneration, and the microenvironment formed during inflammation serves a basis for assembling cells that initiate tissue development and reorganization (Fig. 3). The pro-inflammatory microenvironment facilitates cell growth as well as genome instability, thus being prone to the accumulation of cells with multiple mutations. Furthermore, incipient inflammation compromises the immune system so that the abnormal proliferation of transformed cells is tolerated. Thus, malignant cells build up a tissue that involves tumor-associated macrophages serving a scaffold for invasion and metastasis.[45] In this context, a region harboring DAMP-mediated persistent inflammation provides a perfect nest for tumor progression (Fig. 3). Therapeutics for suppressing inflammation, such as aspirin, may constitute an immune therapy irrespective of the presence of infection.[46] We surmise that two types of inflammation exist, namely tumor-supporting and tumor-suppressing, implying that inflammation is a complex phenomenon consisting of multiple distinct aspects. We have shown that some adjuvants can induce tumor-suppressing inflammation, thereby limiting tumor proliferation by DAMPs.[47] The adjuvant-induced switch of cell death/inflammation signals to an antitumor outcome is an intriguing approach for cancer therapy, particularly in view of the fact that the mechanisms of adjuvant signaling are being increasingly characterized at the molecular level.[48,49] The clarification of the role of adjuvant signaling in compromising tumor progression will lead to the discovery of non-toxic synthetic tumor-regressing molecules with potential as novel anticancer therapeutics.[50]

Acknowledgements

We thank Drs H.H. Aly, R. Takemura, A. Maruyama, Sayuri Yamazaki and J. Kasamatsu in our laboratory for their fruitful discussions. This work was supported in part by Grants-in-Aid from the Ministry of Education, Science and Culture (Specified Project for Advanced Research, MEXT) and the Ministry of Health, Labor and Welfare of Japan and by the Takeda and the Waxmann Foundations. Financial supports by a MEXT Grant-in-Project "the Carcinogenic Spiral," "the National Cancer Center Research and Development Fund (23-A-44)" and the Japan Initiative for Global Research Network on Infectious Diseases (J-GRID) are gratefully acknowledged.

References

1. Kroemer G, Galluzzi L, Vandenabeele P, Abrams J, Alnemri ES, Baehrecke EH, et al.; Nomenclature Committee on Cell Death 2009. Classification of cell death: recommendations of the Nomenclature Committee on Cell Death 2009. Cell Death Differ 2009; 16:3-11; PMID:18846107; http://dx.doi.org/10.1038/cdd.2008.150.
2. Tait SW, Green DR. Caspase-independent cell death: leaving the set without the final cut. Oncogene 2008; 27:6452-61; PMID:18955972; http://dx.doi.org/10.1038/onc.2008.311.
3. Oshiumi H, Sasai M, Shida K, Fujita T, Matsumoto M, Seya T. TIR-containing adapter molecule (TICAM)-2, a bridging adapter recruiting to toll-like receptor 4 TICAM-1 that induces interferon-beta. J Biol Chem 2003; 278:49751-62; PMID:14519765; http://dx.doi.org/10.1074/jbc.M305820200.
4. Ermolaeva MA, Michallet MC, Papadopoulou N, Utermöhlen O, Kranidioti K, Kollias G, et al. Function of TRADD in tumor necrosis factor receptor 1 signaling and in TRIF-dependent inflammatory responses. Nat Immunol 2008; 9:1037-46; PMID:18641654; http://dx.doi.org/10.1038/ni.1638.
5. Feoktistova M, Geserick P, Kellert B, Dimitrova DP, Langlais C, Hupe M, et al. cIAPs block Ripoptosome formation, a RIP1/caspase-8 containing intracellular cell death complex differentially regulated by cFLIP isoforms. Mol Cell 2011; 43:449-63; PMID:21737330; http://dx.doi.org/10.1016/j.molcel.2011.06.011.
6. Medzhitov R, Janeway CA Jr. Innate immunity: the virtues of a nonclonal system of recognition. Cell 1997; 91:295-8; PMID:9363937; http://dx.doi.org/10.1016/S0092-8674(00)80412-2.
7. Iwasaki A, Medzhitov R. Regulation of adaptive *immunity by the innate immune system.* Science 2010; 327:291-5; PMID:20075244; http://dx.doi.org/10.1126/science.1183021.
8. Kawai T, Akira S. Toll-like receptor and RIG-I-like receptor signaling. Ann N Y Acad Sci 2008; 1143:1-20; PMID:19076341; http://dx.doi.org/10.1196/annals.1443.020.
9. Morris S, Swanson MS, Lieberman A, Reed M, Yue Z, Lindell DM, et al. Autophagy-mediated dendritic cell activation is essential for innate cytokine production and APC function with respiratory syncytial virus responses. J Immunol 2011; 187:3953-61; PMID:21911604; http://dx.doi.org/10.4049/jimmunol.1100524.
10. Chen CJ, Kono H, Golenbock D, Reed G, Akira S, Rock KL. Identification of a key pathway required for the sterile inflammatory response triggered by dying cells. Nat Med 2007; 13:851-6; PMID:17572686; http://dx.doi.org/10.1038/nm1603.
11. Kono H, Rock KL. How dying cells alert the immune system to danger. Nat Rev Immunol 2008; 8:279-89; PMID:18340345; http://dx.doi.org/10.1038/nri2215.
12. Cavassani KA, Ishii M, Wen H, Schaller MA, Lincoln PM, Lukacs NW, et al. TLR3 is an endogenous sensor of tissue necrosis during acute inflammatory events. J Exp Med 2008; 205:2609-21; PMID:18838547; http://dx.doi.org/10.1084/jem.20081370.
13. He S, Liang Y, Shao F, Wang X. Toll-like receptors activate programmed necrosis in macrophages through a receptor-interacting kinase-3-mediated pathway. Proc Natl Acad Sci U S A 2011; 108:20054-9; PMID:22123964; http://dx.doi.org/10.1073/pnas.1116302108.
14. Karikó K, Ni H, Capodici J, Lamphier M, Weissman D. mRNA is an endogenous ligand for Toll-like receptor 3. J Biol Chem 2004; 279:12542-50; PMID:14729660; http://dx.doi.org/10.1074/jbc.M310175200.
15. Zhang DW, Shao J, Lin J, Zhang N, Lu BJ, Lin SC, et al. RIP3, an energy metabolism regulator that switches TNF-induced cell death from apoptosis to necrosis. Science 2009; 325:332-6; PMID:19498109; http://dx.doi.org/10.1126/science.1172308.
16. Vandenabeele P, Declercq W, Van Herreweghe F, Vanden Berghe T. The role of the kinases RIP1 and RIP3 in TNF-induced necrosis. Sci Signal 2010; 3:re4; PMID:20354226; http://dx.doi.org/10.1126/scisignal.3115re4.
17. He S, Wang L, Miao L, Wang T, Du F, Zhao L, et al. Receptor interacting protein kinase-3 determines cellular necrotic response to TNF-alpha. Cell 2009; 137:1100-11; PMID:19524512; http://dx.doi.org/10.1016/j.cell.2009.05.021.
18. Cho YS, Challa S, Moquin D, Genga R, Ray TD, Guildford M, et al. Phosphorylation-driven assembly of the RIP1-RIP3 complex regulates programmed necrosis and virus-induced inflammation. Cell 2009; 137:1112-23; PMID:19524513; http://dx.doi.org/10.1016/j.cell.2009.05.037.
19. Kaiser WJ, Upton JW, Long AB, Livingston-Rosanoff D, Daley-Bauer LP, Hakem R, et al. RIP3 mediates the embryonic lethality of caspase-8-deficient mice. Nature 2011; 471:368-72; PMID:21368762; http://dx.doi.org/10.1038/nature09857.
20. Galluzzi L, Brenner C, Morselli E, Touat Z, Kroemer G. Viral control of mitochondrial apoptosis. PLoS Pathog 2008; 4:e1000018; PMID:18516228; http://dx.doi.org/10.1371/journal.ppat.1000018.
21. Upton JW, Kaiser WJ, Mocarski ES. DAI/ZBP1/DLM-1 complexes with RIP3 to mediate virus-induced programmed necrosis that is targeted by murine cytomegalovirus vIRA. Cell Host Microbe 2012; 11:290-7; PMID:22423968; http://dx.doi.org/10.1016/j.chom.2012.01.016.
22. Takaoka A, Wang Z, Choi MK, Yanai H, Negishi H, Ban T, et al. DAI (DLM-1/ZBP1) is a cytosolic DNA sensor and an activator of innate immune response. Nature 2007; 448:501-5; PMID:17618271; http://dx.doi.org/10.1038/nature06013.
23. Shisler JL, Moss B. Immunology 102 at poxvirus U: *avoiding apoptosis. Semin Immunol 2001; 13:67-*72; PMID:11289801; http://dx.doi.org/10.1006/smim.2000.0297.
24. Saeed M, Shiina M, Date T, Akazawa D, Watanabe N, Murayama A, et al. In vivo adaptation of hepatitis C virus in chimpanzees for efficient virus production and evasion of apoptosis. Hepatology 2011; 54:425-33; PMID:21538444; http://dx.doi.org/10.1002/hep.24399.
25. Salaun B, Romero P, Lebecque S. Toll-like receptors' two-edged sword: when immunity meets apoptosis. Eur J Immunol 2007; 37:3311-8; PMID:18034428; http://dx.doi.org/10.1002/eji.200737744.
26. Piccinini AM, Midwood KS. DAMPening inflammation by modulating TLR signalling. Mediators Inflamm. 2010; pii: 672395.
27. Ishii KJ, Kawagoe T, Koyama S, Matsui K, Kumar H, Kawai T, et al. TANK-binding kinase-1 delineates innate and adaptive immune responses to DNA vaccines. Nature 2008; 451:725-9; PMID:18256672; http://dx.doi.org/10.1038/nature06537.
28. Yanai H, Ban T, Wang Z, Choi MK, Kawamura T, Negishi H, et al. HMGB proteins function as universal sentinels for nucleic-acid-mediated innate immune responses. Nature 2009; 462:99-103; PMID:19890330; http://dx.doi.org/10.1038/nature08512.
29. Hiratsuka S, Watanabe A, Sakurai Y, Akashi-Takamura S, Ishibashi S, Miyake K, et al. The S100A8-serum *amyloid A3-TLR4 paracrine cascade establishes a* pre-metastatic phase. Nat Cell Biol 2008; 10:1349-55; PMID:18820689; http://dx.doi.org/10.1038/ncb1794.
30. Ahrens S, Zelenay S, Sancho D, Han P, Kjaer S, Feest C, et al. F-actin is an evolutionarily conserved damage-associated molecular pattern recognized by DNGR-1, a receptor for dead cells. Immunity 2012; 36:635-45; PMID:22483800; http://dx.doi.org/10.1016/j.immuni.2012.03.008.
31. Zhang JG, Czabotar PE, Policheni AN, Caminschi I, Wan SS, Kitsoulis S, et al. The dendritic cell receptor Clec9A binds damaged cells via exposed actin filaments. Immunity 2012; 36:646-57; PMID:22483802; http://dx.doi.org/10.1016/j.immuni.2012.03.009.
32. Tsan MF, Gao B. Heat shock proteins and immune system. J Leukoc Biol 2009; 85:905-10; PMID:19276179; http://dx.doi.org/10.1189/jlb.0109005.
33. Pedra JH, Cassel SL, Sutterwala FS. Sensing pathogens and danger signals by the inflammasome. Curr Opin Immunol 2009; 21:10-6; PMID:19223160; http://dx.doi.org/10.1016/j.coi.2009.01.006.
34. Cassel SL, Joly S, Sutterwala FS. The NLRP3 inflammasome: a sensor of immune danger signals. Semin Immunol 2009; 21:194-8; PMID:19501527; http://dx.doi.org/10.1016/j.smim.2009.05.002.
35. Yu HB, Finlay BB. The caspase-1 inflammasome: a pilot of innate immune responses. Cell Host Microbe 2008; 4:198-208; PMID:18779046; http://dx.doi.org/10.1016/j.chom.2008.08.007.
36. Seya T, Shime H, Ebihara T, Oshiumi H, Matsumoto M. Pattern recognition receptors of innate immunity and their application to tumor immunotherapy. Cancer Sci 2010; 101:313-20; PMID:20059475; http://dx.doi.org/10.1111/j.1349-7006.2009.01442.x.
37. Caskey M, Lefebvre F, Filali-Mouhim A, Cameron MJ, Goulet JP, Haddad EK, et al. Synthetic double-stranded RNA induces innate immune responses similar to a live viral vaccine in humans. J Exp Med 2011; 208:2357-66; PMID:22065672; http://dx.doi.org/10.1084/jem.20111171.
38. Schulz O, Diebold SS, Chen M, Näslund TI, Nolte MA, Alexopoulou L, et al. Toll-like receptor 3 promotes cross-priming to virus-infected cells. Nature 2005; 433:887-92; PMID:15711573; http://dx.doi.org/10.1038/nature03326.
39. Longhi MP, Trumpfheller C, Idoyaga J, Caskey M, Matos I, Kluger C, et al. Dendritic cells require a systemic type I interferon response to mature and induce CD4+ Th1 immunity with poly IC as adjuvant. J Exp Med 2009; 206:1589-602; PMID:19564349; http://dx.doi.org/10.1084/jem.20090247.
40. Chung EY, Kim SJ, Ma XJ. Regulation of cytokine production during phagocytosis of apoptotic cells. Cell Res 2006; 16:154-61; PMID:16474428; http://dx.doi.org/10.1038/sj.cr.7310021.
41. Zhang Y, Kim HJ, Yamamoto S, Kang X, Ma X. Regulation of interleukin-10 gene expression in macrophages engulfing apoptotic cells. J Interferon Cytokine Res 2010; 30:113-22; PMID:20187777; http://dx.doi.org/10.1089/jir.2010.0004.
42. Aderem A, Underhill DM. Mechanisms of phagocytosis in macrophages. Annu Rev Immunol 1999; 17:593-623; PMID:10358769; http://dx.doi.org/10.1146/annurev.immunol.17.1.593.
43. Ricklin D, Hajishengallis G, Yang K, Lambris JD. Complement: a key system for immune surveillance and homeostasis. Nat Immunol 2010; 11:785-97; PMID:20720586; http://dx.doi.org/10.1038/ni.1923.
44. Wakasa K, Shime H, Kurita-Taniguchi M, Matsumoto M, Imamura M, Seya T. Development of monoclonal antibodies that specifically interact with necrotic lymphoma cells. Microbiol Immunol 2011; 55:373-7; PMID:21517948; http://dx.doi.org/10.1111/j.1348-0421.2011.00319.x.
45. Mantovani A. La mala educación of tumor-associated macrophages: Diverse pathways and new players. Cancer Cell 2010; 17:111-2; PMID:20159603; http://dx.doi.org/10.1016/j.ccr.2010.01.019.
46. Chan AT, Ogino S, Fuchs CS. Aspirin and the risk of colorectal cancer in relation to the expression of COX-2. N Engl J Med 2007; 356:2131-42; PMID:17522398; http://dx.doi.org/10.1056/NEJMoa067208.
47. Shime H, Matsumoto M, Oshiumi H, Tanaka S, Nakane A, Iwakura Y, et al. Toll-like receptor 3 signaling converts tumor-supporting myeloid cells to tumoricidal effectors. Proc Natl Acad Sci U S A 2012; 109:2066-71; PMID:22308357; http://dx.doi.org/10.1073/pnas.1113099109.
48. Ishii KJ, Akira S. Toll or toll-free adjuvant path toward the optimal vaccine development. J Clin Immunol 2007; 27:363-71; PMID:17370119; http://dx.doi.org/10.1007/s10875-007-9087-x.
49. Seya T, Matsumoto M. The extrinsic RNA-sensing pathway for adjuvant immunotherapy of cancer. Cancer Immunol Immunother 2009; 58:1175-84; PMID:19184005; http://dx.doi.org/10.1007/s00262-008-0652-9.
50. Galluzzi L, Vacchelli E, Eggermont A, Fridman WH, Galon J, Sautes-Fridman C, et al. Trial Watch: Experimental Toll-like receptor agonists for cancer therapy. OncoImmunol. 2012; 1(5):699-717; PMID: 3429574; http://dx.doi.org/10.4161/onci.20696.

Toll-like receptor 3 signaling converts tumor-supporting myeloid cells to tumoricidal effectors

Hiroaki Shime[a], Misako Matsumoto[a], Hiroyuki Oshiumi[a], Shinya Tanaka[b], Akio Nakane[c], Yoichiro Iwakura[d], Hideaki Tahara[e], Norimitsu Inoue[f], and Tsukasa Seya[a,1]

[a]Department of Microbiology and Immunology, and [b]Department of Cancer Pathology, Graduate School of Medicine, Hokkaido University, Kita-ku, Sapporo 060-8638, Japan; [c]Department of Microbiology and Immunology, Graduate School of Medicine, Hirosaki University, Zaifu-cho, Hirosaki 036-8562, Japan; [d]Laboratory of Molecular Pathogenesis, Center for Experimental Medicine and Systems Biology, and [e]Department of Surgery and Bioengineering, Advanced Clinical Research Center, Institute of Medical Science, University of Tokyo, Shirokanedai, Minato-ku, Tokyo 108-8639, Japan; and [f]Department of Molecular Genetics, Osaka Medical Center for Cancer, Nakamichi, Higashinari-ku, Osaka 537-8511, Japan

Edited by Ruslan Medzhitov, Yale University School of Medicine, New Haven, CT, and approved December 20, 2011 (received for review August 11, 2011)

Smoldering inflammation often increases the risk of progression for malignant tumors and simultaneously matures myeloid dendritic cells (mDCs) for cell-mediated immunity. PolyI:C, a dsRNA analog, is reported to induce inflammation and potent antitumor immune responses via the Toll-like receptor 3/Toll–IL-1 receptor domain-containing adaptor molecule 1 (TICAM-1) and melanoma differentiation-associated protein 5/IFN-β promoter stimulator 1 (IPS-1) pathways in mDCs to drive activation of natural killer cells and cytotoxic T lymphocytes. Here, we found that i.p. or s.c. injection of polyI:C to Lewis lung carcinoma tumor-implant mice resulted in tumor regression by converting tumor-supporting macrophages (Mfs) to tumor suppressors. F4/80$^+$/Gr1$^-$ Mfs infiltrating the tumor respond to polyI:C to rapidly produce inflammatory cytokines and thereafter accelerate M1 polarization. TNF-α was increased within 1 h in both tumor and serum upon polyI:C injection into tumor-bearing mice, followed by tumor hemorrhagic necrosis and growth suppression. These tumor responses were abolished in TNF-α$^{-/-}$ mice. Furthermore, F4/80$^+$ Mfs in tumors extracted from polyI:C-injected mice sustained Lewis lung carcinoma cytotoxic activity, and this activity was partly abrogated by anti–TNF-α Ab. Genes for supporting M1 polarization were subsequently up-regulated in the tumor-infiltrating Mfs. These responses were completely abrogated in TICAM-1$^{-/-}$ mice, and unaffected in myeloid differentiation factor 88$^{-/-}$ and IPS-1$^{-/-}$ mice. Thus, the TICAM-1 pathway is not only important to mature mDCs for cross-priming and natural killer cell activation in the induction of tumor immunity, but also critically engaged in tumor suppression by converting tumor-supporting Mfs to those with tumoricidal properties.

Toll-like receptor | tumor-associated macrophages | TRIF

Inflammation followed by bacterial and viral infections triggers a high risk of cancer and promotes tumor development and progression (1, 2). Long-term use of anti-inflammatory drugs has been shown to reduce—if not eliminate—the risk of cancer, as demonstrated by a clinical study of aspirin and colorectal cancer occurrence (3). Inflammatory cytokines facilitate tumor progression and metastasis in most cases. Innate immune response and the following cellular events are closely concerned with the formation of the tumor microenvironment (4, 5).

By contrast, inflammation induced by microbial preparations was applied to patients with cancer for therapeutic potential as Coley vaccine with some success. A viral replication product, dsRNA and its analog polyI:C (6, 7), induced acute inflammation, and has been expected to be a promising therapeutic agent against cancer. Although polyI:C exerts life-threatening cytokinemia (8), trials for its clinical use as an adjuvant continued because of its high therapeutic potential (9, 10). Pathogen-associated molecular patterns (PAMPs) and host cell factors induced secondary to PAMP–host cell interaction act as a double-edged sword in cancer prognosis and require understanding their multifarious functional properties in the tumor environment.

Recent advances in the study of innate immunity show how polyI:C suppresses tumor progression (11). PolyI:C is a synthetic compound that serves as an agonist for pattern-recognition receptors (PRRs), Toll-like receptor 3 (TLR3), and melanoma differentiation-associated protein 5 (MDA5) (12–14). Although TLR3 and MDA5 signals are characterized as myeloid differentiation factor 88 (MyD88) independent (15, 16), they have immune effector-inducing properties (12–14, 17). TLR3 couples with the Toll–IL-1 receptor domain-containing adaptor molecule 1 (TICAM-1, also known as TRIF), and MDA5 couples with the IFN-β promoter stimulator 1 (IPS-1, also known as Cardif, MAVS, or VISA) (11, 15). Possible functions for the TICAM-1 and IPS-1 signaling pathways have been investigated by using gene-disrupted mice (15); although they activate the same downstream transcription factors NF-κB and IFN regulatory factor 3 (IRF-3) (15, 18), they appear to distinctly modulate myeloid dendritic cells (mDCs) and macrophages (Mfs) to drive effector lymphocytes (19, 20).

Tumor microenvironments frequently involve myeloid-derived suppressor cells (MDSCs), tumor-associated macrophages (TAMs), and immature mDCs (1, 21). These myeloid cells express PRR through which they are functionally activated. Once the inflammation process is triggered, immature mDCs turn mature so that they are capable of antigen cross-presentation and able to activate immune effector cells, which would act to protect the host system and damage the undesirable tumor cells (22). However, TAMs and MDSCs play a major role in establishing a favorable environment for tumor cell development by suppressing antitumor immunity and recruiting host immune cells to support tumor cell survival, motility, and invasion (23–25). Although these myeloid cell scenarios have been studied with interest, how the PRR signal in these myeloid cells links regulation of tumor progression has yet to be elucidated.

Here we show that TICAM-1 but not IPS-1 signal in tumor-infiltrating Mfs is engaged in conversion of the TAM-like Mfs to tumoricidal effectors. We investigated the molecular mechanisms in Mfs underlying the phenotype switch from tumor supporting to tumor suppressing by treating cells with polyI:C and found that the TICAM-1–inducing TNF-α and M1 polarization are crucial for eliciting tumoricidal activity in TAMs.

Results

In Vivo Effect of PolyI:C on Implant Lewis Lung Carcinoma Tumor. I.p. injection of polyI:C rapidly induced hemorrhagic necrosis in 3LL tumors implanted in WT mice, which was established >12 h after polyI:C treatment (Fig. 1*A*). The polyI:C-dependent hemorrhagic necrosis did not occur in TNF-α$^{-/-}$ mice (Fig. 1*A*). Histological and immunohistochemical analysis revealed vascular damage in the necrotic lesion, where disruption of vascular endothelial cells was indicated by fragmented CD31$^+$ marker (Fig. S1). Although the polyI:C signal is delivered by TICAM-1 and IPS-1 adaptors (11, 13), the hemorrhagic necrosis was largely alleviated in TICAM-1$^{-/-}$ mice but not in IPS-1$^{-/-}$ mice (Fig. 1*A*). The results suggest that polyI:C is a reagent that induces Lewis lung carcinoma (3LL) hemorrhagic necrosis, and the TICAM-1 pathway and its products, including TNF-α, are preferentially involved in this response.

3LL implant tumors grew well in WT C57BL6 mice. PolyI:C, when i.p. injected, resulted in tumor growth retardation (Fig. 1*B*). The retardation of tumor growth by polyI:C was also impaired in TNF-α$^{-/-}$ mice (Fig. 1*B*), suggesting that TNF-α is a critical effector for not only induction of hemorrhagic necrosis but also further 3LL tumor regression. To investigate the signaling pathway involved in the tumor growth retardation by polyI:C, we challenged WT, MyD88$^{-/-}$, TICAM-1$^{-/-}$, and IPS-1$^{-/-}$ mice with 3LL implantation and then treated the mice with i.p. injection of polyI:C. 3LL growth retardation was observed in both IPS-1$^{-/-}$ (Fig. 1*C*) and MyD88$^{-/-}$ mice, to a similar extent to WT mice. In contrast, polyI:C-dependent tumor growth retardation was abrogated in TICAM-1$^{-/-}$ mice (Fig. 1*D*). The size differences of the implanted tumors became significant within 2 d after polyI:C treatment, suggesting that the molecular effector for tumor regression is induced early and its upstream is TICAM-1. Similar results were obtained with MC38 implant tumor (Fig. S2*A*), which is TNF-α sensitive and MHC class I positive (Table S1) (26).

PolyI:C is a reagent that induces natural killer (NK) cell activation in MHC class I-negative tumors (12), and 3LL cells are class I negative and NK cell sensitive (Table S1) (27, 28). We tested whether NK cells activated by polyI:C damage the 3LL tumor in mice. Tumor growth was not affected by pretreatment of the mice with anti-NK1.1 Ab in this model (Fig. S3). Thus, NK cells, at least the NK1.1$^+$ cells, have a negligible ability to retard tumor growth in vivo.

PolyI:C Induces TNF-α Through the TICAM-1 Pathway in Mice. To test whether polyI:C treatment had elicited TNF-α production in vivo, we investigated the cytokine profiles of serum from polyI:C-stimulated WT and IPS-1$^{-/-}$ and TICAM-1$^{-/-}$ mice by ELISA. Prominent differences in TNF-α levels were observed in serum collected from polyI:C-injected WT and TICAM-1$^{-/-}$ mice. Serum TNF-α levels in WT and IPS-1$^{-/-}$ mice were significantly higher than that in TICAM-1$^{-/-}$ mice within 1 h after polyI:C injection (Fig. S4 *A* and *B*). IFN-β is a main output for polyI:C stimulation (11), and its production was decreased in TICAM-1$^{-/-}$ mice and totally abrogated in IPS-1$^{-/-}$ mice (Fig. S4*C*). Taken together, the data indicate that the TICAM-1 pathway was able to sustain a high TNF-α level in the early phase of polyI:C treatment, which is independent of IPS-1 and subsequent production of IFN-β.

TICAM-1$^+$ Cells in Tumor Produces TNF-α in Response to PolyI:C Stimulation. Using the 3LL implant WT, IPS-1$^{-/-}$, and TICAM-1$^{-/-}$ mouse models, we tested whether polyI:C-induced early TNF-α was responsible for the lately observed tumor regression. Time-course analyses of the polyI:C-induced TNF-α protein levels were performed by ELISA using serum samples and tumors extracted from the experimental mice. The tumor TNF-α levels in WT and IPS-1$^{-/-}$ mice increased at 2 h after polyI:C i.p. injection (Fig. 2*A*). The serum TNF-α levels in both were rapidly up-regulated within 1 h after polyI:C injection, although in WT the levels continued to increase but in IPS-1$^{-/-}$ mice gradually decreased (Fig. 2*B*). In TICAM-1$^{-/-}$ mice, however, no appreciable up-regulation of TNF-α protein was detected in either tumor or serum samples during the early time-course tested. To test whether the induced TNF-α protein was generated de novo in tumors, we examined the corresponding mRNA levels in excised tumors (Fig. 2*C* and Table S2). The TNF-α mRNA levels peaked between 1 and 2 h after polyI:C injection, whereas the TNF-α protein level was kept high at >2 h after polyI:C injection in tumor as well as serum. In the TICAM-1$^{-/-}$ mice, TNF-α production was largely abrogated in the tumor and serum samples, suggesting that TNF-α was mainly produced and secreted in response to polyI:C stimulation from the TLR3/TICAM-1$^+$ cells within the tumor.

F4/80$^+$/Gr-1$^-$ Mfs in 3LL Tumor Produce TNF-α Leading to Tumor Damage. We next investigated the cell types that had infiltrated the tumor by using various Mf markers in FACS analysis and tumor samples extracted at 1 h after polyI:C injection. We discovered that CD45$^+$ cells in the tumor produced TNF-α in response to polyI:C (Fig. 3*A*). The major population of those CD45$^+$ cells was determined to be of CD11b$^+$ myeloid-lineage cells that coexpressed F4/80$^+$, Gr1$^+$, or CD11c$^+$. A small population of NK1.1$^+$ cells was also detected. CD4$^+$ T cells, CD8$^+$ T cells, and B cells were rarely detected in these implant tumors (Fig. S5*A*). Moreover, F4/80$^+$/Gr-1$^-$ cells were found to be the principal contributors to polyI:C-mediated TNF-α production (Fig. 3 *B* and *C*). F4/80$^+$ cells in 3LL tumor highly expressed macrophage mannose receptor (MMR; CD206), a M2 macrophage marker, in contrast to splenic F4/80$^+$CD11b$^+$ cells. Both TNF-α–producing and –nonproducing F4/80$^+$ cell populations in 3LL tumor showed indistinguishable levels of CD206 (Fig. S6), and dissimilar to MDSCs or splenic Mfs, as determined by the surface marker profiles (Table S3). Thus, the source of the TNF-α–producing cells in tumor is likely F4/80$^+$ Mfs with a TAM-like feature.

We harvested F4/80$^+$ cells from tumor samples extracted from WT and TICAM-1$^{-/-}$ mice at 30 min after polyI:C injection. These cells were used in in vitro experiments to verify the TNF-α–producing abilities and 3LL cytotoxicity properties (Fig. 4 *A* and *B*). WT F4/80$^+$ Mfs exhibited normal TNF-α–producing function and were able to kill 3LL cells upon exposure. This tumoricidal activity was ~50% neutralized by the addition of anti–TNF-α Ab (Fig. 4*C*), although incomplete inhibition by this mAb may reflect participation of other factors in TNF-α cytotoxicity. Furthermore, when active TNF-α protein (rTNF-α) was added exogenously to 3LL cell culture, the cytotoxic effects were still present and occurred in a dose-dependent manner (Fig. 4*D*). TNF-α–producing ability was also observed in F4/80$^+$ cells from implant tumor of MC38, B16D8, or EL4, and only the MC38 tumor was remediable by TICAM-1–derived TNF-α (Fig. S2 *B* and *C*). The MC38 tumor contained the F4/80$^+$/CD11b$^+$/Gr1$^-$ cells, as in the 3LL tumor (Fig. S5*B*).

IFN-β did not enhance rTNF-α–mediated 3LL killing efficacy (Fig. S7*A*), a finding that was consistent with previously published data (29). No effect of IRF3/7 on polyI:C-induced 3LL tumor regression in vivo was confirmed using IRF3/7 double-knockout mice. However, polyI:C-dependent tumor regression was abrogated in 3LL-bearing IFN-α/β receptor (IFNAR)$^{-/-}$ mice (Fig. S7*B*). Quantitative PCR analysis of cells from WT vs. IFNAR$^{-/-}$ tumor-bearing mice revealed that the TLR3 level was basally low and not up-regulated in response to polyI:C in tumor-infiltrating F4/80$^+$ Mfs of IFNAR$^{-/-}$ mice (Fig. S7*C*). Accordingly, the TNF-α level was not up-regulated in tumor and serum in polyI:C-stimulated IFNAR$^{-/-}$ mice (Fig. S7*D*). Thus, basal induction of type I IFN serves as a critical factor for TLR3 function in tumor F4/80$^+$ Mfs to produce TNF-α in vivo. These results suggest that the direct effector for 3LL cytolysis by polyI:C involves TNF-α, which is derived from TICAM-1 downstream independent of the IRF3/7 axis. Our results indicate that cytotoxic TNF-α is produced via a distinct route from initial type I IFN and downstream of TICAM-1 in F4/80$^+$ TAM-like Mfs. Type I IFN do not synergistically act with TNF-α on 3LL killing, but is required to complete the TLR3/TICAM-1 pathway.

These results were confirmed by in vitro assay, wherein the F4/80$^+$ Mfs harvested from 3LL tumors in WT, TICAM-1$^{-/-}$, IPS-1$^{-/-}$, and TLR3$^{-/-}$ mice were stimulated with polyI:C (Fig. S8*A*). Both TNF-α release and 3LL cytotoxic abilities of polyI:C-stimulated F4/80$^+$ Mfs were specifically abrogated by the absence of TICAM-1 and TLR3 (Fig. S8 *A* and *B*). IPS-1 or

Author contributions: H.S., M.M., and T.S. designed research; H.S., H.O., and S.T. performed research; H.O., A.N., Y.I., and H.T. contributed new reagents/analytic tools; M.M. and N.I. analyzed data; and H.S. and T.S. wrote the paper.

The authors declare no conflict of interest.

This article is a PNAS Direct Submission.

[1]To whom correspondence should be addressed. E-mail: seya-tu@pop.med.hokudai.ac.jp.

This article contains supporting information online at www.pnas.org/lookup/suppl/doi:10.1073/pnas.1113099109/-/DCSupplemental.

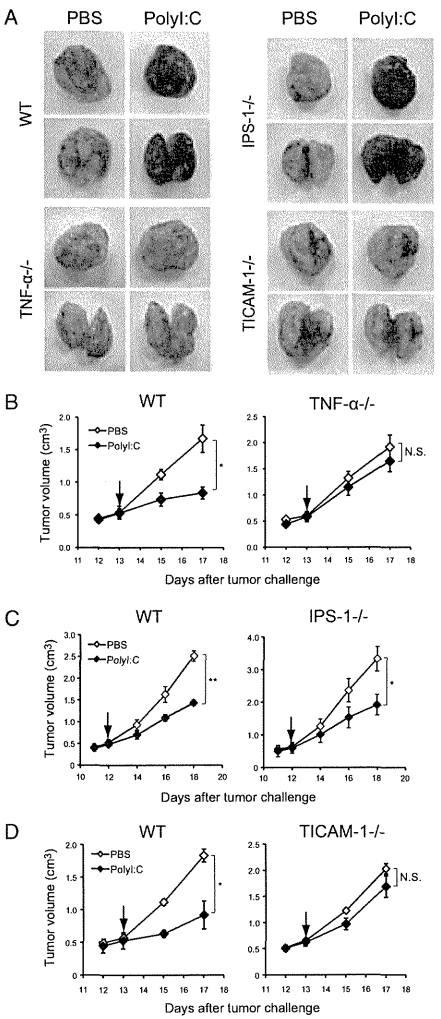

Fig. 1. Antitumor activity of polyI:C against 3LL tumor cells is mediated by the TICAM-1 pathway in vivo. (*A*) Representative photographs of 3LL tumors excised from WT, TNF-$\alpha^{-/-}$, TICAM-$1^{-/-}$, and IPS-$1^{-/-}$ mice. Whole tumor (*Upper*) and bisected tumor (*Lower*) are shown. (*B–D*) On day 0, 3LL tumor cells (3×10^6) were s.c. implanted into B6 WT (*B–D*), TNF-$\alpha^{-/-}$ (*B*), TICAM-$1^{-/-}$ (*C*), and IPS-$1^{-/-}$ (*D*) mice. PolyI:C i.p. injection was started on the day indicated by arrow, then repeated every 4 d. Data are shown as tumor average size ± SE; $n = 3$–4 mice per group. $^*P < 0.05$; $^{**}P < 0.001$. N.S., not significant. A representative experiment of two with similar outcomes is shown.

MyD88 in F4/80$^+$ Mfs had no or minimal effect on the TNF-α tumoricidal effect against 3LL tumors. PolyI:C did not directly exert a cytotoxic effect on 3LL tumor cells (Fig. S8*C*).

Role of the IPS-1 Pathway in F4/80$^+$ Cells. Both TICAM-1 and IPS-1 are known to converge their signals on transcription factors NF-κB and IRF-3, which drive expression of TNF-α and IFN-β, respectively. PolyI:C-induced TNF-α production was reduced in F4/80$^+$ cells extracted from tumors of TICAM-$1^{-/-}$ mice, but not in samples of IPS-$1^{-/-}$ mice. We examined the expression of IFN-β in these cells after polyI:C stimulation. Compared with F4/80$^+$ cells from WT mice, IFN-β expression and production was barely decreased in IPS-$1^{-/-}$ F4/80$^+$ cells, but largely impaired in TICAM-$1^{-/-}$ F4/80$^+$ cells (Fig. S9*A*) as other cytokines tested. M1 Mf-associated cytokines/chemokines were generally reduced in TICAM-$1^{-/-}$ F4/80$^+$ cells compared with WT and IPS-$1^{-/-}$ cells >4 h after polyI:C stimulation (Fig. S9*A*), whereas M2 Mf-associated genes were barely affected by TICAM-1 disruption or polyI:C stimulation (Fig. S9*B*).

Most types of Mfs are known to express TLR3 in mice (30). Messages and proteins for type I IFN induction were conserved in the F4/80$^+$ tumor-infiltrating Mfs (Fig. S10 *A–C*). However, the TLR3 mRNA level was low in macrophage colony-stimulating factor (M-CSF)–derived Mfs compared with TAMs (Fig. S10*D*). We further examined whether IFN-β production might also have relied on the TICAM-1 pathway in other types of Mfs upon stimulation with polyI:C. In contrast to the F4/80$^+$ cells isolated from tumor (Fig. S11 *A* and *B*), the IPS-1 pathway was indispensable for polyI:C-mediated IFN-β production in mouse peritoneal Mfs and M-CSF–induced bone marrow-derived Mfs (Fig. S11 *C* and *E*). However, IPS-1 only slightly participated in polyI:C-mediated TNF-α production in these Mf subsets (Fig. S11 *D* and *F*). It appears then that the IPS-1 pathway is able to signal the presence of polyI:C and subsequently induce type I IFN. TICAM-1 is the protein that induces effective TNF-α in all subsets of Mfs.

PolyI:C Influences Polarization of TAMs. Plasticity is a characteristic feature of Mfs (25). Various factors and signals can influence polarization of Mf cells to induce the M1/M2 transition, which is accompanied by a substantial change in the Mf cell's expression profile of cytokines and chemokines. Previous studies have demonstrated that Mfs that have infiltrated into tumor are of the M2-polarized phenotype, which is known to contribute to tumor progression. To test the effects of polyI:C on the polarization of tumor-infiltrated Mf cells, we analyzed the gene expression profiles of these cells following in vitro polyI:C stimulation, and representative profiles were confirmed by quantitative PCR (Fig. 5 *A* and *B*). The mRNA expressions were increased for M1 Mf markers IL-12p40, IL-6, CXCL11, and IL-1β at 4 h after in vitro polyI:C treatment, as were mRNA levels of IFN-β and TNF-α and ex vivo results. The M2 Mf markers arginase-1 (*Arg1*), chitinase 3-like 3 (*Chi3l3*), and MMR (*Mrc1*) were unchanged, compared with unstimulated levels; however, the M2 Mf marker IL-10, a regulatory cytokine, was induced. In addition, there was no difference observed in the mRNA expression levels of MMP9 (*Mmp9*) and VEGFA (*Vegfa*), both of which are involved in tissue remodeling and angiogenesis events of tumor progression (Fig. 5*C*). The polyI:C-induced M1 markers and IL-10 expression that were up-regulated in WT and IPS-$1^{-/-}$ F4/80$^+$ cells were found to be abrogated in TICAM-$1^{-/-}$ F4/80$^+$ cells (Fig. 5 *A* and *B*), reinforcing the results obtained with F4/80$^+$ Mfs isolated from 3LL tumors in mice injected with polyI:C (Fig. S9 *A* and *B*). It appears that TICAM-1 is responsible for the M1 polarization of F4/80$^+$ Mf cells in tumors, but has no effect on M2 markers. We further examined the expression of IRF-5 and IRF-4, which are considered the master regulators for M1 and M2 polarization, respectively (31, 32). As expected, polyI:C induced IRF-5 mRNA expression, but had no effect on IRF-4 mRNA expression in vitro (Fig. 5 *A* and *B*). Jmjd3, a histone H3K27 demethylase involved in IRF-4 expression, is reportedly induced by TLR stimulation (33). In our study, polyI:C stimulation increased Jmjd3 mRNA in F4/80$^+$ cells

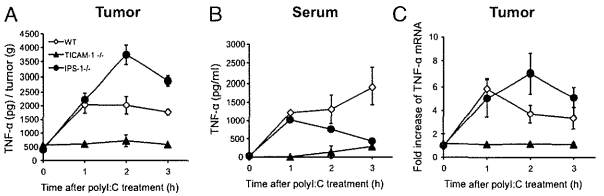

Fig. 2. TNF-α production in tumor and serum of polyI:C-injected 3LL tumor-bearing mice. Mice bearing 3LL tumor were i.p. injected with 200 μg polyI:C. Tumor (*A*) and serum (*B*) were collected at 0, 1, 2, and 3 h after polyI:C injection, and TNF-α concentration was determined by ELISA. TNF-α level in tumor is presented as [TNF-α protein (pg)/tumor weight (g)]. (*C*) Tumors were isolated from polyI:C-injected tumor-bearing WT, TICAM-$1^{-/-}$, and IPS-$1^{-/-}$ mice, and TNF-α mRNA was measured by quantitative PCR; $n = 3$. Data are shown as average ± SD. A representative experiment of two with similar outcomes is shown.

(Fig. 5*B*). The polyI:C-triggered M1 gene expression continued long in tumor-infiltrated Mfs, a finding that may further explain the tumor-suppressing feature of these Mfs, in addition to the concern of early inducing TNF-α.

Discussion

In this study we demonstrated that the tumor-supporting properties of tumor-infiltrating F4/80$^+$ Mfs characterized by M2 markers are dynamic and able to shift to an M1-dominant state upon the particular signal provided by PRRs. In 3LL tumors that express minimal amounts of MHC class I/II and recruit a large amount of myeloid cells, F4/80$^+$ Mfs function to sustain the tumor in the surrounding microenvironment. This tumor-supporting environment can be disrupted by stimulation with an RNA duplex through a TICAM-1 signal and subsequent induction of mediators such as TNF-α. Thus, the TICAM-1 signal in tumor-infiltrating Mfs plays a key role in TNF-α and M1 shift-mediated tumor regression. These results were confirmed using another cell line, MC38 colon adenocarcinoma (34), although MC38 cells express MHC class I. B16D8 melanoma (12) and EL4 lymphoma (35) were resistant to TNF-α, but their F4/80$^+$ Mfs still possessed TNF-α–inducing potential by stimulation with polyI:C; their susceptibilities to polyI:C reportedly depend on other effectors (12, 35). These results may partly explain the reported findings that tumors regressed in patients with simultaneous virus infection (36, 37), and that tumor growth was inhibited by polyI:C injection in tumor-bearing mice (6, 7).

In contrast, polyI:C-stimulated PEC or bone marrow-derived Mfs induce type I IFN via the IPS-1 pathway unlike the case of tumor-infiltrating F4/80$^+$ Mfs. Nevertheless, all of these Mf subsets produce proinflammatory cytokines, including TNF-α, in a TICAM-1–dependent manner. Thus, the key question that arose was why predominant TICAM-1 dependence for polyI:C-mediated production of TNF-α occurred in F4/80$^+$ tumor-infiltrating Mfs leading to tumor regression. A marked finding is that the TLR3 protein level is high in tumor-infiltrating Mfs compared with other sources of Mfs (Fig. S10). In addition, the IPS-1 pathway is unresponsive to polyI:C if the polyI:C is exogenously added to the tumor-infiltrating Mfs without transfection reagents. The cytoplasmic dsRNA sensors normally work for IFN induction in tumor F4/80$^+$ Mfs if the polyI:C is transfected into the cells. TICAM-1–dependent TNF-α production by F4/80$^+$ Mfs (Fig. S11 *D* and *F*) occurs partly because F4/80$^+$ Mfs express a high basal level of TLR3 and fail to take up extrinsic polyI:C into the cytoplasm. Of many subsets of Mfs, these properties (38) are unique to the F4/80$^+$ Mfs.

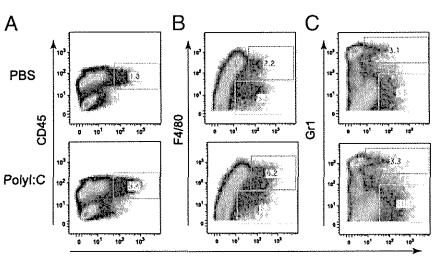

Fig. 3. F4/80$^+$ cells are responsible for the polyI:C-induced elevation of TNF-α production in tumor. Mice bearing 3LL tumors were i.p. injected with 200 μg polyI:C. TNF-α–producing cells in tumors of polyI:C- or PBS-injected mice were examined by immunohistochemical staining and flow cytometry to determine intracellular cytokine expression profiles of CD45$^+$ cells (*A*), F4/80$^+$ cells (*B*), and Gr1$^+$ cells (*C*). CD45$^+$ cells in tumor were gated and are shown in *B* and *C*. A representative experiment of two with similar outcomes is shown. TNF-α$^+$ gating squares are shown in red (positive) and green (negative).

Hemorrhagic necrosis and tumor size reduction are closely correlated with constitutive production of TNF-α (39, 40). The association of PRR-derived TNF-α and hemorrhagic necrosis of tumor has been described earlier. Carswell et al. (41) showed that TNF-α is robustly expressed in mouse serum following treatment with bacillus Calmette–Guérin and endotoxin. Bioassay of TNF-α as reflected by the degree of hemorrhagic necrosis of transplanted Meth A sarcoma in BALB/c mice led the authors to speculate that Mfs are responsible for TNF-α induction. Many years later, Dougherty et al. (42) identified the mechanism responsible for the TNF-α production associated with antitumor activity; macrophages isolated from tumors in mice with inactivating mutation in the TLR4 gene [Lps(d) in C3H/HeJ] expressed 5- to 10-fold less TNF-α than tumors in WT mice. This finding represents a unique recognition of a PRR contributing to the cancer phenotype. Subsequent studies determined that MyD88 is involved in the induction of TNF-α via TLR4 binding to its cognate ligand, lipid A endotoxin (15, 43). Because the TLR3 signal is independent of MyD88, this MyD88 concept is not applicable to the present study on polyI:C-dependent tumor regression.

Alternatively, endotoxin/lipid A may have activated TICAM-1 in previous reports on TLR4-derived TNF-α because TLR4 can recruit TICAM-1 in addition to MyD88 (15). The lipid A derivative monophospholipid A preferentially activates the TICAM-1 pathway of TLR4 (43). It is likely that TICAM-1 participates in TLR4-mediated tumor regression in addition to MyD88, although MyD88 is not involved in the polyI:C signaling. This point was further proven using TNF-$\alpha^{-/-}$ mice: TICAM-1–derived TNF-α in F4/80$^+$ Mf cells has a critical role in the induction of tumor necrosis and regression by polyI:C. The results are consistent with the finding that both TICAM-1 and IPS-1 pathways are able to induce NF-κB activation secondary to polyI:C stimulation, and indeed their signals converge at the IκB kinase complex (18).

TICAM-1 is able to induce many of the IFN-inducible genes that MyD88 cannot in mDCs (44). In both cases of TICAM-1 and MyD88 stimulation, tumor-infiltrating Mfs facilitate the expression of many genes in addition to TNF-α. The M2 phenotype of F4/80$^+$ Mfs or tumor-associated Mfs is modified dependent on these additional factors. IFNAR facilitates polyI:C-mediated tumor regression in tumor-bearing mice, lack of which results in no induction of TLR3 (Fig. S7). Thus, preceding the polyI:C

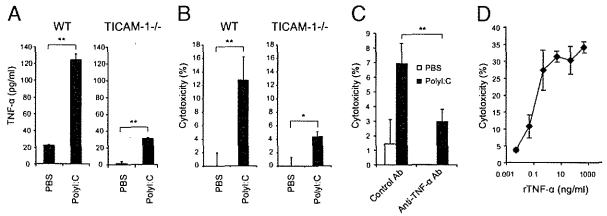

Fig. 4. Poly I:C enhances TNF-α production and cytotoxicity of F4/80$^+$ cells in tumor. Poly I:C (200 μg) or PBS was i.p. injected into 3LL tumor-bearing WT mice. After 30 min, F4/80$^+$ cells isolated from tumor were cultured for 24 h and TNF-α concentration in the conditioned medium was determined by ELISA (*A*). In parallel, the cytotoxicity of tumor-infiltrating F4/80$^+$ cells against 3LL tumor cells was measured by ^{51}Cr-release assay (*B*). Anti–TNF-α neutralization antibody or control antibody was added (10 μg/mL) to mixed culture of isolated tumor-infiltrating F4/80$^+$ cells and 3LL tumor cells (*C*). (*D*) Cytotoxic activity of TNF-α against 3LL tumor cells. Recombinant TNF-α was added to ^{51}Cr-labeled 3LL tumor cell culture at various concentrations. After 20 h, cytotoxicity was measured; $n = 3$. Data are shown as average ± SD. $*P < 0.05$, $**P < 0.001$. A representative experiment of three with similar outcomes is shown.

response, minute type I IFN of undefined source has to be provided to set the TLR3/TICAM-1 pathway, which may primarily fail in IFNAR$^{-/-}$ mice. Cellular effectors, cytotoxic T lymphocyte (CTL) and NK cells, are induced secondary to activation of IFN-inducible genes in a late phase of poly I:C-stimulated myeloid cells (45–47). The relationship among the TICAM-1–mediated type I IFN liberation, these late-phase effectors, and tumor regression remains an open question in this setting.

M1 Mf cells function to protect the host against tumors by producing large amounts of inflammatory cytokines and activating the immune response (48, 49). However, distinct types of M2 cells differentiate when monocytes are stimulated with IL-4 and IL-13 (M2a), immune complexes/TLR ligands (M2b), or IL-10 and glucocorticoids (M2c) (50). In our study, poly I:C stimulation led to incremental expression of the M1 Mf-related genes. In contrast, poly I:C stimulation was not associated with M2 polarization, except for IL-10. Other genes related to angiogenesis and extravasation were not affected by poly I:C treatment. Thus, poly I:C was able to induce the characteristic M1 conversion and, in turn, contribute to tumor regression. It is notable that TAM cells usually have defective and delayed NF-κB activation in response to different proinflammatory signals, such as expression of cytotoxic mediators NO, cytokines, TNF-α, and IL-12 (51–53). These observations are in apparent contrast with the function of other resident Mf species. This discrepancy may again reflect a dynamic change in the tumor microenvironment during tumor progression.

In line with our findings, virus infection has been observed to instigate tumor regression in patients with cancer (36, 54). Gene therapy for cancer patients using virus-derived vectors has proved effective in reducing tumors in clinic (36, 37). Administration of dsRNA elicits IFN induction, NK cell activation, and CTL proliferation for antitumor effectors in vivo (19, 55). This is a unique finding that tumor-infiltrating Mfs are a target of dsRNA and converted from tumor supporters to tumoricidal effectors. Hence, the antitumor effect of dsRNA adjuvant is ultimately based on the liberation of type I IFN, functional maturation of mDCs, and modulation of tumor-infiltrating Mfs, where TICAM-1 is a crucial transducer in eliciting antitumor immunity.

Methods

Inbred C57BL/6 WT mice were purchased from CLEA Japan, Inc. TICAM-1$^{-/-}$ and IPS-1$^{-/-}$ mice were generated in our laboratory and maintained as described previously. IRF-3/7 double-KO mice were a gift from T. Taniguchi

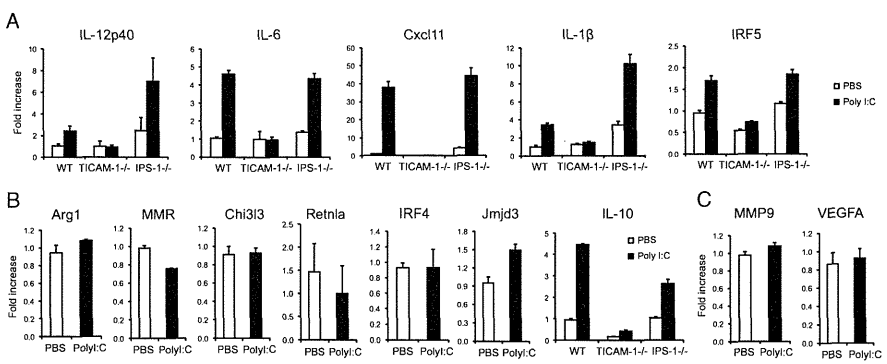

Fig. 5. Poly I:C induces M1 polarization of TAMs. F4/80$^+$ cells were isolated from 3LL tumor and stimulated with poly I:C (50 μg/mL) for 4 h. Total RNA was extracted and used to analyze the transcript expression levels of M1 (*A*) and M2 (*B* and *C*) markers; $n = 3$. Data are shown as average ± SD. A representative experiment of two with similar outcomes is shown.

(University of Tokyo, Tokyo, Japan). TNF-α$^{-/-}$ mice were kindly provided by A. Nakane (Hirosaki University, Aomori, Japan) and Y. Iwakura (University of Tokyo). Mice 6–10 wk of age were used in all experiments. 3LL lung cancer cells were cultured at 37 °C under 5% CO_2 in RPMI containing 10% FCS, penicillin, and streptomycin. This study was carried out in strict accordance with the recommendations in the Guide for the Care and Use of Laboratory Animals of the National Institutes of Health. The protocol was approved by the Committee on the Ethics of Animal Experiments in the Animal Safety Center, Hokkaido University, Japan. All mice were used according to the guidelines of the Institutional Animal Care and Use Committee of Hokkaido University, who approved this study as no. 08-0290, "Analysis of Anti-Tumor Immune Response Induced by the Activation of Innate Immunity."

Other detailed methods are provided in *SI Methods*.

ACKNOWLEDGMENTS. We thank Dr. T. Taniguchi (University of Tokyo) and D. M. Segal (EIB/NCI, Bethesda, MD) for kindly providing us with IRF-3/7 double KO mice and mAb against mouse TLR3. This work was supported in part by Grants-in-Aid from the Ministry of Education, Science, and Culture (MEXT), "the Carcinogenic Spiral" a MEXT Grant-in-Project, and the Ministry of Health, Labor, and Welfare of Japan, the Takeda Foundation, the Akiyama Foundation, and the Waxman Foundation.

1. Grivennikov SI, Greten FR, Karin M (2010) Immunity, inflammation, and cancer. *Cell* 140:883–899.
2. de Visser KE, Eichten A, Coussens LM (2006) Paradoxical roles of the immune system during cancer development. *Nat Rev Cancer* 6:24–37.
3. Chan AT, Ogino S, Fuchs CS (2007) Aspirin and the risk of colorectal cancer in relation to the expression of COX-2. *N Engl J Med* 356:2131–2142.
4. Rakoff-Nahoum S, Medzhitov R (2007) Regulation of spontaneous intestinal tumorigenesis through the adaptor protein MyD88. *Science* 317:124–127.
5. Chen GY, Shaw MH, Redondo G, Núñez G (2008) The innate immune receptor Nod1 protects the intestine from inflammation-induced tumorigenesis. *Cancer Res* 68:10060–10067.
6. Sarma PS, Shiu G, Neubauer RH, Baron S, Huebner RJ (1969) Virus-induced sarcoma of mice: Inhibition by a synthetic polyribonucleotide complex. *Proc Natl Acad Sci USA* 62:1046–1051.
7. Levy HB, Law LW, Rabson AS (1969) Inhibition of tumor growth by polyinosinic-polycytidylic acid. *Proc Natl Acad Sci USA* 62:357–361.
8. Absher M, Stinebring WR (1969) Toxic properties of a synthetic double-stranded RNA. Endotoxin-like properties of poly I. poly C, an interferon stimulator. *Nature* 223:715–717.
9. Talmadge JE, et al. (1985) Immunomodulatory effects in mice of polyinosinic-polycytidylic acid complexed with poly-L-lysine and carboxymethylcellulose. *Cancer Res* 45:1058–1065.
10. Longhi MP, et al. (2009) Dendritic cells require a systemic type I interferon response to mature and induce CD4$^+$ Th1 immunity with poly IC as adjuvant. *J Exp Med* 206:1589–1602.
11. Matsumoto M, Seya T (2008) TLR3: Interferon induction by double-stranded RNA including poly(I:C). *Adv Drug Deliv Rev* 60:805–812.
12. Akazawa T, et al. (2007) Antitumor NK activation induced by the Toll-like receptor 3-TICAM-1 (TRIF) pathway in myeloid dendritic cells. *Proc Natl Acad Sci USA* 104:252–257.
13. Miyake T, et al. (2009) Poly I:C-induced activation of NK cells by CD8 alpha$^+$ dendritic cells via the IPS-1 and TRIF-dependent pathways. *J Immunol* 183:2522–2528.
14. McCartney S, et al. (2009) Distinct and complementary functions of MDA5 and TLR3 in poly(I:C)-mediated activation of mouse NK cells. *J Exp Med* 206:2967–2976.
15. Oshiumi H, Matsumoto M, Funami K, Akazawa T, Seya T (2003) TICAM-1, an adaptor molecule that participates in Toll-like receptor 3-mediated interferon-beta induction. *Nat Immunol* 4:161–167.
16. Yoneyama M, et al. (2005) Shared and unique functions of the DExD/H-box helicases RIG-I, MDA5, and LGP2 in antiviral innate immunity. *J Immunol* 175:2851–2858.
17. Takeuchi O, Akira S (2010) Pattern recognition receptors and inflammation. *Cell* 140:805–820.
18. Sasai M, et al. (2006) NAK-associated protein 1 participates in both the TLR3 and the cytoplasmic pathways in type I IFN induction. *J Immunol* 177:8676–8683.
19. Seya T, Matsumoto M (2009) The extrinsic RNA-sensing pathway for adjuvant immunotherapy of cancer. *Cancer Immunol Immunother* 58:1175–1184.
20. Iwasaki A, Medzhitov R (2010) Regulation of adaptive immunity by the innate immune system. *Science* 327:291–295.
21. Condeelis J, Pollard JW (2006) Macrophages: Obligate partners for tumor cell migration, invasion, and metastasis. *Cell* 124:263–266.
22. Schuler G, Schuler-Thurner B, Steinman RM (2003) The use of dendritic cells in cancer immunotherapy. *Curr Opin Immunol* 15:138–147.
23. Murdoch C, Muthana M, Coffelt SB, Lewis CE (2008) The role of myeloid cells in the promotion of tumour angiogenesis. *Nat Rev Cancer* 8:618–631.
24. Borrello MG, Degl'Innocenti D, Pierotti MA (2008) Inflammation and cancer: The oncogene-driven connection. *Cancer Lett* 267:262–270.
25. Biswas SK, Mantovani A (2010) Macrophage plasticity and interaction with lymphocyte subsets: Cancer as a paradigm. *Nat Immunol* 11:889–896.
26. Farma JM, et al. (2007) Direct evidence for rapid and selective induction of tumor neovascular permeability by tumor necrosis factor and a novel derivative, colloidal gold bound tumor necrosis factor. *Int J Cancer* 120:2474–2480.
27. Masuda H, et al. (2002) High levels of RAE-1 isoforms on mouse tumor cell lines assessed by the anti-pan-Rae-1 polyclonal antibody confers tumor cell cytotoxicity on mouse NK cells. *Biochem Biophys Res Commun* 290:140–145.
28. Smyth MJ, et al. (2004) NKG2D recognition and perforin effector function mediate effective cytokine immunotherapy of cancer. *J Exp Med* 200:1325–1335.
29. Remels L, Fransen L, Huygen K, De Baetselier P (1990) Poly I:C activated macrophages are tumoricidal for TNF-α-resistant 3LL tumor cells. *J Immunol* 144:4477–4486.
30. Jelinek I, et al. (2011) TLR3-specific double-stranded RNA oligonucleotide adjuvants induce dendritic cell cross-presentation, CTL responses, and antiviral protection. *J Immunol* 186:2422–2429.
31. Krausgruber T, et al. (2011) IRF5 promotes inflammatory macrophage polarization and TH1-TH17 responses. *Nat Immunol* 12:231–238.
32. Satoh T, et al. (2010) The Jmjd3-Irf4 axis regulates M2 macrophage polarization and host responses against helminth infection. *Nat Immunol* 11:936–944.
33. De Santa F, et al. (2007) The histone H3 lysine-27 demethylase Jmjd3 links inflammation to inhibition of polycomb-mediated gene silencing. *Cell* 130:1083–1094.
34. Zitvogel L, et al. (1995) Cancer immunotherapy of established tumors with IL-12. Effective delivery by genetically engineered fibroblasts. *J Immunol* 155:1393–1403.
35. Abe R, Peng T, Sailors J, Bucala R, Metz CN (2001) Regulation of the CTL response by macrophage migration inhibitory factor. *J Immunol* 166:747–753.
36. Russell SJ (2002) RNA viruses as virotherapy agents. *Cancer Gene Ther* 9:961–966.
37. Aghi M, Martuza RL (2005) Oncolytic viral therapies—the clinical experience. *Oncogene* 24:7802–7816.
38. Watanabe A, et al. (2011) Raftlin is involved in the nucleocapture complex to induce poly(I:C)-mediated TLR3 activation. *J Biol Chem* 286:10702–10711.
39. Mocellin S, Rossi CR, Pilati P, Nitti D (2005) Tumor necrosis factor, cancer and anticancer therapy. *Cytokine Growth Factor Rev* 16:35–53.
40. Balkwill F (2009) Tumour necrosis factor and cancer. *Nat Rev Cancer* 9:361–371.
41. Carswell EA, et al. (1975) An endotoxin-induced serum factor that causes necrosis of tumors. *Proc Natl Acad Sci USA* 72:3666–3670.
42. Dougherty ST, Eaves CJ, McBride WH, Dougherty GJ (1997) Molecular mechanisms regulating TNF-alpha production by tumor-associated macrophages. *Cancer Lett* 111:27–37.
43. Mata-Haro V, et al. (2007) The vaccine adjuvant monophosphoryl lipid A as a TRIF-biased agonist of TLR4. *Science* 316:1628–1632.
44. Ebihara T, et al. (2010) Identification of a poly(I:C)-inducible membrane protein that participates in dendritic cell-mediated natural killer cell activation. *J Exp Med* 207:2675–2687.
45. Akazawa T, et al. (2004) Adjuvant-mediated tumor regression and tumor-specific cytotoxic response are impaired in MyD88-deficient mice. *Cancer Res* 64:757–764.
46. Akazawa T, et al. (2007) Tumor immunotherapy using bone marrow-derived dendritic cells overexpressing Toll-like receptor adaptors. *FEBS Lett* 581:3334–3340.
47. Schulz O, et al. (2005) Toll-like receptor 3 promotes cross-priming to virus-infected cells. *Nature* 433:887–892.
48. Mantovani A, Sica A, Locati M (2007) New vistas on macrophage differentiation and activation. *Eur J Immunol* 37:14–16.
49. Martinez FO, Helming L, Gordon S (2009) Alternative activation of macrophages: An immunologic functional perspective. *Annu Rev Immunol* 27:451–483.
50. Mantovani A, et al. (2004) The chemokine system in diverse forms of macrophage activation and polarization. *Trends Immunol* 25:677–686.
51. Sica A, et al. (2000) Autocrine production of IL-10 mediates defective IL-12 production and NF-kappa B activation in tumor-associated macrophages. *J Immunol* 164:762–767.
52. Torroella-Kouri M, et al. (2005) Diminished expression of transcription factors nuclear factor kappaB and CCAAT/enhancer binding protein underlies a novel tumor evasion mechanism affecting macrophages of mammary tumor-bearing mice. *Cancer Res* 65:10578–10584.
53. Biswas SK, et al. (2006) A distinct and unique transcriptional program expressed by tumor-associated macrophages (defective NF-kappaB and enhanced IRF-3/STAT1 activation). *Blood* 107:2112–2122.
54. Bluming AZ, Ziegler JL (1971) Regression of Burkitt's lymphoma in association with measles infection. *Lancet* 2:105–106.
55. Matsumoto M, Oshiumi H, Seya T (2011) Antiviral responses induced by the TLR3 pathway. *Rev Med Virol* 21:67–77.

JVI
Journals.ASM.org

The Toll-Like Receptor 3-Mediated Antiviral Response Is Important for Protection against Poliovirus Infection in Poliovirus Receptor Transgenic Mice

Yuko Abe,[a] Ken Fujii,[a] Noriyo Nagata,[b] Osamu Takeuchi,[c] Shizuo Akira,[c] Hiroyuki Oshiumi,[d] Misako Matsumoto,[d] Tsukasa Seya,[d] and Satoshi Koike[a]

Neurovirology Project, Tokyo Metropolitan Institute of Medical Science, 2-1-6 Kamikitazawa, Setagaya-ku, Tokyo 156-8506, Japan[a]; Department of Pathology, National Institute of Infectious Diseases, 4-7-1 Gakuen, Musashimurayama, Tokyo 208-0011, Japan[b]; Laboratory of Host Defense, WPI Immunology Frontier Research Center (IFReC), Osaka University, 3-1 Yamada-oka, Suita, Osaka 565-0871, Japan[c]; and Department of Microbiology and Immunology, Hokkaido University Graduate School of Medicine, Kita 15, Nishi 7, Kita-ku, Sapporo 060-8638, Japan[d]

RIG-I-like receptors and Toll-like receptors (TLRs) play important roles in the recognition of viral infections. However, how these molecules contribute to the defense against poliovirus (PV) infection remains unclear. We characterized the roles of these sensors in PV infection in transgenic mice expressing the PV receptor. We observed that alpha/beta interferon (IFN-α/β) production in response to PV infection occurred in an MDA5-dependent but RIG-I-independent manner in primary cultured kidney cells *in vitro*. These results suggest that, similar to the RNA of other picornaviruses, PV RNA is recognized by MDA5. However, serum IFN-α levels, the viral load in nonneural tissues, and mortality rates did not differ significantly between MDA5-deficient mice and wild-type mice. In contrast, we observed that serum IFN production was abrogated and that the viral load in nonneural tissues and mortality rates were both markedly higher in TIR domain-containing adaptor-inducing IFN-β (TRIF)-deficient and TLR3-deficient mice than in wild-type mice. The mortality rate of MyD88-deficient mice was slightly higher than that of wild-type mice. These results suggest that multiple pathways are involved in the antiviral response in mice and that the TLR3-TRIF-mediated signaling pathway plays an essential role in the antiviral response against PV infection.

Poliovirus (PV), which belongs to the genus *Enterovirus* in the family *Picornaviridae*, is the causative agent of poliomyelitis (38). The host range of PV is restricted to primates (18). This species' tropism is determined primarily by the cellular PV receptor (PVR; CD155), which gives the virus access to susceptible cells (14–16, 20). Mice are generally not susceptible to PV. However, transgenic mice expressing human PVR (PVR-tg mice) become susceptible to PV and develop a paralytic disease similar to human poliomyelitis after the administration of PV intravenously, intraperitoneally, intracerebrally, or intramuscularly but not orally (26, 40). PV shows a neurotropic phenotype in both humans and PVR-tg mice. PV preferentially replicates in neurons, especially in motor neurons in the anterior or ventral horn of the spinal cord and in the brainstem. However, the efficiency of PV replication is low in nonneural tissues (4, 25). We previously found that innate immune responses that are mediated by type I interferons (IFNs) play important roles in controlling viral replication in nonneural tissues and in the mortality rates of PVR-tg mice (19). In PVR-tg mice deficient in IFNAR1, PV efficiently replicates in nonneural tissues such as the liver, pancreas, and spleen, which are not normal targets of PV. IFNAR1-deficient mice die after the inoculation of a small amount of PV by peripheral routes. The results suggest that the type I IFN response forms an innate immune barrier that prevents PV replication in nonneural tissues and subsequent PV invasion of the central nervous system (CNS). This response therefore plays important roles in the tissue tropism and pathogenicity of PV (25).

The sensors that are involved in the production of type I IFNs in response to RNA viral infections have been recently identified and characterized (1, 46–48). The RIG-I-like receptors (RLRs) retinoic-acid-inducible gene 1 (RIG-I) and melanoma differentiation-associated gene 5 (MDA5) are expressed in the cytoplasm of all cell types, with the exception of plasmacytoid dendritic cells (pDCs). RIG-I and MDA5 have RNA binding domains and differentially recognize specific characteristics of nonself viral RNAs (17, 22, 36, 37). In addition, RLRs have DExD/H box RNA helicase domains (51) that activate downstream signaling pathways resulting in the activation of IFN regulatory factor 3 (IRF-3) and IRF-7 (53). TLR3 and TLR7 are the sensors for viral double-stranded RNA (dsRNA) and single-stranded RNA, respectively (2, 8, 12). TLR3 is expressed in the endosome of macrophages and conventional dendritic cells (DCs) (28) but not in pDCs. TLR3 is also expressed in a variety of epithelial cells, including airway, uterine, corneal, vaginal, cervical, biliary, and intestinal epithelial cells, which may function as efficient barriers to infection. The TLR3-mediated signaling pathway is transmitted through Toll–interleukin-1 (IL-1) receptor (TIR)-containing adaptor molecule 1, which is also known as TIR domain-containing adaptor inducing IFN-β (TRIF), and finally results in the activation of IRF3 and IRF7 (13, 34, 51). TLR7 is specifically expressed in the endosome of pDCs and contributes to the production of a large amount of IFNs in response to many RNA virus infections (5, 7). TLR7 signaling is mediated by the adaptor molecule myeloid differentiation factor 88 (MyD88). These sensors do not contribute equally to the antiviral response to each viral infection. The type I IFN production that is induced by these sensors occurs in a virus-specific and cell-specific manner (21, 23). For example, RIG-I plays an important role in the antiviral response to Newcastle disease virus, influenza A virus, Sendai virus, vesicular stomatitis virus, Japanese encephalitis virus, and hepatitis C virus. However, MDA5 is important in the response to infection with picornaviruses, such as encephalomyocarditis virus (EMCV) (10, 23). Although RNA viruses produce dsRNA during the replication step, the protective effect of the TLR3-mediated pathway is not clear (9). In a previous study, TLR3 expression was found to cause severe encephalitis in West Nile virus (WNV) infection (50). How these sensor molecules contribute to the recognition of PV infection is not understood. The aim of the present study was to determine the role of these sensors in the response to PV infection in transgenic mice expressing human PVR. We generated PVR-tg mice deficient in these sensor and adaptor molecules. Our results demonstrate that the MDA5-, TRIF- and MyD88-mediated pathways contribute to the antiviral response against PV infection and that the TLR3-TRIF-mediated pathway plays a pivotal role in this response.

Received 29 May 2011 Accepted 20 October 2011
Published ahead of print 9 November 2011
Address correspondence to Satoshi Koike, koike-st@igakuken.or.jp.

doi:10.1128/JVI.05245-11

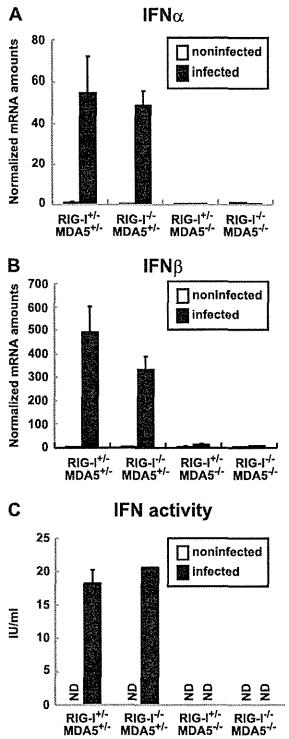

FIG 1 Production of IFNs in primary cultured kidney cells prepared from RIG-I- and MDA5-deficient mice. Kidney cells were pretreated with 100 U of IFN-β for 2 h and infected with PV at an MOI of 10. RNA was prepared from the infected cells at 6 hpi. The amounts of IFN-α mRNA (A) and IFN-β mRNA (B) were determined using quantitative real-time PCR. Cells were prepared in duplicate, and the experiments were repeated three times. Representative data are shown. The amount of IFN activity in the supernatant of infected kidney cells at 8 hpi was determined by the cytopathic effect dye uptake method using L929 cells (C). ND, not detected.

MATERIALS AND METHODS

Cells and viruses. An AGMK cell line, JVK-03 (24), was maintained in Eagle's minimum essential medium containing 5% fetal bovine serum. PV type I Mahoney, a strain derived from the infectious cDNA clone pOM, was used in this study (45). The virus was propagated in JVK-03, and the viral titer was determined using the plaque assay. Primary cultured kidney cells were prepared from transgenic and knockout mice as previously described (54).

Transgenic and knockout mice and infection experiments. All experiments using mice were performed in accordance with the Guidelines for the Care and Use of Laboratory Animals of the Tokyo Metropolitan Institute of Medical Science. ICR-PVRTg21 mice (26) were mated with RIG-I$^{-/-}$ and/or MDA5$^{-/-}$ mice (21) in the ICR background because it is difficult to maintain RIG-I$^{-/-}$ mice in other genetic backgrounds. We mated mice and obtained littermates with the genotypes RIG-I$^{+/-}$ MDA5$^{+/-}$, RIG-I$^{-/-}$ MDA5$^{+/-}$, RIG-I$^{+/-}$ MDA5$^{-/-}$, and RIG-I$^{-/-}$ MDA5$^{-/-}$ to use in experiments. C57BL/6 (B6)-PVRTg21 mice were mated with MDA5$^{-/-}$ mice, TRIF$^{-/-}$ mice, MyD88$^{-/-}$ mice, and TLR3$^{-/-}$ mice (51) in the B6 background (backcrossed 7 to 10 times). IFNAR1$^{-/-}$ PVR-tg mice were previously described (19). Because all of the mice that were used in the present study were in the PVR-tg background, we omitted the notation "PVR-tg" for simplicity in this report. Six- to 7-week-old mice were used for infection experiments. The survival and clinical symptoms of the mice were observed daily for 3 weeks. At the first sign of severe neurological symptoms, the mice were sacrificed as a humane endpoint.

Measurement of IFN levels. IFN-α levels in the sera were determined using an enzyme-linked immunosorbent assay (ELISA). The ELISA kit for IFN-α was purchased from PBL Biochemical Laboratories. Mouse IFN activity in the supernatants of PV-infected kidney cells was measured by the cytopathic effect dye uptake method using L929 cells (54, 55). Recombinant mouse IFN-β (Toray) was used as the standard for unit definition.

Quantitative real-time reverse transcription (RT)-PCR. RNA was isolated from the tissues of infected mice or infected cells using the Isogen RNA extraction kit (Nippon Gene). DNase I treatment and cDNA synthesis were performed as previously described (54). The amounts of the mRNAs for IFN-α, IFN-β, OAS1a, and IRF-7 were determined using real-time RT-PCR with an ABI Prism 7500 (Applied Biosystems) as previously described (54).

RESULTS

IFN production in primary cultured kidney cells is dependent on MDA5. We examined whether, similar to EMCV infection, PV infection is recognized by MDA5 *in vitro*. We mated PVR-tg mice with MDA5-deficient and RIG-I-deficient mice to generate RIG-I$^{+/-}$ MDA5$^{+/-}$, RIG-I$^{-/-}$ MDA5$^{+/-}$, RIG-I$^{+/-}$ MDA5$^{-/-}$, and RIG-I$^{-/-}$ MDA5$^{-/-}$ mice in the ICR background. We prepared primary cultured kidney cells from mice with these genotypes to determine the role of RLRs. After cultivation for approximately 1 week, the cells that became confluent were infected with PV at a multiplicity of infection (MOI) of 10. RNA was recovered from the infected cells at 6 hpi, and the amounts of the mRNAs for IFN-α and IFN-β were determined using real-time RT-PCR. Kid-

ney cells that were not pretreated with IFN-β before PV infection showed rapid cytopathic effect progression and did not produce IFN mRNA (data not shown). This result is consistent with our previous observations (54). We therefore pretreated cells with 100 U of IFN-β for 2 h and infected them with PV. As we reported previously, the IFN-treated kidney cells became resistant to PV infection, PV replication was severely inhibited, and IFN production was observed (54). Under this condition, we determined the sensor responsible for IFN production. We observed the induction of both IFN-α (Fig. 1A) and IFN-β mRNAs (Fig. 1B) in cells that were isolated from RIGI-I$^{+/-}$ MDA5$^{+/-}$ mice and RIGI-I$^{-/-}$ MDA5$^{+/-}$ mice but not from RIGI-I$^{+/-}$ MDA5$^{-/-}$ mice or RIGI-I$^{-/-}$ MDA5$^{-/-}$ mice. The induced IFN proteins were not detected by ELISA due to a very small amount of IFNs produced in the supernatants. However, IFN activity was detected in the supernatants of PV-infected kidney cells prepared from RIGI-I$^{+/-}$ MDA5$^{+/-}$ mice and RIGI-I$^{-/-}$ MDA5$^{+/-}$ mice but not from RIGI-I$^{+/-}$ MDA5$^{-/-}$ mice or RIGI-I$^{-/-}$ MDA5$^{-/-}$ mice using the cytopathic effect dye uptake method (Fig. 1C). These results suggest that PV infection is recognized by MDA5 but not RIG-I in primary murine kidney cells, which is consistent with previous reports demonstrating that MDA5 is essential for the detection of picornaviruses (10, 23). However, MDA5-mediated IFN production was observed only when cells had been primed with a low dose of IFNs.

IFN responses of MDA5-deficient mice are not significantly different from those of wild-type mice. We hypothesized that MDA5 plays an important role in the type I IFN response upon PV infection *in vivo*. We examined the serum IFN-α levels in PVR-tg mice intravenously infected with 2×10^7 PFU of PV using ELISA. Their serum IFN-α level was initially observed at 9 hpi, peaked at 12 hpi, and began to decline at 24 hpi (Fig. 2A). We then determined the serum IFN-α levels of the knockout mice at 12 hpi. Unexpectedly, similar serum IFN-α levels were detected in RIG-I$^{+/-}$ MDA5$^{+/-}$, RIG-I$^{+/-}$ MDA5$^{-/-}$, RIG-I$^{-/-}$ MDA5$^{+/-}$, and RIG$^{-/-}$ MDA5$^{-/-}$ mice infected with PV (Fig. 2B).

We monitored the induction of mRNAs for the IFN-stimulated genes (ISGs), OAS1a (Fig. 3A) and IRF-7 (Fig. 3B), in the brain, spinal cord, liver, spleen, and kidney using real-time RT-PCR. Among the organs tested, the expression levels of these ISGs were the highest in the spleen. However, the expression profiles of these genes were essentially the same in all organs. In accordance with the elevated serum IFN levels, the induction of ISGs in various organs was observed in all mice (Fig. 3A and B). The results suggest that MDA5 does not play a critical role in IFN production and subsequent ISG induction in response to PV infection *in vivo*.

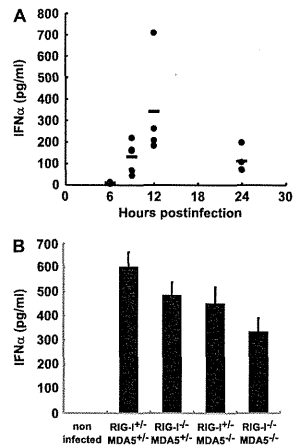

FIG 2 Production of serum IFN-α in RIG-I- and MDA5-deficient mice. (A) Time course of IFN-α levels in serum. PVR-tg mice in the B6 background (n = 4 or n = 5) were intravenously infected with 2×10^7 PFU of PV. Serum samples were collected at the indicated time points, and the concentration of IFN-α was determined using ELISA. (B) IFN-α levels of RIG-I- and MDA5-deficient mice in the ICR background (n = 8) at 12 hpi were compared. The experiments were repeated twice, and representative data are shown.

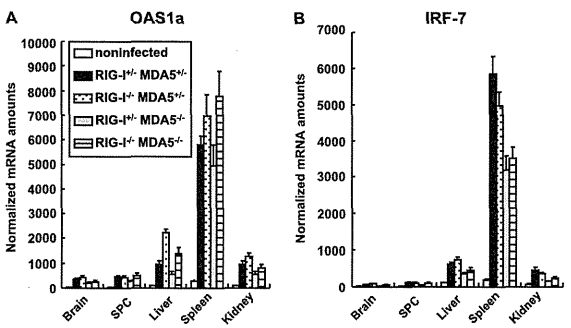

FIG 3 ISG induction in RIG-I- and MDA5-deficient mice. Mice (n = 4) were intravenously infected with 2×10^7 PFU of PV. At 12 hpi, RNA was isolated from the indicated tissues of the infected mice and OAS1a (A) and IRF-7 (B) mRNA levels were determined using quantitative real-time PCR. The experiments were repeated twice, and representative data are shown. SPC, spinal cord.

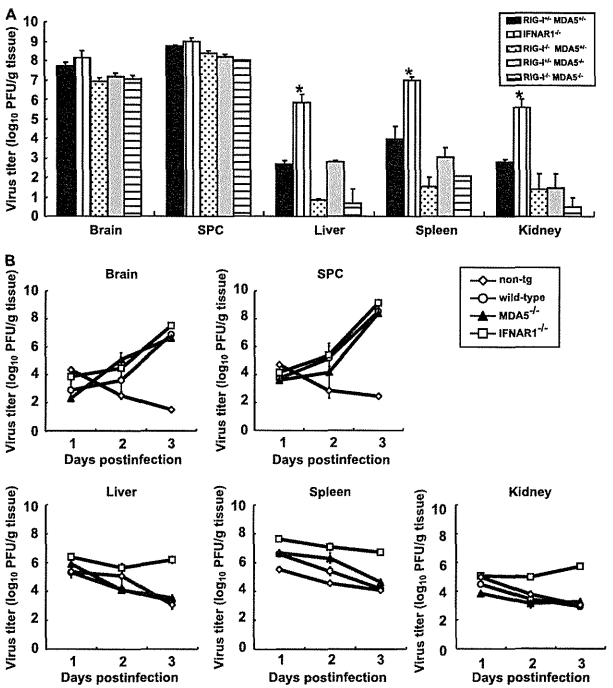

FIG 4 (A) PV replication in RIG-I- and MDA5-deficient mice. RIGI-I$^{+/-}$ MDA5$^{+/-}$, RIGI-I$^{-/-}$ MDA5$^{+/-}$, RIGI-I$^{-/-}$ MDA5$^{+/-}$, and RIGI-I$^{-/-}$ MDA5$^{-/-}$ mice in the ICR background and IFNAR1$^{-/-}$ mice in the B6 background (n = 3) were intravenously infected with 2×10^7 PFU of PV. Infected mice were paralyzed or dead at 3 to 5 days postinfection. The tissues of the paralyzed mice were collected, and the viral titers were determined using a plaque assay (*, $P < 0.01$ by t test compared to RIGI-I$^{+/-}$ MDA5$^{+/-}$ mice). (B) PV replication kinetics in MDA5-deficient mice. Nontransgenic (non-tg) mice, wild-type mice, MDA5$^{-/-}$ mice, and IFNAR1$^{-/-}$ mice in the B6 background (n = 3) were infected as described above. Tissues were collected daily, and viral titers were determined. SPC, spinal cord.

PV replication in nonneural tissues and mortality rates of mice deficient in RIG-I-like receptors. We have previously shown that the IFN-α/β response forms an innate immune barrier to prevent PV replication in nonneural tissues and PV invasion of the CNS (19, 25). Therefore, we evaluated PV replication in neural and nonneural tissues in RLR-deficient mice. The mice were infected with 2×10^7 PFU of PV, which is approximately 100 times higher than the 50% lethal doses for all mouse strains. The infected mice showed paralysis by 3 to 5 days postinfection. The brain, spinal cord, liver, spleen, and kidney of the paralyzed mice were recovered, and their viral titers were determined (Fig. 4A). PV was recovered from the CNS of the paralyzed mice almost equally among the genotypes. The viral titers recovered from the liver, spleen, and kidney of IFNAR1$^{-/-}$ mice were significantly higher than those of wild-type mice, as previously described (19). However, PV titers that were recovered from these organs of RIG-I$^{-/-}$ MDA5$^{+/-}$, RIG-I$^{+/-}$ MDA5$^{-/-}$, and RIG-I$^{-/-}$ MDA5$^{-/-}$ mice were as low as or lower than those in the organs of RIG-I$^{+/-}$ MDA5$^{+/-}$ mice. We then examined virus replication kinetics using nontransgenic mice, wild-type mice, IFNAR$^{-/-}$ mice, and MDA5$^{-/-}$ mice in the B6 background (Fig. 4B). The viral load in the CNS increased in a similar fashion among the transgenic mouse strains. However, the viral load kinetics in the liver, spleen, and kidney of wild-type and MDA5$^{-/-}$ mice were similar to those of nontransgenic mice. The values for nontransgenic mice indicate the kinetics of clearance of inoculated virus. The results indicated that PV replication was severely inhibited in the liver, spleen, and kidney of wild-type and MDA5$^{-/-}$ mice. This inhibition correlated well with the induction of serum IFNs in MDA5$^{-/-}$ mice (Fig. 2). The PV antigen was detected in neurons in the CNS but not in other tissues in all knockout mice (Table 1). This result indicates that the lack of RLRs did not alter the tissue tropism of PV. These data suggest that inhibition of PV replication in nonneural tissues is not dependent on RLRs and that MDA5-independent mechanisms are the major contributors in controlling PV replication.

We examined the mortality rates of RIG-I$^{+/-}$ MDA5$^{+/-}$, RIG-I$^{-/-}$ MDA5$^{+/-}$, RIG-I$^{+/-}$ MDA5$^{-/-}$, and RIG-I$^{-/-}$ MDA5$^{-/-}$

TABLE 1 PV antigens in RIG-I- and MDA5-deficient mice

Organ or tissue	No. of PV antigen-positive mice/no. of mice tested			
	RIG-I$^{+/-}$ MDA5$^{+/-}$	RIG-I$^{-/-}$ MDA5$^{+/-}$	RIG-I$^{+/-}$ MDA5$^{-/-}$	RIG-I$^{-/-}$ MDA5$^{-/-}$
Brain	4/4	3/3	4/4	4/4
Spinal cord	4/4	3/3	4/4	4/4
Heart	0/4	0/3	0/4	0/4
Lung	0/4	0/3	0/4	0/4
Liver	0/4	0/3	0/4	0/4
Kidney	0/4	0/3	0/4	0/4
Spleen	0/4	0/3	0/4	0/4
Pancreas	0/4	0/3	0/4	0/4
Intestine	0/4	0/3	0/4	0/4
Adipose tissue	0/4	0/3	0/4	0/4

mice in the ICR background after intravenous infection with PV at 10^3, 10^4, and 10^5 PFU (Fig. 5A, B, and C). The mortality rates of these mice did not differ significantly from each other. We observed that the mortality rates of RIG-I$^{+/-}$ MDA5$^{-/-}$ mice that were inoculated with 10^4 PFU of PV was slightly higher than the mice of other genotypes. However, significant differences were not observed in mice that were inoculated with the other doses. Similar experiments were performed using MDA5$^{-/-}$ and MDA5$^{+/-}$ mice in the B6 background (Fig. 5D, E, and F). We did not observe significant differences between the MDA5$^{-/-}$ and MDA5$^{+/-}$ mice. The mortality rate of MDA5$^{-/-}$ mice was slightly higher than that of MDA5$^{+/-}$ mice that were inoculated with 10^5 PFU of PV. However, the opposite trend was observed when mice

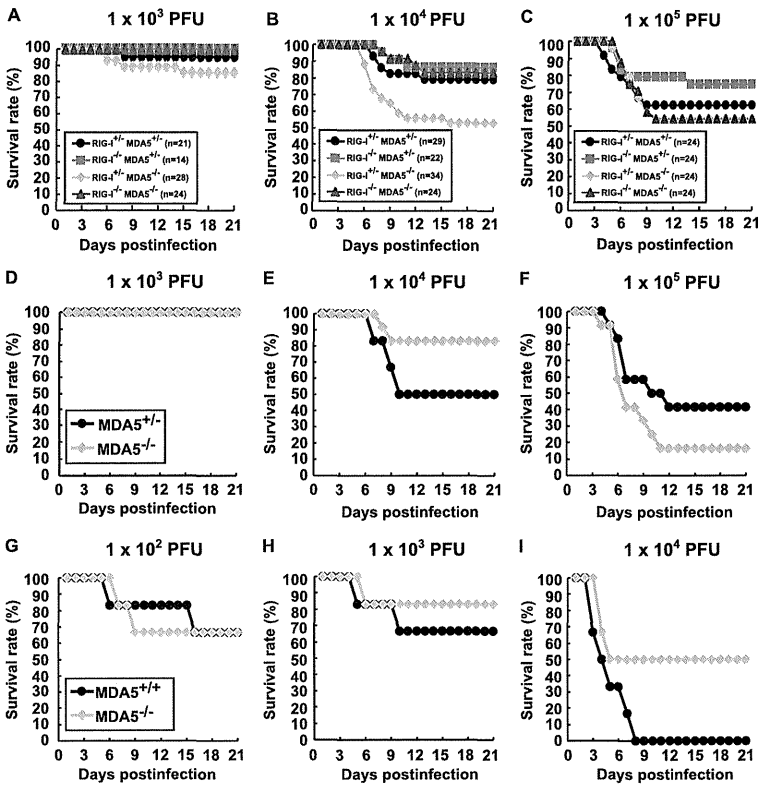

FIG 5 Mortality rates of RIG-I- and MDA5-deficient mice. Littermates of the genotypes indicated were obtained by mating RIGI-I$^{+/-}$ MDA5$^{+/-}$ and RIGI-I$^{-/-}$ MDA5$^{-/-}$ mice in the ICR background. The mice were infected intravenously with 10^3 (A), 10^4 (B), or 10^5 (C) PFU of PV. The results shown are the sums of several independent experiments. The total numbers of mice of the different genotypes that were used are boxed, and the doses used are shown at the top. Littermates of MDA5$^{+/-}$ and MDA5$^{-/-}$ mice were obtained in the B6 background. The mice (n = 12) were intravenously infected with 10^3 (D), 10^4 (E), or 10^5 (F) of PV. MDA5$^{+/+}$ and MDA5$^{-/-}$ mice (n = 6) were intracerebrally infected with 10^2 (G), 10^3 (H), or 10^4 (I) PFU of PV, respectively. We monitored the survival rates of the mice for 3 weeks after infection.

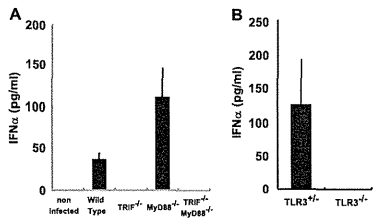

FIG 6 Production of serum IFN-α in TRIF-, MyD88-, and TLR3-deficient mice. Mice (n = 3 or 8) were intravenously infected with 10^7 PFU of PV. IFN-α levels of TRIF- and MyD88-deficient mice (A) and TLR3-deficient mice (B) at 12 hpi were compared. The experiments were repeated twice, and representative data are shown.

were inoculated with 10^4 PFU of PV. We suspect that the slight difference between the mortality rates of wild-type and MDA5$^{-/-}$ mice was in the range of experimental fluctuation, and thus, the disruption of MDA5 did not significantly influence the mortality rate. In order to determine if the same is true when mice are infected by other routes, we inoculated wild-type and MDA5$^{-/-}$ mice with PV intracerebrally and compared their mortality rates (Fig. 5G to I). Their mortality rates did not differ significantly. These results suggest that MDA5 does not make a great contribution to the protection of mice, at least after intracerebral and intravenous infections. Taken together, the MDA5-mediated response does not play a dominant role in IFN production, ISG induction, or inhibition of PV replication *in vivo*, unlike the MDA5-mediated effects on EMCV infection.

IFN response in TRIF- and MyD88-deficient mice. Because the experiments with MDA5-deficient mice suggested the existence of other protective mechanisms in PV infection, we investigated the role of TLRs using TRIF- and MyD88-deficient mice. PVR-tg mice were mated with TRIF$^{-/-}$ and/or MyD88$^{-/-}$ mice in the B6 background. Serum IFN-α of mice infected with 10^7 PFU of PV was measured using ELISA at 12 hpi (Fig. 6A). Interestingly, serum IFN production in response to PV infection was abrogated in TRIF$^{-/-}$ mice. Because TRIF acts as an adaptor for TLR3 and TLR4, we tested whether the same phenomenon occurs in TLR3$^{-/-}$ mice. Serum IFN induction was not observed in TLR3-deficient mice (Fig. 6B). These results suggest that the TLR3-mediated pathway is essential for IFN production in response to PV infection.

We next assessed the induction of mRNAs for OAS1a (Fig. 7A) and IRF-7 (Fig. 7B) in various organs using real-time RT-PCR. The induction of OAS1a and IRF-7 was observed in all mice. Although serum IFN production was abrogated in TRIF$^{-/-}$ mice and TRIF$^{-/-}$ MyD88$^{-/-}$ mice (Fig. 6), a significant level of ISG mRNA was induced. However, the induction levels were slightly lower than those in wild-type mice in some cases. The results suggest that the TRIF-mediated pathway contributes to ISG expression mainly through the induction of serum IFNs in response to PV infection and that some other mechanisms may also contribute to ISG expression.

PV replication in nonneural tissues and mortality rates of TRIF- and MyD88-deficient mice. The brain, spinal cord, liver, spleen, and kidney of paralyzed mice were recovered, and viral titers were determined (Fig. 8). PV was recovered from the CNS of TRIF$^{-/-}$, MyD88$^{-/-}$, and TLR3$^{-/-}$ mice, and the titers were not different from those of wild-type mice. However, the viral titers of the liver, spleen, and kidney of TRIF$^{-/-}$ and TLR3$^{-/-}$ mice were significantly higher than those of wild-type mice but lower than those of IFNAR1$^{-/-}$ mice. We then examined the virus replication kinetics in TRIF$^{-/-}$ mice (Fig. 8B). The viral load in the CNS increased in TRIF$^{-/-}$ mice similarly to that in other mice. In accordance to the absence of serum IFN (Fig. 2), the viral loads in the liver, spleen, and kidney of TRIF$^{-/-}$ mice increased, while the viral loads in these organs of wild-type mice decreased. PV antigens were detected in the CNS of all of the knockout mice. In addition, PV antigens were detected in the adipose tissue, pancreas, and kidney of several TRIF$^{-/-}$ and MyD88$^{-/-}$ mice (Table 2). These results suggest that these tissues support viral multiplication in these knockout mice and that the TLR-mediated signaling pathways contribute to the regulation of PV replication in nonneural tissues.

The mortality rates of TRIF$^{-/-}$, MyD88$^{-/-}$, and TLR3$^{-/-}$

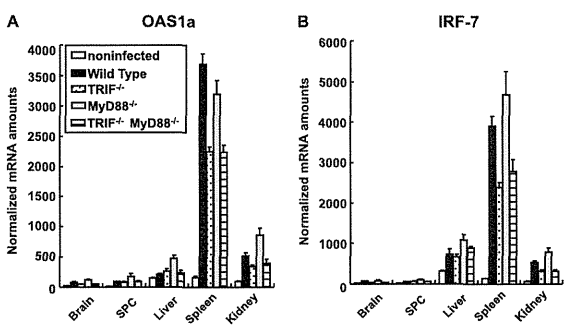

FIG 7 ISG induction in TRIF- and MyD88-deficient mice. Mice (n = 4) were intravenously infected with 10^7 PFU of PV. At 12 hpi, RNA was isolated from the indicated tissues of the infected mice and OAS1a (A) and IRF-7 (B) mRNA levels were determined by quantitative real-time PCR. The experiments were repeated twice, and representative data are shown. SPC, spinal cord.

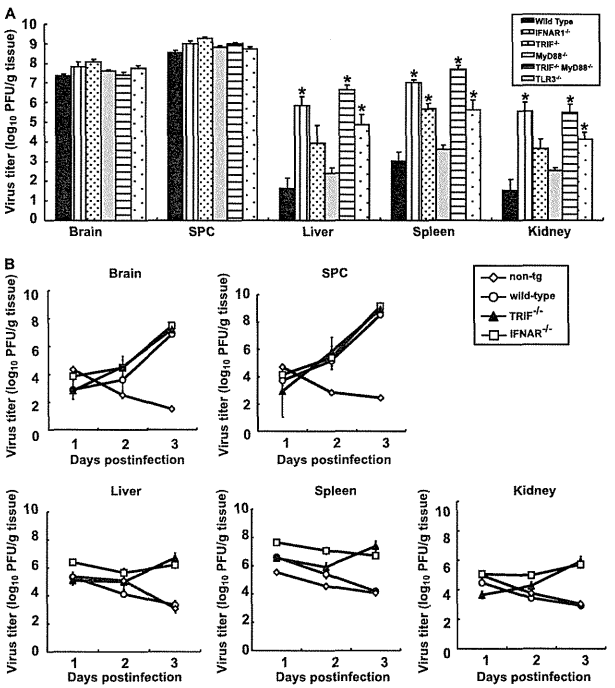

FIG 8 (A) PV replication in TRIF- and MyD88-deficient mice. Wild-type ($n = 4$), TRIF$^{-/-}$ ($n = 4$), MyD88$^{-/-}$ ($n = 6$), TRIF$^{-/-}$ MyD88$^{-/-}$ ($n = 4$), TLR3$^{-/-}$ ($n = 5$), and IFNAR1$^{-/-}$ ($n = 4$) mice were intravenously infected with 10^7 PFU of PV. The infected mice were paralyzed or dead at 3 to 5 days postinfection. The indicated tissues were collected, and viral titers were determined using a plaque assay (*, $P < 0.01$ by t test compared to wild-type mice). (B) PV replication kinetics in TRIF-deficient mice. Nontransgenic mice, wild-type mice, TRIF$^{-/-}$ mice, and IFNAR1$^{-/-}$ mice ($n = 3$) were infected as described above. Tissues were collected daily, and viral titers were determined. The results for nontransgenic (non-tg) mice, wild-type mice, and IFNAR1$^{-/-}$ mice are the same as those in Fig. 4B. SPC, spinal cord.

TABLE 2 PV antigens in TRIF- and MyD88-deficient mice

Organ or tissue	No. of PV antigen-positive mice/no. of mice tested			
	Wild type	TRIF$^{-/-}$	MyD88$^{-/-}$	TRIF$^{-/-}$ MyD88$^{-/-}$
Brain	6/6	8/8	9/9	6/6
Spinal cord	6/6	8/8	9/9	6/6
Heart	0/6	0/8	0/8	0/6
Lung	0/6	0/8	0/8	0/6
Liver	0/6	0/8	0/9	0/6
Kidney	0/6	0/8	2/9	0/5
Spleen	0/6	0/8	0/9	0/6
Pancreas	2/6	0/8	7/9	4/6
Intestine	0/6	0/8	0/9	0/6
Adipose tissue	0/6	2/8	2/9	3/6

mice were compared (Fig. 9). Approximately 25% of the TRIF$^{-/-}$ mice died after infection with 10^2 PFU of PV, and almost all of the mice died after infection with more than 10^3 PFU of PV (Fig. 9A). Approximately 20% and 60% of the MyD88$^{-/-}$ mice died after infection with 10^3 and 10^4 PFU of PV, respectively (Fig. 9B and C). TRIF$^{-/-}$ MyD88$^{-/-}$ mice were the most susceptible. In total, 70% of the mice died after infection with 10^2 PFU of PV (Fig. 9A). The mortality rate of TRIF$^{-/-}$ MyD88$^{-/-}$ mice was very close to that of IFNAR1$^{-/-}$ mice (19). The mortality rate of TLR3$^{-/-}$ mice was similar to that of TRIF$^{-/-}$ mice (Fig. 9D, E, and F). These results suggest that the TRIF-mediated and MyD88-mediated antiviral responses contribute to the host's defense against PV infection and that the TLR3-TRIF-mediated response has the most dominant effect.

DISCUSSION

Each virus infects different cell types and has a characteristic mode of replication. In mammalian hosts, several viral RNA sensors,

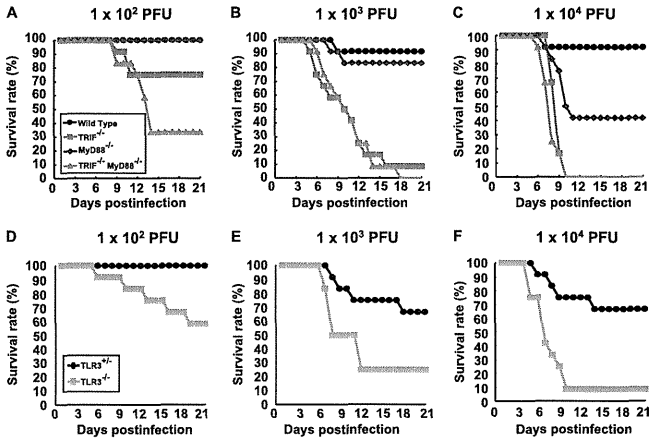

FIG 9 Mortality rates of TRIF-, MyD88-, and TLR3-deficient mice. (A) Wild-type, TRIF$^{-/-}$, MyD88$^{-/-}$, and TRIF$^{-/-}$ MyD88$^{-/-}$ mice ($n = 12$) were intravenously inoculated with the indicated doses of PV. (B) Littermates of TLR3$^{+/-}$ and TLR3$^{-/-}$ mice ($n = 12$) were used.

which are expressed in different cell types and recognize different molecular patterns, have evolved to counteract a variety of viruses. In the present study, we demonstrated that the MDA5-, TRIF-, and MyD88-mediated pathways contribute to the recognition of PV infection and that the TLR3-TRIF-mediated pathway plays the most important role in the antiviral response. Since all of the phenotypes shown after PV infection in the TRIF$^{-/-}$ mice and TLR3$^{-/-}$ mice are very similar to each other, we think that the contribution of the TLR3-mediated response is dominant and that of the TLR4-mediated response is negligible.

Previous reports have revealed that IFN is produced efficiently in EMCV-infected fibroblasts in an MDA5-dependent manner and that MDA5 contributes to the induction of serum IFNs and the protection of mice against EMCV (10, 23). Because EMCV belongs to the family *Picornaviridae*, we hypothesized that MDA5 also contributes to IFN induction in response to PV infection. However, the MDA5-dependent pathway did not play a dominant role in the defense against PV infection. Therefore, we speculate that PV uses mechanisms different from those of EMCV to strongly suppress IFN production *in vivo*. Indeed, IFN production in cultured cells in response to PV infection was observed only when the cells were pretreated with a low dose of IFNs. In addition, the amount of IFN produced was much lower than that produced in response to EMCV infection (Fig. 1). This result suggests that IFN induction in infected cells is suppressed and that this PV-mediated effect may be stronger than that of EMCV. Translational shutoff may be one of the reasons for this difference. PV 3A protein causes a change in membrane trafficking that prevents protein secretion and may also contribute to the suppression of IFN production (6). Caspase-dependent cleavage of MDA5 (3) and IPS-1 (39) in PV-infected cells has been reported. Through these possible mechanisms, PV may induce the suppression of IFN production in mice *in vivo*, and the MDA5-mediated pathway does not play an essential role in the host response, unlike in EMCV infection. PV and EMCV seemed to use different strategies to counteract the host innate immune system, even though PV and EMCV belong to the same family. Thus, TLR3 became the sensor that functions most effectively for PV as a result of PV evolution. Although the TLR3-TRIF-mediated pathway plays a dominant role, the fact that significant ISG induction was observed in PV-infected TRIF$^{-/-}$ and TRIF$^{-/-}$ MyD88$^{-/-}$ mice (Fig. 7) suggested that other mechanisms also operate in combination with this pathway.

The viral loads in the nonneural tissues of TLR3- and TRIF-deficient mice were much higher than those in wild-type mice, whereas the viral loads in the CNS were not significantly different in paralyzed mice (Fig. 8). These results suggest that the TLR3-TRIF-mediated pathway inhibits viral replication mainly before viral invasion of the CNS rather than after invasion and that this response plays an important role in preventing the viral invasion of the CNS. In the CNS, replication of PV was not effectively inhibited, even in wild-type mice. This result is consistent with our previous results obtained using IFNAR1$^{-/-}$ mice and suggests that the antivirus response in the CNS is different from that in nonneural tissues upon PV infection (19). The cell tropism of PV may influence the efficiency of the immune response. For example, if PVR is expressed in TLR3-expressing cells, then PV replication would be detected immediately after infection. Alternatively, if PV infection *in vivo* occurs in the vicinity of TLR3-expressing immune cells such as DCs and macrophages, PV-infected cells may readily be captured by TLR3-expressing cells, thereby facilitating efficient cross-priming (27, 44) of PV RNA. PV infects neurons almost exclusively and not other cell types in the CNS. If neurons do not have the ability to induce a strong TLR3-mediated antiviral response upon PV infection, the CNS may be more defective in the innate immune response than nonneural tissues are. This may be one of the reasons why PV replicates preferentially in the CNS. Further studies on PV pathogenesis related to the innate

immune response will make a great contribution to elucidating the mechanisms of PV tissue tropism.

TLR3 recognizes dsRNA. However, the protective role of TLR3 in the response to many RNA viral infections is not clear (9, 29, 43). A previous study has demonstrated that WNV, which is an encephalitis virus belonging to the family *Flaviviridae*, causes more severe encephalitis in mice with intact TLR3 than in TLR3$^{-/-}$ mice. Peripheral WNV infection leads to a breakdown of the blood-brain barrier (BBB) and enhances brain infection in wild-type mice but not in TLR3$^{-/-}$ mice (50). In contrast, a protective role of the TLR3-mediated pathway in PV infection was clearly demonstrated in the present study. PV enters the CNS directly across the BBB via a PVR-independent mechanism (52) and from the neuromuscular junction via retrograde axonal transport (31–33). Because PV originally possesses two entry pathways into the CNS, the generation of a new entry pathway, even if it did occur, might not increase its deteriorative effect.

Interestingly, protective roles of the TLR3-mediated pathway have been reported for group B coxsackievirus (30, 41, 42), human rhinovirus (49), and EMCV (11) infections. Riad et al. (41) demonstrated that TRIF$^{-/-}$ mice showed severe myocarditis after CVB3 infection and IFN-β treatment improved virus control and reduced cardiac inflammation. Richer et al. (42) reported that TLR3$^{-/-}$ mice produced reduced proinflammatory mediators and were unable to control CVB4 replication at the early stages of infection, resulting in severe cardiac damage. They also showed that adoptive transfer of wild-type macrophages into TLR3$^{-/-}$ mice challenged with CVB4 resulted in greater survival, suggesting the importance of the TLR3-mediated pathway in the macrophage. Negishi et al. (30) reported that TLR3$^{-/-}$ mice showed vulnerability to CVB3 and that TLR3 signaling is linked to the activation of the type II IFN system. Since CVB3 does not induce robust type I IFNs, they suggested that the TLR3 type II IFN pathway serves as an "ace in the hole" in infections with such viruses. PV is similar to CVB3 because type I IFN production is low. However, in our preliminary experiments on PV infection in IFN-$\gamma^{-/-}$ PVR-tg mice, type II IFN did not make a significant contribution to the pathogenesis of PV. Taken together, these results suggest a critical role for the TLR3-mediated pathway, but the precise mechanisms leading to host protection are still controversial and the downstream events of TLR3 signaling after picornavirus infection remain to be elucidated.

Because the above-mentioned viruses are picornaviruses, picornavirus RNA may be easily detected by TLR3. There may be a common RNA structure in the genome or in the replication intermediates of these viruses that is detected by TLR3. Alternatively, picornaviral RNA may replicate in a compartment in which TLR3 can easily access the replicating dsRNA. To investigate these hypotheses, identification of the cells responsible for IFN production is an important step. Oshiumi et al. demonstrated that splenic CD8α^+ CD11c$^+$ cells, bone marrow-derived macrophages, and DCs are able to elicit IFN in response to PV infection (35). Further studies using this virus-cell system will elucidate the molecular recognition pattern in the PV genome, the precise mechanism of PV RNA recognition in TLR3-expressing cells, and the roles of these cells in the prevention of PV dissemination in the body.

ACKNOWLEDGMENTS

We thank Takashi Fujita, Mitsutoshi Yoneyama, Hiroki Kato, Masahiro Yamamoto, Satoshi Uematsu, Seiya Yamayoshi, Akira Ainai, Hideki Hasegawa, and Takashi Kawanishi for helpful discussions and technical assistance.

This work was supported, in part, by Grants-in-Aid from the Ministry of Education, Culture, Sports, Science and Technology, Japan (Grants-in-Aid for Scientific Research on Priority Areas no. 21022053), and Grants-in-Aid for Research on Emerging and Re-emerging Infectious Diseases from the Ministry of Health, Labor and Welfare, Japan.

REFERENCES

1. **Akira S, Uematsu S, Takeuchi O.** 2006. Pathogen recognition and innate immunity. Cell **124**:783–801.
2. **Alexopoulou L, Holt AC, Medzhitov R, Flavell RA.** 2001. Recognition of double-stranded RNA and activation of NF-kappaB by Toll-like receptor 3. Nature **413**:732–738.
3. **Barral PM, et al.** 2007. MDA-5 is cleaved in poliovirus-infected cells. J. Virol. **81**:3677–3684.
4. **Bodian D.** 1959. Poliomyelitis: pathogenesis and histopathology, p 479–518. *In* Rivers TM, Horsfall FL, Jr (ed), Viral and rickettsial infections of man, vol 3. J. B. Lippincott, Philadelphia, PA.
5. **Cella M, et al.** 1999. Plasmacytoid monocytes migrate to inflamed lymph nodes and produce large amounts of type I interferon. Nat. Med. **5**:919–923.
6. **Choe SS, Dodd DA, Kirkegaard K.** 2005. Inhibition of cellular protein secretion by picornaviral 3A proteins. Virology **337**:18–29.
7. **Colonna M, Trinchieri G, Liu YJ.** 2004. Plasmacytoid dendritic cells in immunity. Nat. Immunol. **5**:1219–1226.
8. **Diebold SS, Kaisho T, Hemmi H, Akira S, Reis e Sousa C.** 2004. Innate antiviral responses by means of TLR7-mediated recognition of single-stranded RNA. Science **303**:1529–1531.
9. **Edelmann KH, et al.** 2004. Does Toll-like receptor 3 play a biological role in virus infections? Virology **322**:231–238.
10. **Gitlin L, et al.** 2006. Essential role of mda-5 in type I IFN responses to polyriboinosinic:polyribocytidylic acid and encephalomyocarditis picornavirus. Proc. Natl. Acad. Sci. U. S. A. **103**:8459–8464.
11. **Hardarson HS, et al.** 2007. Toll-like receptor 3 is an essential component of the innate stress response in virus-induced cardiac injury. Am. J. Physiol. Heart Circ. Physiol. **292**:H251–H258.
12. **Hemmi H, et al.** 2002. Small anti-viral compounds activate immune cells via the TLR7 MyD88-dependent signaling pathway. Nat. Immunol. **3**:196–200.
13. **Hoebe K, et al.** 2003. Identification of Lps2 as a key transducer of MyD88-independent TIR signalling. Nature **424**:743–748.
14. **Holland JJ.** 1961. Receptor affinities as major determinants of enterovirus tissue tropisms in humans. Virology **15**:312–326.
15. **Holland JJ, Mc LL, Syverton JT.** 1959. Mammalian cell-virus relationship. III. Poliovirus production by non-primate cells exposed to poliovirus ribonucleic acid. Proc. Soc. Exp. Biol. Med. **100**:843–845.
16. **Holland JJ, McLaren LC, Syverton JT.** 1959. The mammalian cell-virus relationship. IV. Infection of naturally insusceptible cells with enterovirus ribonucleic acid. J. Exp. Med. **110**:65–80.
17. **Hornung V, et al.** 2006. 5′-Triphosphate RNA is the ligand for RIG-I. Science **314**:994–997.
18. **Hsiung GD, Black FL, Henderson JR.** 1964. Susceptibility of primates to viruses in relation to taxonomic classification, p 1–23. *In* Buettner-Jaenusch J (ed), Evolutionary and genetic biology of primates, vol 2. Academic Press, New York, NY.
19. **Ida-Hosonuma M, et al.** 2005. The alpha/beta interferon response controls tissue tropism and pathogenicity of poliovirus. J. Virol. **79**:4460–4469.
20. **Ida-Hosonuma M, et al.** 2003. Host range of poliovirus is restricted to simians because of a rapid sequence change of the poliovirus receptor gene during evolution. Arch. Virol. **148**:29–44.
21. **Kato H, et al.** 2005. Cell type-specific involvement of RIG-I in antiviral response. Immunity **23**:19–28.
22. **Kato H, et al.** 2008. Length-dependent recognition of double-stranded ribonucleic acids by retinoic acid-inducible gene-I and melanoma differentiation-associated gene 5. J. Exp. Med. **205**:1601–1610.
23. **Kato H, et al.** 2006. Differential roles of MDA5 and RIG-I helicases in the recognition of RNA viruses. Nature **441**:101–105.
24. **Koike S, et al.** 1992. A second gene for the African green monkey poliovirus receptor that has no putative N-glycosylation site in the functional N-terminal immunoglobulin-like domain. J. Virol. **66**:7059–7066.
25. **Koike S, Nomoto A.** 2010. Poliomyelitis, p 339–351. *In* Ehrenfeld E, Domingo E, Roos RP (ed), The picornaviruses. ASM Press, Washington, DC.
26. **Koike S, et al.** 1991. Transgenic mice susceptible to poliovirus. Proc. Natl. Acad. Sci. U. S. A. **88**:951–955.
27. **Kramer M, et al.** 2008. Phagocytosis of picornavirus-infected cells induces an RNA-dependent antiviral state in human dendritic cells. J. Virol. **82**:2930–2937.
28. **Matsumoto M, et al.** 2003. Subcellular localization of Toll-like receptor 3 in human dendritic cells. J. Immunol. **171**:3154–3162.
29. **Matsumoto M, Oshiumi H, Seya T.** 2011. Antiviral responses induced by the TLR3 pathway. Rev. Med. Virol. **21**:67–77.
30. **Negishi H, et al.** 2008. A critical link between Toll-like receptor 3 and type II interferon signaling pathways in antiviral innate immunity. Proc. Natl. Acad. Sci. U. S. A. **105**:20446–20451.
31. **Ohka S, et al.** 2004. Receptor (CD155)-dependent endocytosis of poliovirus and retrograde axonal transport of the endosome. J. Virol. **78**:7186–7198.
32. **Ohka S, et al.** 2009. Receptor-dependent and -independent axonal retrograde transport of poliovirus in motor neurons. J. Virol. **83**:4995–5004.
33. **Ohka S, Yang WX, Terada E, Iwasaki K, Nomoto A.** 1998. Retrograde transport of intact poliovirus through the axon via the fast transport system. Virology **250**:67–75.
34. **Oshiumi H, Matsumoto M, Funami K, Akazawa T, Seya T.** 2003. TICAM-1, an adaptor molecule that participates in Toll-like receptor 3-mediated interferon-beta induction. Nat. Immunol. **4**:161–167.
35. **Oshiumi H, et al.** 12 October 2011, posting date. The TLR3-TICAM-1 pathway is mandatory for innate immune responses to poliovirus infection. J. Immunol. [Epub ahead of print.] doi:10.4049/jimmunol.1101503.
36. **Pichlmair A, et al.** 2006. RIG-I-mediated antiviral responses to single-stranded RNA bearing 5′-phosphates. Science **314**:997–1001.
37. **Pichlmair A, et al.** 2009. Activation of MDA5 requires higher-order RNA structures generated during virus infection. J. Virol. **83**:10761–10769.
38. **Racaniello VR.** 2007. Picornaviridae: the viruses and their replication, p 795–838. *In* Knipe DM, Howley PM (ed), Fields virology, 5th ed. Lippincott Williams & Wilkins, Philadelphia, PA.
39. **Rebsamen M, Meylan E, Curran J, Tschopp J.** 2008. The antiviral adaptor proteins Cardif and Trif are processed and inactivated by caspases. Cell Death Differ. **15**:1804–1811.
40. **Ren RB, Costantini F, Gorgacz EJ, Lee JJ, Racaniello VR.** 1990. Transgenic mice expressing a human poliovirus receptor: a new model for poliomyelitis. Cell **63**:353–362.
41. **Riad A, et al.** 2011. TRIF is a critical survival factor in viral cardiomyopathy. J. Immunol. **186**:2561–2570.
42. **Richer MJ, Lavallee DJ, Shanina I, Horwitz MS.** 2009. Toll-like receptor 3 signaling on macrophages is required for survival following coxsackievirus B4 infection. PLoS One **4**:e4127.
43. **Schröder M, Bowie AG.** 2005. TLR3 in antiviral immunity: key player or bystander? Trends Immunol. **26**:462–468.
44. **Schulz O, et al.** 2005. Toll-like receptor 3 promotes cross-priming to virus-infected cells. Nature **433**:887–892.
45. **Shiroki K, et al.** 1995. A new *cis*-acting element for RNA replication within the 5′ noncoding region of poliovirus type 1 RNA. J. Virol. **69**:6825–6832.
46. **Takeuchi O, Akira S.** 2009. Innate immunity to virus infection. Immunol. Rev. **227**:75–86.
47. **Takeuchi O, Akira S.** 2008. MDA5/RIG-I and virus recognition. Curr. Opin. Immunol. **20**:17–22.
48. **Takeuchi O, Akira S.** 2007. Recognition of viruses by innate immunity. Immunol. Rev. **220**:214–224.
49. **Wang Q, et al.** 2009. Role of double-stranded RNA pattern recognition receptors in rhinovirus-induced airway epithelial cell responses. J. Immunol. **183**:6989–6997.
50. **Wang T, et al.** 2004. Toll-like receptor 3 mediates West Nile virus entry into the brain causing lethal encephalitis. Nat. Med. **10**:1366–1373.
51. **Yamamoto M, et al.** 2003. Role of adaptor TRIF in the MyD88-independent Toll-like receptor signaling pathway. Science **301**:640–643.
52. **Yang WX, et al.** 1997. Efficient delivery of circulating poliovirus to the central nervous system independently of poliovirus receptor. Virology **229**:421–428.
53. **Yoneyama M, et al.** 2004. The RNA helicase RIG-I has an essential function in double-stranded RNA-induced innate antiviral responses. Nat. Immunol. **5**:730–737.
54. **Yoshikawa T, et al.** 2006. Role of the alpha/beta interferon response in the acquisition of susceptibility to poliovirus by kidney cells in culture. J. Virol. **80**:4313–4325.
55. **Yousefi S, Escobar MR, Gouldin CW.** 1985. A practical cytopathic effect/dye-uptake interferon assay for routine use in the clinical laboratory. Am. J. Clin. Pathol. **83**:735–740.

Contents lists available at SciVerse ScienceDirect

Virus Research

journal homepage: www.elsevier.com/locate/virusres

Identification of host genes showing differential expression profiles with cell-based long-term replication of hepatitis C virus RNA

Hiroe Sejima, Kyoko Mori, Yasuo Ariumi [1], Masanori Ikeda, Nobuyuki Kato*

Department of Tumor Virology, Okayama University Graduate School of Medicine, Dentistry, and Pharmaceutical Sciences, 2-5-1, Shikata-cho, Okayama 700-8558, Japan

ARTICLE INFO

Article history:
Received 5 February 2012
Received in revised form 18 April 2012
Accepted 19 April 2012
Available online 1 May 2012

Keywords:
HCV
HCV RNA replication system
Li23 cells
Long-term RNA replication
Upregulated host genes
Downregulated host genes

ABSTRACT

Persistent hepatitis C virus (HCV) infection frequently causes hepatocellular carcinoma. However, the mechanisms of HCV-associated hepatocarcinogenesis and disease progression are unclear. Although the human hepatoma cell line, HuH-7, has been widely used as the only cell culture system for robust HCV replication, we recently developed new human hepatoma Li23 cell line-derived OL, OL8, OL11, and OL14 cells, in which genome-length HCV RNA (O strain of genotype 1b) efficiently replicates. OL, OL8, OL11, and OL14 cells were cultured for more than 2 years. We prepared cured cells from OL8 and OL11 cells by interferon-γ treatment. The cured cells were also cultured for more than 2 years. cDNA microarray and RT-PCR analyses were performed using total RNAs prepared from these cells. We first selected several hundred highly or moderately expressed probes, the expression levels of which were upregulated or downregulated at ratios of more than 2 or less than 0.5 in each set of compared cells (e.g., parent OL8 cells versus OL8 cells cultured for 2 years). From among these probes, we next selected those whose expression levels commonly changed during a 2-year culture of genome-length HCV RNA-replicating cells, but which did not change during a 2-year culture period in cured cells. We further examined the expression levels of the selected candidate genes by RT-PCR analysis using additional specimens from the cells cultured for 3.5 years. Reproducibility of the RT-PCR analysis using specimens from recultured cells was also confirmed. Finally, we identified 5 upregulated genes and 4 downregulated genes, the expression levels of which were irreversibly altered during 3.5-year replication of HCV RNA. These genes may play roles in the optimization of the environment in HCV RNA replication, or may play key roles in the progression of HCV-associated hepatic diseases.

1. Introduction

Hepatitis C virus (HCV) is a causative agent of chronic hepatitis, which progresses to liver cirrhosis and hepatocellular carcinoma (HCC) (Choo et al., 1989; Saito et al., 1990; Thomas, 2000). However, the mechanisms of HCV-associated hepatocarcinogenesis and disease progression are still unclear. HCV is an enveloped virus with a positive single-stranded 9.6 kb RNA genome, which encodes a large polyprotein precursor of approximately 3000 amino acid residues. This polyprotein is cleaved by a combination of the host and viral proteases into at least 10 proteins in the following order: Core, envelope 1 (E1), E2, p7, nonstructural protein 2 (NS2), NS3, NS4A, NS4B, NS5A, and NS5B (Hijikata et al., 1991, 1993; Kato et al., 1990).

The initial development of a cell culture-based replicon system (Lohmann et al., 1999) and a genome-length HCV RNA-replication system (Ikeda et al., 2002) using genotype 1b strains enabled the rapid progression of investigations into the mechanisms underlying HCV replication (Bartenschlager, 2005; Lindenbach and Rice, 2005). Furthermore, these RNA replication systems have been improved such that they have become suitable for the screening of anti-HCV reagents by the introduction of reporter genes such as luciferase (Ikeda et al., 2005; Krieger et al., 2001). Moreover, in 2005, an efficient virus production system using the JFH1 genotype 2a strain was developed using human hepatoma cell line HuH-7-derived cells (Wakita et al., 2005). However, to date, HuH-7-derived cells are used as the only cell culture system for robust HCV replication (Bartenschlager and Sparacio, 2007; Lindenbach and Rice, 2005). Most studies of HCV replication or anti-HCV reagents are currently carried out using a HuH-7-derived cell culture system. Therefore, it remains unclear whether or not recent advances obtained from the HuH-7-derived cell culture system reflect the general features of HCV replication or anti-HCV targets. To resolve this issue, we aimed to find a cell line other than HuH-7 that enables robust HCV replication. We recently found a new human hepatoma cell line, Li23, that enables efficient HCV RNA replication and persistent HCV production (Kato et al., 2009b). In that study, we established genome-length HCV RNA replicating cell lines, OL (polyclonal; a mixture of approximately 200 clones), OL8 (monoclonal), OL11 (monoclonal), and OL14 (monoclonal), and characterized them (Kato et al., 2009b). We further developed Li23-derived drug assay systems (ORL8 and ORL11) (Kato et al., 2009b), which are relevant to the HuH-7-derived OR6 assay system (Ikeda et al., 2005). Since we demonstrated that the gene expression profile of Li23 cells was distinct from that of HuH-7 cells (Mori et al., 2010), we expected to find that the host factors required for HCV replication or anti-HCV targets in Li23-derived cells would also be distinct from those in HuH-7-derived cells. Indeed, we found that treatment of the cells with approximately 10 μM (a clinically achievable concentration) of ribavirin, an anti-HCV drug, efficiently inhibited HCV RNA replication in both the Li23-derived ORL8 and ORL11 assay systems, but not in the HuH-7-derived OR6 assay system (Mori et al., 2011). We further demonstrated that more than half of the 26 anti-HCV reagents that have been reported by other groups as anti-HCV candidates using HuH-7-derived assay systems other than OR6 assay system exhibited different anti-HCV activities from those of the previous studies (Ueda et al., 2011). In addition, we observed that the anti-HCV activities evaluated by the OR6 and ORL8 assay systems were also frequently different (Ueda et al., 2011). Furthermore, Li23-derived cells showed epidermal growth factor (EGF)-dependent growth (Kato et al., 2009b)-like immortalized or primary hepatocyte cells (e.g., PH5CH8 (Ikeda et al., 1998)), whereas HuH-7-derived cells can grow in an EGF-independent manner. Our findings, when taken together, suggested that a study using Li23-derived cells might yield unexpected results, since only HuH-7-derived cells are commonly used in a wide range of HCV studies.

Moreover, our findings to date suggested that the long-term replication of HCV RNA may cause irreversible changes in the gene expression profiles of host cells, yielding an environment for facilitative viral replication or progression of a malignant phenotype. To investigate this possibility, we carried out cDNA microarray and/or reverse transcription-polymerase chain reaction (RT-PCR) analyses using Li23-derived cells (OL, OL8, OL11, and OL14) in order to identify host genes for which expression levels were irreversibly altered by the long-term replication of HCV RNA. Here we report the identification of such host genes.

2. Materials and methods

2.1. Cell culture

The Li23 cell line consists of human hepatoma cells from a Japanese male (age 56) was established and characterized in 2009 (Kato et al., 2009b). Li23 cells were maintained in modified culture medium for the PH5CH8 human immortalized hepatocyte cell line (Ikeda et al., 1998), as described previously (Kato et al., 2009b). Genome-length HCV RNA-replicating cells (Li23-derived OL, OL8, OL11, and OL14 cells) were also maintained in the medium for the Li23 cells in the presence of 0.3 mg/mL of G418 (Geneticin, Invitrogen, Carlsbad, CA). Cured cells (OL8c and OL11c cells), from which the HCV RNA had been eliminated by interferon (IFN)-γ treatment (Abe et al., 2007), were cultured in the medium for the Li23 cells. These cells were passaged every 7 days for 3.5 years. In this study, OL, OL8, OL11, OL14, OL8c, and OL11c cells were renamed as OL(0Y), OL8(0Y), OL11(0Y), OL14(0Y), OL8c(0Y), and OL11c(0Y) cells, respectively, to specify the time at which the cells were established. These "0Y" cells of passage number 3 were used in this study. Two-year cultures of OL(0Y), OL8(0Y), OL11(0Y), OL14(0Y), OL8c(0Y), and OL11c(0Y) cells were designated as OL(2Y), OL8(2Y), OL11(2Y), OL14(2Y), OL8c(2Y), and OL11c(2Y) cells, respectively. The 3.5-year cultures of OL8(0Y), OL11(0Y), OL8c(0Y), and OL11c(0Y) cells were designated as OL8(3.5Y), OL11(3.5Y), OL8c(3.5Y), and OL11c(3.5Y) cells, respectively. The cured cells obtained from OL8(2Y) and OL11(2Y) cells by IFN-γ treatment (Abe et al., 2007) were designated as OL8(2Y)c and OL11(2Y)c cells, respectively, and were maintained in the medium for the Li23 cells.

2.2. cDNA microarray analysis

OL(0Y), OL(2Y), OL8(0Y), OL8(2Y), OL11(0Y), OL11(2Y), OL8c(0Y), OL8c(2Y), OL11c(0Y), and OL11c(2Y) cells were cultured in the medium without G418 during a few passages, and then these cells (1×10^6 each) were plated onto 10-cm diameter dishes and cultured for 2 or 3 days. Total RNAs from these cells (approximately 70–80% confluency) were prepared using the RNeasy extraction kit (QIAGEN, Hilden, Germany). As previously described (Kato et al., 2009b; Mori et al., 2010), cDNA microarray analysis was performed by Dragon Genomics Center of Takara Bio. (Otsu, Japan) through an authorized Affymetrix service provider using the GeneChip Human Genome U133 Plus 2.0 Array. Differentially expressed genes were selected by comparing the arrays from the genome-length HCV RNA-replicating cells, and the selected genes were further compared with the arrays from the cured cells (see Fig. 2 for details).

2.3. RT-PCR

We performed RT-PCR in order to detect cellular mRNA as described previously (Dansako et al., 2003). Briefly, total RNA (2 μg) was reverse-transcribed with M-MLV reverse trascriptase (Invitrogen) using an oligo dT primer (Invitrogen) according to the manufacturer's protocol. One-tenth of the synthesized cDNA was used for the PCR. The primers arranged for this study are listed in Table 1.

2.4. Quantitative RT-PCR analysis

The quantitative RT-PCR analysis for HCV RNA was performed using a real-time LightCycler PCR (Roche Diagnostics, Basel, Switzerland) as described previously (Ikeda et al., 2005; Kato et al., 2009b). Quantitative RT-PCR analysis for the mRNAs of the selected genes was also performed using a real-time LightCycler PCR. The primer sets used in this study are listed in Table 1.

2.5. Western blot analysis

The preparation of cell lysates, sodium dodecyl sulfate–polyacrylamide gel electrophoresis, and immunoblotting analysis with a PVDF membrane were performed as previously described (Kato et al., 2003). The antibodies used for the O strain in this study were those against Core (CP9, CP11, and CP14 monoclonal antibodies [Institute of Immunology, Tokyo, Japan]; a polyclonal antibody [a generous gift from Dr. M. Kohara, Tokyo Metropolitan Institute of Medical Science]), E1 and NS5B (a generous gift from Dr. M. Kohara), and NS3 (Novocastra Laboratories, Newcastle upon Tyne, UK). β-Actin antibody (Sigma, St. Louis, MO)

Abbreviations: HCV, hepatitis C virus; HCC, hepatocellular carcinoma; E1, envelope 1; EGF, epidermal growth factor; RT-PCR, reverse transcription-polymerase chain reaction; IFN, interferon; ACSM3, acyl-CoA synthetase medium-chain family member 3; ANGPT1, angiopoietin 1; CDKN2C, cyclin-dependent kinase inhibitor 2C; PLA1A, phospholipase A1 member A; SEL1L3, Sel-1 suppressor of lin-12-like 3; SLC39A4, solute carrier family 39 member 4; TBC1D4, TBC1 domain family member 4; WISP3, WNT1 inducible signaling pathway protein 3; ANXA1, annexin A1; AREG, amphiregulin; BASP1, brain abundant, membrane attached signal protein 1; CIDEC, cell death activator CIDE-3; CPB2, carboxypeptidase B2; HSPA6, heat-shock 70 kDa protein B'; PI3, peptidase inhibitor 3; SLC1A3, solute carrier family 1 member 3; THSD4, thrombospondin type-1 domain-containing protein 4; ICAM-1, intercellular adhesion molecule-1; ALXR, ANXA1 receptor.

* Corresponding author. Tel.: +81 86 235 7385; fax: +81 86 235 7392.
E-mail address: nkato@md.okayama-u.ac.jp (N. Kato).
[1] Present address: Center For AIDS Research, Kumamoto University, Kumamoto 860-0811, Japan.

0168-1702/$ – see front matter © 2012 Elsevier B.V. All rights reserved.
http://dx.doi.org/10.1016/j.virusres.2012.04.008

Table 1
Primers used for RT-PCR analysis.

Gene (accession no.)	Direction	Nucleotide sequence (5′–3′)	Products (bp)	Gene (accession no.)	Direction	Nucleotide sequence (5′–3′)	Products (bp)
Acyl-CoA synthetase medium-chain family member 3 (*ACSM3*; NM_005622)	Forward	GCATTCAAGTTCTACCCAACCGAC	258	Brain abundant, membrane attached signal protein 1 (BASP1; NM_006317)	Forward	GGATGAATGCCAGCTTTCAGACAG	247
	Reverse	GGCTGCTGACAACAGCTGACTC			Reverse	ACTCGAACTGCAATGAACGCAGAC	
Angiopoietin 1 (ANGPT1; NM_001146)	Forward	ATACAACATCGTGAACATGGAAGTC	287	Cell death activator CIDE-3 (CIDEC; NM_022094)	Forward	GATCTCTACAAGCTCGAACCCACAG	265
	Reverse	CCGTCTAAGATCAGGCTCCTCTC			Reverse	GACAGGTCGGGATAAGGGATGAG	
Cyclin-dependent kinase inhibitor 2C (*CDKN2C*; NM_001262)	Forward	AACACCGAACTGGTTTCGCTGTC	246	Carboxypeptidase B2 (CPB2; NM_001872)	Forward	GCAACTGTCTCTAGTAGCCAGTG	242
	Reverse	CATAGAGCCTGGCCAAATCACAG			Reverse	CAGCCGCAAAAGCTTCTCTACAG	
Phospholipase A1 member A (*PLA1A*; NM_015900)	Forward	GGAGTTTCACTTGAAGGAACTGAG	292	Heat shock 70 kDa protein 8 (HSPA8; NM_002155)	Forward	TGAAGCCGAGCAGTACAAGGCTG	235
	Reverse	GTTCACTGGTTCAGGTAAGCAGAC			Reverse	CTCCCTCTTCGATGCTCATACTC	
Sel-1 suppressor of lin-12-like 3 (*SEL1L3*; NM_015187)	Forward	ACCTCGCACTTCGCGGCTTCTCTG	212	Peptidase inhibitor 3 (PI3; NM_002638)	Forward	GCTTCTACAGCGCAGCTGTCACG	276[a]
	Reverse	AGAGGCATCTCGCAGCTGGAGTC			Reverse	CCGCAACAGCCTTCACAGCAC	
Solute carrier family 39 member 4 (*SLC39A4*; NM_017767)	Forward	GCCTCGTTCCTCACGTAGCACTC	158	Peptidase inhibitor 3 (PI3; NM_002638)	Forward	GCTTCTACAGCGCAGCTGTCACG	241[b]
	Reverse	GAAGCGTGATCTCATCCTCCGTACAG			Reverse	GCAGTCAGTATCTTTCAAGCAGC	
TBC1 domain family member 4 (*TBC1D4*; NM_014832)	Forward	GGAGAGGGCCAATAGCCAACTG	198	Solute carrier family member 3 (SLC1A3; NM_004172)	Forward	CAATGGCGTGGACAAACCGCGTC	240
	Reverse	AGCTTCCGGAGTTGCTCCACTG			Reverse	CCGACAGATGTCAGCACAATGAC	
WNT1 inducible signaling pathway protein 3 (*WISP3*; NM_003880)	Forward	AGAGATGCTGTATCCCTAATAAGTC	129	Thrombospondin type-1 domain-containing protein 4 (THSD4; NM_024817)	Forward	TGGAGTCAGTGTTCCATCGAGTG	275
	Reverse	CAGGTTCCTCGCAGTTTCTCTGAC			Reverse	GCGTCACACAGCGTTACTTACAGCTC	
Annexin A1 (ANXA1; NM_000700)	Forward	GACTTGGCGTGATTCAGATGCCAG	192	Glyceraldehyde-3-phosphate dehydrogenase (GAPDH; NM_002046)	Forward	GACTCATCGACCACACTCCATCC	334
	Reverse	AATGTCACCTTTCAACTCCAGGTC			Reverse	GAGGAGACCACCTGGTGCTCAG	
Amphiregulin (*AREG*; NM_001657)	Forward	CGGGAGCCCGACTATGACTACTC	391				
	Reverse	AACGCCAGCTATCGCCTCCTAATGC					

[a] This primer set was used for RT-PCR analysis.
[b] This primer set was used for quantitative RT-PCR analysis.

was used as the control for the amount of protein loaded per lane. Immunocomplexes were detected by the Renaissance enhanced chemiluminescence assay (PerkinElmer Life Sciences, Boston, MA).

2.6. Statistical analysis

Statistical comparison of the mRNA levels between the various time points was performed using Student's *t*-test. *P* values of less than 0.05 were considered statistically significant.

3. Results

3.1. Efficient replication of genome-length HCV RNA is maintained in long-term cell culture

To prepare specimens for the cDNA microarray analysis, genome-length HCV RNA-replicating OL(0Y), OL8(0Y), OL11(0Y), and OL14(0Y) cells were cultured for 2 years, and were designated as OL(2Y), OL8(2Y), OL11(2Y), and OL14(2Y) cells, respectively. OL8c(0Y) and OL11c(0Y) cells were also cultured for 2 years, and were designated as OL8c(2Y) and OL11c(2Y) cells, respectively. We observed that the growth rates of all cell lines increased in a time-dependent manner, while the appreciable changes of cell shapes were not observed. The doubling time of genome-length HCV RNA-replicating cells (OL(0Y), OL8(0Y), OL11(0Y), and OL14(0Y)) and cured cells (OL8c(0Y) and OL11c(0Y)) was approximately 41 h and 32 h, respectively. After 2-year culture, these values reduced to approximately 28 h and 23 h.

Using the total RNA specimens obtained from genome-length HCV RNA-replicating cells, the levels of genome-length HCV RNAs were examined by quantitative RT-PCR analysis. The results revealed that the levels of the genome-length HCV RNAs had increased in all cases after a 2-year period of HCV RNA replication (Fig. 1). The levels of HCV proteins (Core, E1, NS3, and NS5B) were also examined by Western blot analysis. The E1, NS3, and NS5B were detected in all specimens, except for the Li23 cells, although a little larger size of E1 was additionally detected in the specimens from 2-year culture (Fig. 1). This phenomenon may indicate the appearance of additional N-glycosylation sites by mutations caused during the 2-year replication of the HCV RNA, as observed in a previous report (Mori et al., 2008). However, genetic analysis of HCV RNAs from 2-year culture of OL8, OL11, and OL14 cell series has detected no additional N-glycosylation sites by mutations (Kato et al., unpublished results). Therefore, the mobility change of E1 may be due to the other modifications such as O-glycosylation. In addition, Core was not detected in the cultures of OL11(2Y) cells, even when polyclonal anti-Core antibody was used (Fig. 1). A similar phenomenon was observed in a previous study using HuH-7-derived genome-length HCV RNA-replicating cells (Kato et al., 2009a). In that study, we showed that the Core region was not deleted, but mutated at several positions within the epitopes of the anti-Core antibody (Kato et al., 2009a). The results of genetic analysis using Li23-derived cells as described above (Kato et al., unpublished results) were also similar with those in the previous study using HuH-7-derived cells (Kato et al., 2009a).

3.2. Selection of genes showing irreversible changes with long-term HCV RNA replication

To identify those genes whose expression levels were irreversibly altered by the long-term replication of HCV RNA, we performed a combination of cDNA microarray and RT-PCR analyses using several Li23-derived cell lines. An outline of the selection process performed in this study is provided in Fig. 2. The first microarray analysis I was carried out by the comparison of OL(0Y) cells versus OL(2Y) cells, OL8(0Y) cells versus OL8(2Y) cells, and

Fig. 1. Characterization of genome-length HCV RNA-replicating cells in long-term cell culture. The upper panel shows the results of a quantitative RT-PCR analysis of intracellular genome-length HCV RNA. Total RNAs from OL(0Y), OL8(0Y), OL11(0Y), and OL14(0Y) cells after 2 years [OL(2Y), OL8(2Y), OL11(2Y), and OL14(2Y)] in culture, as well as total RNAs from the parental OL(0Y), OL8(0Y), OL11(0Y), and OL14(0Y) cells were used for the analysis. Total RNA from Li23 cells was used as a negative control. The lower panel shows the results of the Western blot analysis. Cellular lysates from cells used for quantitative RT-PCR were also used for comparison. HCV Core, E1, NS3, and NS5B were detected by Western blot analysis. β-Actin was used as a control for the amount of protein loaded per lane. A single asterisk indicates that the anti-Core polyclonal antibody was used for detection. A double asterisk indicates that a mixture of three kinds (CP9, CP11, and CP14) of anti-Core monoclonal antibodies was used for detection.

OL11(0Y) cells versus OL11(2Y) cells. In this step, we selected those genes whose expression levels commonly showed changes in at least two of three comparative analyses to avoid the bias caused by the difference of cell clonality, since OL(0Y) was a polyclonal cell line, while OL8(0Y) and OL11(0Y) were monoclonal cell lines (Kato et al., 2009b). As regards the selected genes, a microarray analysis II was performed in which OL8c(0Y) cells were compared to OL8c(2Y) cells, and OL11c(0Y) cells were compared to OL11c(2Y) cells. In this step, the genes were excluded from those selected by the microarray analysis I if their expression levels had changed during the 2-year culture of cured cells. As regards the selected genes, we next performed a RT-PCR analysis I to examine the reproducibility of changes in gene expression levels. In this step, we added the results of a new comparative series, OL14(0Y) versus OL14(2Y), to arrive at the judgment to advance to the next step of analysis. We selected genes for which expression levels had changed in more than five of six comparative series (Fig. 2). At the last step, we confirmed by RT-PCR analysis II whether or not the expression levels of the selected genes in OL8(2Y) or OL11(2Y) cells had changed by HCV RNA replication. When the gene expression levels had not changed in two comparative series (OL8(2Y) versus OL8(2Y)c and OL11(2Y) versus OL11(2Y)c), the genes were selected as the candidates exhibiting irreversible changes after 2-year HCV RNA replication.

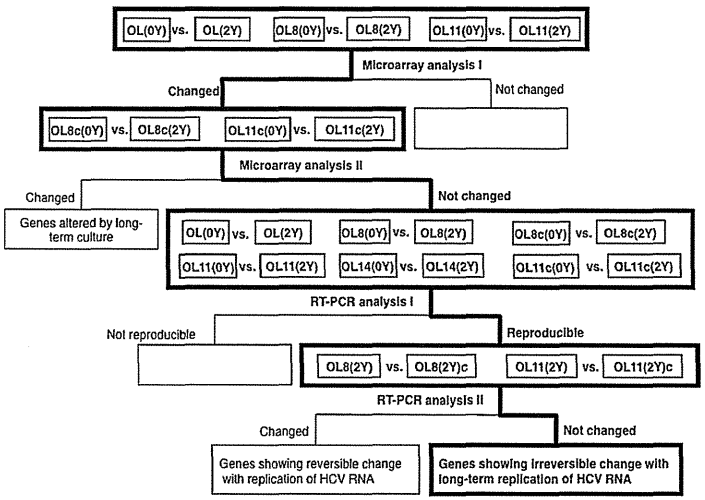

Fig. 2. Outline of selection process performed in this study. To obtain the objective genes, cDNA microarray analyses I and II were performed, and then RT-PCR analyses I and II were also performed.

3.3. Selection and expression profiles of genes showing upregulated expression during long-term HCV RNA replication

The process outlined in Fig. 2 was used to identify those genes that exhibited irreversibly upregulated expression during the 2-year replication of HCV RNA. Microarray analysis I revealed 1912, 1148, and 1633 probes, the expression levels of which were upregulated at a ratio of more than 2 in the case of OL(0Y) cells versus OL(2Y) cells, OL8(0Y) cells versus OL8(2Y) cells, and OL11(0Y) cells versus OL11(2Y) cells, respectively. To avoid the possibility that the genes showing low expression level are selected, the ratios and expression values were used in combination for the selection. As the minimum expression level, more than 100 (actual value of measurement), which was detectable within 30 cycles in RT-PCR analysis, was adopted. From among these probes, we selected those showing ratios of more than 4 with an expression level of more than 100, or those showing ratios of more than 3 with an expression level of more than 200, or those showing an expression level of 1000. By this selection process, 559, 237, and 368 genes (redundant probes excluded) were assigned in the case of OL(0Y) cells versus OL(2Y) cells, OL8(0Y) cells versus OL8(2Y) cells, and OL11(0Y) cells versus OL11(2Y) cells, respectively (Fig. 3A). At this step, we obtained 51 genes as candidates exhibiting upregulation in more than two of three comparisons. Based on the results of the subsequent microarray analysis II, we further selected 14 genes from a total of 51 genes, because the expression levels of the remaining 37 genes increased during the 2-year culture of cured cells (Fig. 3B). The list of these genes was shown in Supplemental Table 1. As regards the 14 selected genes, we performed an RT-PCR analysis I to confirm the results obtained by the cDNA microarray analysis and to examine the status of gene expression in an additional comparison of OL14(0Y) cells versus OL14(2Y) cells. This analysis revealed that the mRNA levels of 6 of 14 genes showed no enhancement in two of four comparative series (data not shown). Therefore, in this step, these 6 genes were excluded from the candidate genes. However, the mRNA levels of the remaining 8 genes (acyl-CoA synthetase medium-chain family member 3 [*ACSM3*], angiopoietin 1 [*ANGPT1*], cyclin-dependent kinase inhibitor 2C [*CDKN2C*], phospholipase A1 member A [*PLA1A*], Sel-1 suppressor of lin-12-like 3 [*SEL1L3*], solute carrier family 39 member 4 [*SLC39A4*], TBC1 domain family member 4 [*TBC1D4*], and WNT1 inducible signaling pathway protein 3 [*WISP3*]) were enhanced in more than three of four comparative series (Fig. 3C). Furthermore, we demonstrated by RT-PCR analysis II that the expression levels of these 8 genes did not return to initial levels, even after elimination of HCV RNA from OL8(2Y) or OL11(2Y) cells (Fig. 3C). It was noteworthy that the mRNA levels of the *ANGPT1* and *PLA1A* genes were enhanced in all comparative series (Fig. 3C).

3.4. Selection and expression profiles of genes showing downregulated expression during long-term HCV RNA replication

To obtain genes showing irreversibly downregulated expression during the 2-year HCV RNA replication period, we performed a selection of genes according to the methods described for the selection of upregulated genes. The first microarray analysis I in this series revealed 1901, 2128, and 1579 probes whose expression levels were downregulated at a ratio of less than 0.5 in the case of OL(0Y) cells versus OL(2Y) cells, OL8(0Y) cells versus OL8(2Y) cells, and OL11(0Y) cells versus OL11(2Y) cells, respectively. As described in Section 3.3, the ratios and expression values were used in combination for the selection. From among these probes, we selected those showing ratios of less than 0.25 with an initial expression level of more than 1000 (actual value of measurement), or those showing ratios of less than 0.33 with an initial expression level of more than 200, or those showing an initial expression level of 100. By this selection process, 828, 622, and 466 genes (redundant probes excluded) were assigned in the case of OL(0Y) cells versus OL(2Y) cells, OL8(0Y) cells versus OL8(2Y) cells, and OL11(0Y) cells versus OL11(2Y) cells, respectively (Fig. 4A). At this step, we obtained 236 genes as candidates showing downregulation in more than two of three comparisons. Based on the results

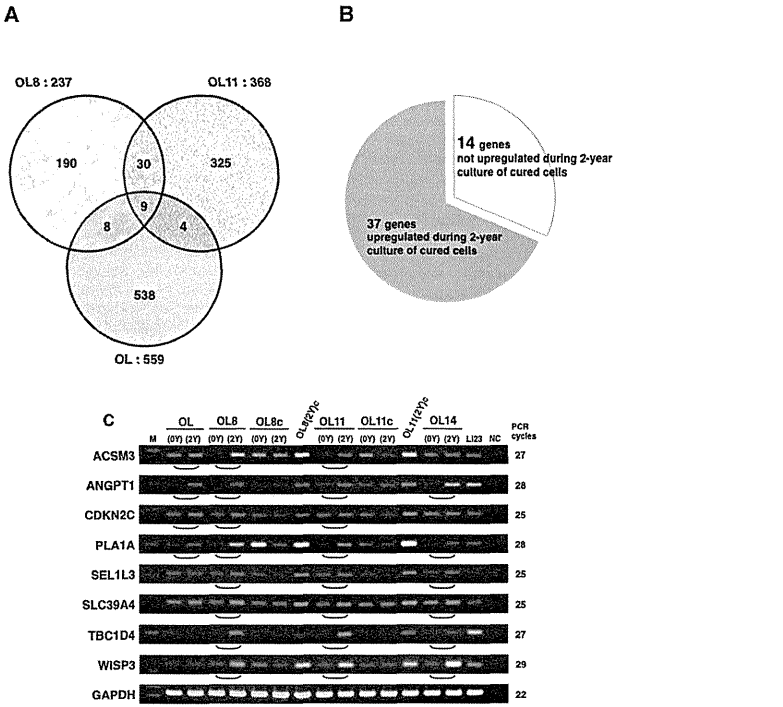

Fig. 3. Identification of genes irreversibly upregulated during 2-year replication of HCV RNA. (A) Upregulated genes obtained by microarray analysis I shown in Fig. 2. Genes whose expression levels were upregulated at ratios of more than 2 in the case of OL(0Y) versus OL(2Y) cells, OL8(0Y) versus OL8(2Y) cells, or OL11(0Y) versus OL11(2Y) cells were selected, and 51 genes upregulated in at least two of three comparisons were obtained. (B) Further selection by microarray analysis II, shown in Fig. 2. Genes whose expression levels were upregulated during 2-year culture (OL8c(2Y) or OL11c(2Y) cells) of the cured OL8c(0Y) or OL11c(0Y) cells were eliminated. (C) Expression profiles of upregulated genes. RT-PCR analyses I and II shown in Fig. 2 were performed as described in Section 2. PCR products were detected by staining with ethidium bromide after separation by electrophoresis on 3% agarose gels. The round parenthesis indicates the comparative series showing the upregulated expression.

of the second microarray analysis II, we were able to select 17 genes from a total of 236 genes, as the expression levels of most of the genes had decreased during the 2-year culture of cured cells (Fig. 4B). The list of these genes was shown in Supplemental Table 2. As regards the 17 selected genes, we performed an initial RT-PCR analysis I to confirm the results obtained by the microarray analysis I and to examine the status of gene expression by additional comparison of OL14(0Y) cells versus OL14(2Y) cells. This analysis revealed that the mRNA levels of 8 of 17 genes showed no suppression in more than two of four comparative series (data not shown). Therefore, these 8 genes were excluded from the candidate genes in this step. However, the mRNA levels of the remaining 9 genes (annexin A1 [*ANXA1*], amphiregulin [*AREG*], brain abundant, membrane attached signal protein 1 [*BASP1*], cell death activator CIDE-3 [*CIDEC*], carboxypeptidase B2 [*CPB2*], heat-shock 70 kDa protein B' [*HSPA6*], peptidase inhibitor 3 [*PI3*], solute carrier family 1 member 3 [*SLC1A3*], and thrombospondin type-1 domain-containing protein 4 [*THSD4*]) were suppressed in more than three of four comparative series (Fig. 4C). Furthermore, we demonstrated by RT-PCR analysis II that the expression levels of these 9 genes did not return to initial levels, even after the elimination of HCV RNA from OL8(2Y) or OL11(2Y) cells (Fig. 4C). It is noteworthy that the mRNA levels of *BASP1*, *CIDEC*, *HSPA6*, and *PI3* genes were suppressed in all comparative series (Fig. 4C).

3.5. Expression profiles of selected genes during 3.5-year replication of HCV RNA

As described above, we selected 8 upregulated genes and 9 downregulated genes, the expression levels of which had irreversibly changed after a 2-year period of HCV RNA replication. However, reproducibility of the RT-PCR analysis using total RNA specimens prepared from independent recultured cells would be needed or arriving at a reliable conclusion. Furthermore, in this context, it would also be important to clarify whether or not these irreversible changes in RNA expression levels remained stable or were further enhanced during HCV RNA replication if the cells were cultured for a period of more than 2 years. Since the OL8(2Y), OL8c(2Y), OL11(2Y), and OL11c(2Y) cells were continuously cultured for a period of up to 3.5 years, they were used as OL8(3.5Y), OL8c(3.5Y), OL11(3.5Y), and OL11c(3.5Y) cells with the recultured OL8(0Y), OL8(2Y), OL8c(0Y), OL8c(2Y), OL11(0Y),

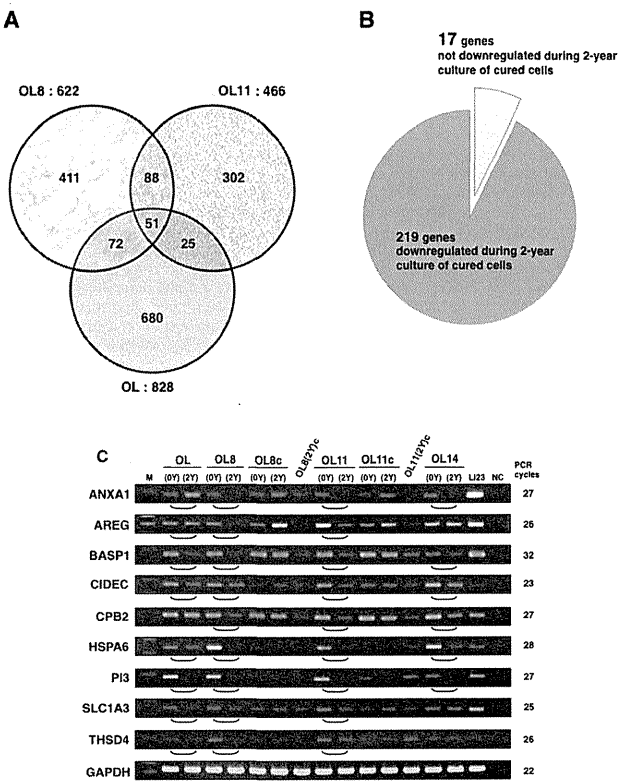

Fig. 4. Identification of genes irreversibly downregulated during 2-year replication of HCV RNA. (A) Downregulated genes obtained by microarray analysis I shown in Fig. 2. Genes were selected whose expression levels were downregulated at ratios of less than 0.5 in the case of OL(0Y) versus OL(2Y) cells, OL8(0Y) versus OL8(2Y) cells, and OL11(0Y) versus OL11(2Y) cells. A total of 236 genes were obtained that were downregulated in at least two of three comparisons. (B) Further selection by microarray analysis II shown in Fig. 2. Genes whose expression levels were downregulated during 2-year culture (OL8c(2Y) or OL11c(2Y)) of the cured OL8c(0Y) or OL11c(0Y) cells were eliminated. (C) Expression profiles of downregulated genes. RT-PCR analyses I and II, shown in Fig. 2, were performed as described in Fig. 3C. The round parenthesis indicates the comparative series showing the downregulated expression.

OL11(2Y), OL11c(0Y), and OL11c(2Y) cells, respectively, for the RT-PCR analysis in order to address the questions raised above. We first performed RT-PCR analysis of the genes indicated in Figs. 3C and 4C. The results revealed that most of the genes examined showed reproducible results, as shown in Figs. 3C and 4C (data not shown). However, no reproducible results were obtained regarding *ACSM3* selected as an upregulated gene and *HSPA6* selected as a downregulated gene (data not shown), suggesting that the mRNA levels of both genes were sensitively affected by the cell culture conditions (e.g., cell density). Regarding the remaining 7 upregulated and 8 downregulated genes, we next performed a quantitative RT-PCR analysis using the total RNA specimens prepared from OL8(0Y), OL8(2Y), OL8(3.5Y), OL11(0Y), OL11(2Y), OL11(3.5Y), OL8c(0Y), OL8c(2Y), OL8c(3.5Y), OL11c(0Y), OL11c(2Y), and OL11c(3.5Y) cells.

As regards the upregulated genes, statistically significant differences between their mRNA levels of HCV RNA-replicating cells and their cured counterparts during the culture for a period of up to 3.5 years were observed in the case of 5 genes (*WISP3*, *TBC1D4*, *ANGPT1*, *SEL1L3*, and *CDKN2C*) (Fig. 5). However, such a significant difference was not maintained for a period up to 3.5 years in the case of *PLA1A* gene (OL8(3.5Y) cells versus OL8c(3.5Y) cells) and *SLC39A4* gene (OL11(3.5Y) cells versus OL11c(3.5Y) cells) (Fig. 5). These results suggest that the upregulated expression of *PLA1A* or *SLC39A4* gene is not irreversible change by long-term replication of HCV RNA. A drastic difference between mRNA levels in HCV RNA-replicating cells versus cured cells was observed in the case of the genes *WISP3* and *TBC1D4* (Fig. 5).

As for the downregulated genes, the results revealed that 4 genes (*BASP1*, *CPB2*, *ANXA1*, and *SLC1A3*) showed statistically significant differences between their mRNA levels of HCV RNA-replicating cells and their cured counterparts during the culture for a period of up to 3.5 years (Fig. 6). However, such a significant difference was not continuously observed for a period up to 3.5 years in the case of 3 genes (*AREG*, *CIDEC*, and *THSD4*) (Fig. 6), although the expression levels (except for AREG in the OL11 series and CIDEC in the OL8 series) at 2 years in cell culture showed reproducible

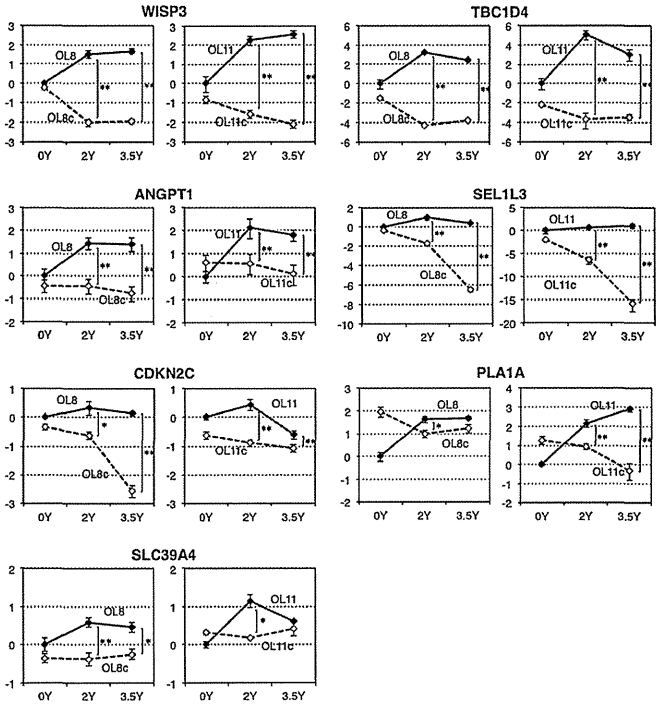

Fig. 5. Expression levels of genes selected as upregulated genes in 3.5-year cell culture. Quantitative RT-PCR analysis using the total RNAs derived from OL8(0Y), OL8(2Y), OL8(3.5Y), OL8c(0Y), OL8c(2Y), OL8c(3.5Y), OL11(0Y), OL11(2Y), OL11(3.5Y), OL11c(0Y), OL11c(2Y), and OL11c(3.5Y) cells was performed as described in Section 2. Experiments were done in triplicate. The vertical lines indicate the expression levels, with the fold in the scale of log 2, when the level in OL8(0Y) or OL11(0Y) cells was assigned to be 1. Asterisks indicate significant differences between mRNA levels of HCV RNA-replicating cells and their cured counterparts. $^{*}P < 0.05$; $^{**}P < 0.01$.

differences, as depicted in Fig. 4C. Quantitative RT-PCR analysis revealed that the expression levels of *PI3* gene drastically decreased during 3.5-year culture of cured cells, although *PI3* gene expression was very low level in cured cells (Fig. 6). These results suggest that the downregulated expression of *AREG*, *CIDEC*, *THSD4*, or *PI3* gene is not irreversible change by long-term replication of HCV RNA. The most drastic difference between mRNA levels of HCV RNA-replicating cells and their cured counterparts was observed in the case of the *BASP1* gene (Fig. 6).

4. Discussion

In this study, we performed cDNA microarray and RT-PCR analyses using genome-length HCV RNA-replicating Li23-derived cells cultured for 2 years after the cells had been established as cell lines, and we performed quantitative RT-PCR analyses using these cells and additional cells cultured for a period of up to 3.5 years. Consequently, we identified 5 genes (*WISP3*, *TBC1D4*, *ANGPT1*, *SEL1L3*, and *CDKN2C*) showing irreversible upregulated expression, and 4 genes (*BASP1*, *CPB2*, *ANXA1*, and *SLC1A3*) showing irreversible downregulated expression with the persistent 3.5-year replication of HCV RNA.

Two possibilities can be considered as plausible biological explanations for the irreversible changes in expression levels of these identified genes. First, it is possible that these genes play roles in the optimization of the environment in HCV RNA replication. Indeed, in the present study, we observed that the levels of HCV RNAs increased in all cases after constitutive HCV RNA replication of 2 years (Fig. 1). However, the expression levels of these genes did not differ between HCV RNA-replicating cells and the corresponding cured cells at the time at which the cells were first established (Figs. 5 and 6). Since, to date, no studies reported in the literature have demonstrated that these genes are required for HCV RNA replication or that the level of HCV RNA replication is regulated by these genes, further comparative analysis such as the quantification of HCV RNA levels in the cells forced to express these genes will be needed to clarify these points.

A second possible explanation for the observed irreversible changes would be that these genes play roles in the progression of HCV-associated hepatic diseases. We focused on this possibility, due to the number of reports in the literature regarding these genes.

Among the upregulated genes identified in this study, *WISP3* is most interesting. WISP3 is a Wnt1-inducible cysteine-rich protein (CCN6) that belongs to the CCN family. Previous studies have

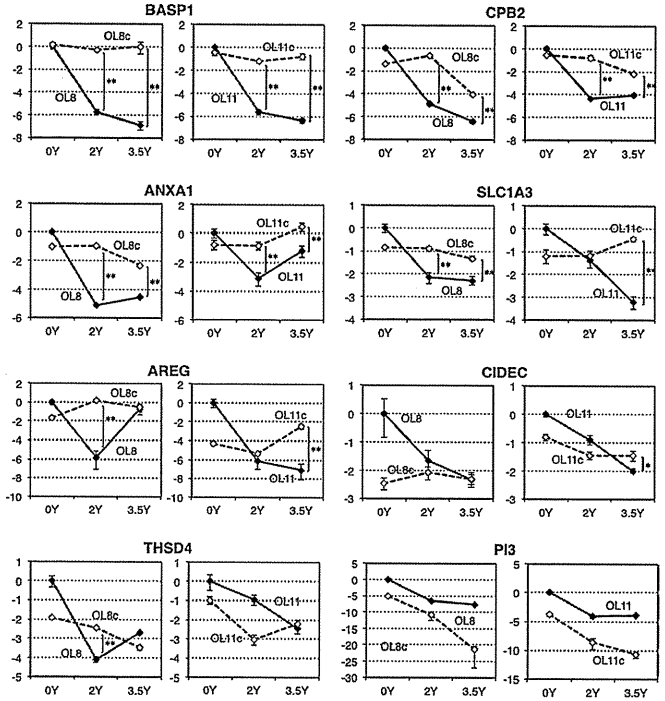

Fig. 6. Expression levels of genes selected as downregulated genes in 3.5-year cell culture. Quantitative RT-PCR analysis was performed as shown in Fig. 5, and the obtained results are also presented as shown in Fig. 5.

linked the overexpression of WISP3/CCN6 to colon cancer (Pennica et al., 1998; Thorstensen et al., 2001), suggesting that overexpression of this protein is associated with the development of this type of cancer. However, recent studies revealed that WISP3 exerts both tumor-growth and invasion-inhibitory functions in inflammatory breast cancer and aggressive non-inflammatory breast cancer (Huang et al., 2008, 2010). Although the role of WISP3 in the development of symptomatic cancer is controversial and unproven, enhancement of WISP3 expression in liver tissue may be involved in the progression of hepatic cancer. On the other hand, it was recently reported that WISP3 increased the migration and the expression of intercellular adhesion molecule-1 (ICAM-1) in human chondrosarcoma cells (Fong et al., 2012). Since ICAM-1 may facilitate the movement of cells through the extracellular matrix, ICAM-1 is expected to play an important role in cancer cell invasion and metastasis (Huang et al., 2004). Therefore, irreversible enhancement of WISP3 by long-term HCV RNA replication, as shown in this study, may be involved in tumor invasion or metastasis, i.e., the transition to the aggressive phenotype of human cancers. However, we could not confirm an enhancement of ICAM-1 expression in our microarray analysis. Therefore, further experiments will be necessary to clarify the biological significance of enhanced WISP3 expression by HCV.

TBC1D4 is also of interest as an enhanced gene during the long-term replication of HCV RNA. TBC1D4 was discovered as a substrate phosphorylated by insulin-activated serine–threonine kinase Akt (Kane et al., 2002). This protein, which was initially designated as AS160 (Akt substrate of 160 kDa), has a GTPase-activating protein (GAP) and shows GAP activity with Rab 2A, 8A, 10, and 14, which participate in the translocation of the GLUT4 glucose transporter from intracellular storage vesicles to the plasma membrane (Mïinea et al., 2005). Therefore, TBC1D4 functions as a Rab inhibitor in insulin-regulated GLUT4 trafficking (Rowland et al., 2011). Since we observed the enhancement of TBC1D4 expression in this study, we simply inferred that insulin-dependent glucose uptake might be suppressed in long-term cultured cells replicating HCV RNA. However, we found very low levels of expression of GLUT4 in the Li23-derived cells used in this study, suggesting that an enhancement of TBC1D4 may be involved in the trafficking of molecule(s) other than the GLUT4 transporter.

Among the downregulated genes identified in this study, three genes of interest showing altered expression levels were clearly identified by quantitative RT-PCR. The first of the three is *BASP1*, which was originally isolated as a membrane-bound phosphoprotein abundant in nerve terminals (Mosevitsky et al., 1997). Although the function of BASP1 in the nervous system is still unclear, it has been reported to be a transcriptional co-suppressor for Wilms' tumor suppressor protein WT1 (Carpenter et al., 2004). In addition, it has also been found that BASP1 can inhibit cellular transformation by the *v-Myc* oncogene, and can block the

regulation of Myc target genes (Hartl et al., 2009). These studies suggest that BASP1 probably acts as a tumor suppressor. Furthermore, it has been reported that BASP1 is suppressed by the methylation of the *BASP1* gene in a significant proportion of HCCs, and the suppression of this gene has been identified as a useful biomarker for the early diagnosis of HCC (Moribe et al., 2008; Tsunedomi et al., 2010). In this context, the suppression of BASP1 expression observed in this study may be due to the methylation of the *BASP1* gene. If so, this type of methylation would likely be induced during the long-term replication of HCV RNA, as the long-term culture of cured cells did not induce a suppression of BASP1 expression. To obtain additional information, we compared the mRNA levels of *BASP1* among HuH-7-derived HCV RNA-replicating O cells, those cells cultured for 2 years, and the corresponding cured cells (Ikeda et al., 2005; Kato et al., 2009a). The preliminary results revealed that the mRNA levels of *BASP1* in these cells were remarkably lower than those in the Li23-derived cells, and no significant differences were observed among the HuH-7-derived cells (data not shown). These results are consistent with the results in a previous report (Tsunedomi et al., 2010) describing hypermethylation of the *BASP1* gene in HuH-7 cells. However, we observed that the mRNA levels of *BASP1* in Li23-derived cells (e.g., OL8, OL11) were similar to those in the immortalized hepatocyte PH5CH8 and NKNT3 cell lines (Ikeda et al., 1998; Naka et al., 2006), suggesting that the methylation status of the *BASP1* gene in these cell lines is lower than that of HuH-7 cells. The results, taken together, led us to speculate that persistent HCV replication may induce the methylation of the *BASP1* gene, although no association of BASP1 suppression with the aggressive phenotype of HCC has been reported to date. To clarify this point, further analysis will be needed.

A second intriguing gene is *CPB2*, which is produced mainly by the liver and circulates in plasma as a plasminogen-bound zymogen. Thus far, it is known that CPB2 potently attenuates fibrinolysis by removing the fibrin C-terminal residues that are needed for the binding and activation of plasminogen (Redlitz et al., 1995). On the other hand, several proinflammatory mediators (e.g., C5a, osteopontin, and bradykinin) have been identified as substrates of CPB2 in vitro (Myles et al., 2003; Sharif et al., 2009). Therefore, it has been considered that CPB2 may serve an anti-inflammatory function. Indeed, a recent study demonstrated that CPB2 plays a central role in down-regulating C5a-mediated inflammatory responses in autoimmune arthritis in mice and humans (Song et al., 2011). These findings led to the hypothesis that the suppression of CPB2 in HCV-infected hepatocytes leads to the proinflammatory status in vivo. The specific suppression of CPB2 obtained as an HCV-induced irreversible change in host cells supports the above hypothesis. Furthermore, since it has been reported that C5 is a quantitative trait gene that modifies liver fibrogenesis in mice and humans, and that it plays a causative role in human liver fibrosis (Hillebrandt et al., 2005), the suppression of CPB2 during the long-term replication of HCV RNA may be involved in liver fibrogenesis.

The third gene of interest in this context is *ANXA1*, a member of the superfamily of annexin proteins that bind acidic phospholipids with high affinity in the presence of Ca^{2+}. ANXA1 is found in many differentiated cells, particularly those of the myeloid lineage, and is known to be a downstream mediator of glucocorticoids (Yazid et al., 2010). Recent reports have shown that glucocorticoids can differentially affect the ANXA1 pathway in cells of the innate and adaptive immune system, and that ANXA1 is an important mediator of the anti-inflammatory effects of glucocorticoids (Perretti and D'Acquisto, 2009). Furthermore, it was reported recently that ANXA1 is an endogenous inhibitor of NF-κB which can be induced in human cancer cells and mice by anti-inflammatory glucocorticoids and modified nonsteroidal anti-inflammatory drugs (Zhang et al., 2010). The suppression of NF-κB activity by the binding of ANXA1 to the p65 subunit of NF-κB was accompanied by enhanced apoptosis and inhibition of cell growth. In this context, the irreversible suppression of ANXA1 observed in the present study may weaken the anti-inflammatory effects of glucocorticoids. However, in our microarray analysis, no expression of the ANXA1 receptor (ALXR; formyl peptide receptor 2 known as ALXR in humans) was observed. Therefore, it is unlikely that Li23-derived cells respond to glucocorticoids in an autocrine manner leading to the anti-inflammatory state, although secreted ANXA1 may interact with its target cells in a paracrine manner. On the other hand, ANXA1 has been shown to be strongly suppressed in prostate cancer (Xin et al., 2003), head and neck cancer (Garcia Pedrero et al., 2004), and esophageal cancer (Hu et al., 2004). Moreover, a recent study showed that ANXA1 regulates the proliferative functions of estrogens in MCF-7 breast cancer cells (Ang et al., 2009). In that study, it was revealed that high physiologic pregnancy levels (up to 100 nM) of estrogen enhanced ANXA1 expression and induced a growth arrest of MCF-7 cells, whereas physiologic levels of estrogen (1 nM) induced the proliferation of these cells. Furthermore, silencing of ANXA1 expression using ANXA1 siRNA reversed this estrogen-dependent proliferation as well as growth arrest [51]. These results suggest that ANXA1 may act as a tumor suppressor gene and modulate the proliferation function of estrogens. In this context, suppression of ANXA1 expression by long-term HCV RNA replication may modulate cell proliferation. Therefore, it is of interest whether ANXA1 acts as an anti-proliferative mediator on the Li23-derived hepatoma cell lines used in this study. To clarify this point, further experiments involving ANXA1 overexpression or silencing will be needed.

This study revealed irreversible changes in host gene expression due to the long-term replication of HCV RNA in cell culture, but not with simple long-term cell culture in the absence of HCV. However, we can not exclude completely the possibility that G418, but not HCV, cause the irreversible changes in the gene expression profiles of Li23-derived cells, since HCV RNA replicating cells were cultured under selective pressure of G418, while the control cured cells were cultured in the absence of G418, except for a few passages before mRNA profiling. To resolve this issue, a long-term culture of G418-resistant cured cells may be the best way, however, it would take a long time to obtain the conclusion. Alternatively, to examine this point, regarding the genes selected in this study, we fortunately could compare the mRNA levels by RT-PCR analysis among HuH-7-derived HCV RNA-replicating O cells, those cells cultured for 2 years, and the corresponding cured cells obtained in previous studies (Ikeda et al., 2005; Kato et al., 2009a). The results revealed that eight genes except for *BASP1*, which was very low expression level in HuH-7-derived cells, showed no such upregulated or downregulated expression profiles obtained in this study (data not shown). Therefore, it is unlikely that the genes identified in this study have been selected by the long-term treatment with G418.

Although we have not yet clarified how these irreversible changes in the expression of identified genes modify cellular function, we may speculate about the nature of the functional changes in several of these genes, as described above. Additional studies using primary hepatocytes or immortalized noncancerous hepatocytes will be needed to clarify the biological significance of expressional changes of the identified genes. Such studies would lead to a better understanding of the mechanisms underlying the long-term persistent replication of HCV RNA that account for how such long-term replication modifies gene function in host cells.

Acknowledgements

We thank N. Kawahara, T. Nakamura, and K. Takeshita for their technical assistances. This work was supported by grants-in-aid for research on hepatitis from the Ministry of Health, Labor, and

Welfare of Japan. K.M. was supported by a Research Fellowship for Young Scientists from the Japan Society for the Promotion of Science.

Appendix A. Supplementary data

Supplementary data associated with this article can be found, in the online version, at http://dx.doi.org/10.1016/j.virusres.2012.04.008.

References

Abe, K., Ikeda, M., Dansako, H., Naka, K., Kato, N., 2007. Cell culture-adaptive NS3 mutations required for the robust replication of genome-length hepatitis C virus RNA. Virus Research 125, 88–97.

Ang, E.Z.-F., Nguyen, H.T., Sim, H.-L., Putti, T.C., Lim, L.H., 2009. Annexin-1 regulates growth arrest induced by high levels of estrogen in MCF-7 breast cancer cells. Molecular Cancer Research 7, 266–274.

Bartenschlager, R., 2005. The hepatitis C virus replicon system: from basic research to clinical application. Journal of Hepatology 43, 210–216.

Bartenschlager, R., Sparacio, S., 2007. Hepatitis C virus molecular clones and their replication capacity in vivo and in cell culture. Virus Research 127, 195–207.

Carpenter, B., Hill, K.J., Charalambous, M., Wagner, K.J., Lahiri, D., James, D.I., Andersen, J.S., Schumacher, V., Royer-Pokora, B., Mann, M., Ward, A., Roberts, S.G.E., 2004. BASP1 is a transcriptional cosuppressor for the Wilms' tumor suppressor protein WT1. Molecular and Cell Biology 24, 537–549.

Choo, Q., Kuo, G., Weiner, A., Overby, L., Bradley, D., Houghton, M., 1989. Isolation of a cDNA clone derived from a blood-borne non-A, non-B viral hepatitis genome. Science 244, 359–362.

Dansako, H., Naganuma, A., Nakamura, T., Ikeda, F., Nozaki, A., Kato, N., 2003. Differential activation of interferon-inducible genes by hepatitis C virus core protein mediated by the interferon stimulated response element. Virus Research 97, 17–30.

Fong, Y.-C., Lin, C.-Y., Su, Y.-C., Chen, W.-C., Tsai, F.-J., Tsai, C.-H., Huang, C.-Y., Tang, C.-H., 2012. CCN6 enhances ICAM-1 expression and cell motility in human chondrosarcoma cells. Journal of Cellular Physiology 227, 223–232.

Garcia Pedrero, J.M., Fernandez, M.P., Morgan, R.O., Herrero Zapatero, A., Gonzalez, M.V., Suarez Nieto, C., Rodrigo, J.P., 2004. Annexin A1 down-regulation in head and neck cancer is associated with epithelial differentiation status. American Journal of Pathology 164, 73–79.

Hartl, M., Nist, A., Khan, M.I., Valovka, T., Bister, K., 2009. Inhibition of Myc-induced cell transformation by brain acid-soluble protein 1 (BASP1). Proceedings of the National Academy of Sciences of the United States of America 106, 5604–5609.

Hijikata, M., Kato, N., Ootsuyama, Y., Nakagawa, M., Shimotohno, K., 1991. Gene mapping of the putative structural region of the hepatitis C virus genome by in vitro processing analysis. Proceedings of the National Academy of Sciences of the United States of America 88, 5547–5551.

Hijikata, M., Mizushima, H., Tanji, Y., Komoda, Y., Hirowatari, Y., Akagi, T., Kato, N., Kimura, K., Shimotohno, K., 1993. Proteolytic processing and membrane association of putative nonstructural proteins of hepatitis C virus. Proceedings of the National Academy of Sciences of the United States of America 90, 10773–10777.

Hillebrandt, S., Wasmuth, H.E., Weiskirchen, R., Hellerbrand, C., Keppeler, H., Werth, A., Schirin-Sokhan, R., Wilkens, G., Geier, A., Lorenzen, J., Koehl, J., Gressner, A.M., Matern, S., Lammert, F., 2005. Complement factor 5 is a quantitative trait gene that modifies liver fibrogenesis in mice and humans. Nature Genetics 37, 835–843.

Hu, N., Flaig, M.J., Su, H., Shou, J.-Z., Roth, M.J., Li, W.-J., Wang, C., Goldstein, A.M., Li, G., Emmert-Buck, M.R., Taylor, P.R., 2004. Comprehensive characterization of annexin I alterations in esophageal squamous cell carcinoma. Clinical Cancer Research 10, 6013–6022.

Huang, W., Gonzalez, M.E., Toy, K.A., Banerjee, M., Kleer, C.G., 2010. Blockade of ccn6 (WISP3) activates growth factor–independent survival and resistance to anoikis in human mammary epithelial cells. Cancer Research 70 (8), 3340–3350.

Huang, W., Zhang, Y., Varambally, S., Chinnaiyan, A.M., Banerjee, M., Merajver, S.D., Kleer, C.G., 2008. Inhibition of CCN6 (Wnt-1-induced signaling protein 3) down-regulates E-cadherin in the breast epithelium through induction of snail and ZEB1. American Journal of Pathology 172 (4), 893–904.

Huang, W.-C., Chan, S.-T., Yang, T.-L., Tzeng, C.-C., Chen, C.-C., 2004. Inhibition of ICAM-1 gene expression, monocyte adhesion and cancer cell invasion by targeting IKK complex: molecular and functional study of novel alpha-methylene-butyrolactone derivatives. Carcinogenesis 25, 1925–1934.

Ikeda, M., Abe, K., Dansako, H., Nakamura, T., Naka, K., Kato, N., 2005. Efficient replication of a full-length hepatitis C virus genome, strain O, in cell culture, and development of a luciferase reporter system. Biochemical and Biophysical Research Communications 329, 1350–1359.

Ikeda, M., Sugiyama, K., Mizutani, T., Tanaka, T., Tanaka, K., Sekihara, H., Shimotohno, K., Kato, N., 1998. Human hepatocyte clonal cell lines that support persistent replication of hepatitis C virus. Virus Research 56, 157–167.

Ikeda, M., Yi, M., Li, K., Lemon, S.M., 2002. Selectable subgenomic and genome-length dicistronic RNAs derived from an infectious molecular clone of the HCV-N strain of hepatitis C virus replicate efficiently in cultured Huh7 cells. Journal of Virology 76, 2997–3006.

Kane, S., Sano, H., Liu, S.C.H., Asara, J.M., Lane, W.S., Garner, C.C., Lienhard, G.E., 2002. A method to identify serine kinase substrates. Akt phosphorylates a novel adipocyte protein with a Rab GTPase-activating protein (GAP) domain. Journal of Biological Chemistry 277, 22115–22118.

Kato, N., Abe, K., Mori, K., Ariumi, Y., Dansako, H., Ikeda, M., 2009a. Genetic variability and diversity of intracellular genome-length hepatitis C virus RNA in long-term cell culture. Archives of Virology 154, 77–85.

Kato, N., Hijikata, M., Ootsuyama, Y., Nakagawa, M., Ohkoshi, S., Sugimura, T., Shimotohno, K., 1990. Molecular cloning of the human hepatitis C virus genome from Japanese patients with non-A, non-B hepatitis. Proceedings of the National Academy of Sciences of the United States of America 87, 9524–9528.

Kato, N., Mori, K., Abe, K., Dansako, H., Kuroki, M., Ariumi, Y., Wakita, T., Ikeda, M., 2009b. Efficient replication systems for hepatitis C virus using a new human hepatoma cell line. Virus Research 146, 41–50.

Kato, N., Sugiyama, K., Namba, K., Dansako, H., Nakamura, T., Takami, M., Naka, K., Nozaki, A., Shimotohno, K., 2003. Establishment of a hepatitis C virus subgenomic replicon derived from human hepatocytes infected in vitro. Biochemical and Biophysical Research Communications 306, 756–766.

Krieger, N., Lohmann, V., Bartenschlager, R., 2001. Enhancement of hepatitis C virus RNA replication by cell culture-adaptive mutations. Journal of Virology 75, 4614–4624.

Lindenbach, B.D., Rice, C.M., 2005. Unravelling hepatitis C virus replication from genome to function. Nature 436, 933–938.

Lohmann, V., Korner, F., Koch, J.-O., Herian, U., Theilmann, L., Bartenschlager, R., 1999. Replication of subgenomic hepatitis C virus RNAs in a hepatoma cell line. Science 285, 110–113.

Miinea, C.P., Sano, H., Kane, S., Sano, E., Fukuda, M., Peränen, J., Lane, W.S., Lienhard, G.E., 2005. As160, the Akt substrate regulating GLUT4 translocation, has a functional Rab GTPase-activating protein domain. Biochemical Journal 391, 87–93.

Mori, K., Abe, K., Dansako, H., Ariumi, Y., Ikeda, M., Kato, N., 2008. New efficient replication system with hepatitis C virus genome derived from a patient with acute hepatitis c. Biochemical and Biophysical Research Communications 371, 104–109.

Mori, K., Ikeda, M., Ariumi, Y., Dansako, H., Wakita, T., Kato, N., 2011. Mechanism of action of ribavirin in a novel hepatitis C virus replication cell system. Virus Research 157, 61–70.

Mori, K., Ikeda, M., Ariumi, Y., Kato, N., 2010. Gene expression profile of Li23, a new human hepatoma cell line that enables robust hepatitis C virus replication: comparison with HuH-7 and other hepatic cell lines. Hepatology Research 40, 1248–1253.

Moribe, T., Iizuka, N., Miura, T., Stark, M., Tamatsukuri, S., Ishitsuka, H., Hamamoto, Y., Sakamoto, K., Tamesa, T., Oka, M., 2008. Identification of novel aberrant methylation of BASP1 and SRD5A2 for early diagnosis of hepatocellular carcinoma by genome-wide search. International Journal of Oncology 33, 949–958.

Mosevitsky, M.I., Capony, J.P., Skladchikova, G.Y., Novitskaya, V.A., Plekhanov, A.Y., Zakharov, V.V., 1997. The BASP1 family of myristoylated proteins abundant in axonal termini. Primary structure analysis and physico-chemical properties. Biochimie 79, 373–384.

Myles, T., Nishimura, T., Yun, T.H., Nagashima, M., Morser, J., Patterson, A.J., Pearl, R.G., Leung, L.L.K., 2003. Thrombin activatable fibrinolysis inhibitor, a potential regulator of vascular inflammation. Journal of Biological Chemistry 278, 51059–51067.

Naka, K., Dansako, H., Kobayashi, N., Ikeda, M., Kato, N., 2006. Hepatitis C virus NS5B delays cell cycle progression by inducing interferon- via toll-like receptor 3 signaling pathway without replicating viral genomes. Virology 346, 348–362.

Pennica, D., Swanson, T.A., Welsh, J.W., Roy, M.A., Lawrence, D.A., Lee, J., Brush, J., Taneyhill, L.A., Deuel, B., Lew, M., Watanabe, C., Cohen, R.L., Melhem, M.F., Finley, G.G., Quirke, P., Goddard, A.D., Hillan, K.J., Gurney, A.L., Botstein, D., Levine, A.J., 1998. WISP genes are members of the connective tissue growth factor family that are up-regulated in Wnt-1-transformed cells and aberrantly expressed in human colon tumors. Proceedings of the National Academy of Sciences of the United States of America 95, 14717–14722.

Perretti, M., D'Acquisto, F., 2009. Annexin A1 and glucocorticoids as effectors of the resolution of inflammation. Nature Reviews Immunology 9, 62–70.

Redlitz, A., Tan, A.K., Eaton, D.L., Plow, E.F., 1995. Plasma carboxypeptidases as regulators of the plasminogen system. Journal of Clinical Investigation 96, 2534–2538.

Rowland, A.F., Fazakerley, D.J., James, D.E., 2011. Mapping insulin/GLUT4 circuitry. Traffic 12, 672–681.

Saito, I., Miyamura, T., Ohbayashi, A., Harada, H., Katayama, T., Kikuchi, S., Watanabe, Y., Koi, S., Onji, M., Ohta, Y., Choo, Q., Houghton, M., Kuo, G., 1990. Hepatitis C virus infection is associated with the development of hepatocellular carcinoma. Proceedings of the National Academy of Sciences of the United States of America 87, 6547–6549.

Sharif, S.A., Du, X., Myles, T., Song, J.J., Price, E., Lee, D.M., Goodman, S.B., Nagashima, M., Morser, J., Robinson, W.H., Leung, L.L.K., 2009. Thrombin-activatable carboxypeptidase B cleavage of osteopontin regulates neutrophil survival and synoviocyte binding in rheumatoid arthritis. Arthritis and Rheumatism 60, 2902–2912.

Song, J.J., Hwang, I., Cho, K.H., Garcia, M.A., Kim, A.J., Wang, T.H., Lindstrom, T.M., Lee, A.T., Nishimura, T., Zhao, L., Morser, J., Nesheim, M., Goodman, S.B., Lee, D.M., Bridges Jr., S.L., Gregersen, P.K., Leung, L.L., Robinson, W.H., 2011. Plasma carboxypeptidase B downregulates inflammatory responses in autoimmune arthritis. Journal of Clinical Investigation 121, 3517–3527.

Thomas, D., 2000. Hepatitis C epidemiology. Current Topics in Microbiology and Immunology 242, 25–41.

Thorstensen, L., Diep, C.B., Meling, G.I., Aagesen, T.H., Ahrens, C.H., Rognum, T.O., Lothe, R.A., 2001. Wnt1 inducible signaling pathway protein 3, WISP-3, a novel target gene in colorectal carcinomas with microsatellite instability. Gastroenterology 121, 1275–1280.

Tsunedomi, R., Ogawa, Y., Iizuka, N., Sakamoto, K., Tamesa, T., Moribe, T., Oka, M., 2010. The assessment of methylated BAPS1 and SRD5A2 levels in the detection of early hepatocellular carcinoma. International Journal of Oncology 36, 205–212.

Ueda, Y., Mori, K., Ariumi, Y., Ikeda, M., Kato, N., 2011. Plural assay systems derived from different cell lines and hepatitis C virus strains are required for the objective evaluation of anti-hepatitis C virus reagents. Biochemical and Biophysical Research Communications 409, 663–668.

Wakita, T., Pietschmann, T., Kato, T., Date, T., Miyamoto, M., Zhao, Z., Murthy, K., Habermann, A., Krausslich, H.-G., Mizokami, M., Bartenschlager, R., Liang, T.J., 2005. Production of infectious hepatitis C virus in tissue culture from a cloned viral genome. Nature Medicine 11, 791–796.

Xin, W., Rhodes, D.R., Ingold, C., Chinnaiyan, A.M., Rubin, M.A., 2003. Dysregulation of the annexin family protein family is associated with prostate cancer progression. American Journal of Pathology 162, 255–261.

Yazid, S., Ayoub, S.S., Solito, E., McArthur, S., Vo, P., Dufton, N., Flower, R.J., 2010. Anti-allergic drugs and the annexin-A1 system. Pharmacological Report 62, 511–517.

Zhang, Z., Huang, L., Zhao, W., Rigas, B., 2010. Annexin 1 induced by anti-inflammatory drugs binds to NF-kappaB and inhibits its activation: anticancer effects in vitro and in vivo. Cancer Research 70, 2379–2388.

Development of hepatitis C virus production reporter-assay systems using two different hepatoma cell lines

Midori Takeda,[1] Masanori Ikeda,[1] Yasuo Ariumi,[1]† Takaji Wakita[2] and Nobuyuki Kato[1]

Correspondence
Masanori Ikeda
maikeda@md.okayama-u.ac.jp

[1]Department of Tumor Virology, Okayama University, Graduate School of Medicine, Dentistry and Pharmaceutical Sciences, Okayama 700-8544, Japan

[2]Department of Virology II, National Institute of Infectious Disease, Tokyo 162-8640, Japan

A hepatitis C virus (HCV) infection system was developed previously using the HCV JFH-1 strain (genotype 2a) and HuH-7 cells, and this cell culture is so far the only robust production system for HCV. In patients with chronic hepatitis C, the virological effects of pegylated interferon and ribavirin therapy differ depending on the HCV strain and the genetic background of the host. Recently, we reported the hepatoma-derived Li23 cell line, in which the JFH-1 life cycle is reproduced at a level almost equal to that in HuH-7-derived RSc cells. To monitor the HCV life cycle more easily, we here developed JFH-1 reporter-assay systems using both HuH-7- and Li23-derived cell lines. To identify any genetic mutations by long-term cell culture, HCV RNAs in HuH-7 cells were amplified 130 days after infection and subjected to sequence analysis to find adaptive mutation(s) for robust virus replication. We identified two mutations, H2505Q and V2995L, in the NS5B region. V2995L but not H2505Q enhanced JFH-1 RNA replication. However, we found that H2505Q but not V2995L enhanced HCV RNA replication of strain O (genotype 1b). We also selected highly permissive D7 cells by serial subcloning of Li23 cells. The expression levels of claudin-1 and Niemann–Pick C1-like 1 in D7 cells are higher than those in parental Li23 cells. In this study, we developed HCV JFH-1 reporter-assay systems using two distinct hepatoma cell lines, HuH-7 and Li23. The mutations in NS5B resulted in different effects on strains O and JFH-1 HCV RNA replication.

Received 21 December 2011
Accepted 26 March 2012

INTRODUCTION

Hepatitis C virus (HCV) infection frequently causes chronic hepatitis and leads to liver cirrhosis and hepatocellular carcinoma. Elimination of HCV by antiviral reagents seems to be the most efficient therapy to prevent fatality.

HCV belongs to the family *Flaviviridae* and contains a positive ssRNA genome of 9.6 kb. The HCV genome encodes a single polyprotein precursor of approximately 3000 aa, which is cleaved by host and viral proteases into at least 10 proteins in the following order: Core, envelope 1 (E1), E2, p7, non-structural 2 (NS2), NS3, NS4A, NS4B, NS5A and NS5B (Kato, 2001; Kato *et al.*, 1990; Tanaka *et al.*, 1996).

Evaluation of anti-HCV reagents was difficult before the development of the HCV replicon system (Lohmann *et al.*, 1999). The HCV replicon system enabled investigation of anti-HCV reagents and the cellular factors involved in HCV RNA replication. Following introduction of the replicon system, genome-length HCV RNA-replication systems and reporter-assay systems were also developed (Ikeda *et al.*, 2002, 2005; Lohmann *et al.*, 2001; Pietschmann *et al.*, 2002). In 2005, an HCV infection system was developed using the genotype 2a JFH-1 strain (Lindenbach *et al.*, 2005; Wakita *et al.*, 2005; Zhong *et al.*, 2005). The JFH-1 infection system has been used to study not only viral RNA replication, but also virus infection and release. This HCV cell-culture system was developed using the human hepatoma cell line HuH-7 and, thus far, HuH-7 is the only cell line to exhibit robust HCV production. Therefore, we intended to test the susceptibility of various other cell lines to HCV RNA replication. We reported previously that the hepatoma cell line Li23 supports robust HCV RNA replication and is also susceptible to authentic JFH-1 infection (Kato *et al.*, 2009). Microarray analysis revealed that HuH-7 and Li23 cells exhibited distinct gene-expression profiles (Mori *et al.*, 2010). For example, we identified three genes (New York oesophageal squamous cell carcinoma 1, β-defensin-1 and galectin-3) showing Li23-specific expression. Using HuH-7 and Li23 cells in combination with HCV strain O (genotype 1b), we developed drug-assay systems (OR6 and ORL8, respectively) by introducing the *Renilla* luciferase (RL) gene (Ikeda *et al.*, 2005; Kato *et al.*, 2009). We found and reported that the sensitivities to anti-HCV reagents were different between the HuH-7 and Li23 assay systems; for example, the Li23 assay system was 10 times more sensitive to ribavirin than the HuH-7 assay system (Mori *et al.*, 2011). Methotrexate showed very strong anti-HCV activity in the Li23 assay system, although it showed very weak anti-HCV activity in the HuH-7 assay system (Ueda *et al.*, 2011). These results encouraged us to develop a JFH-1 reporter-assay system using HuH-7 and Li23 cells. This JFH-1 reporter-assay system not only facilitated monitoring of virus infection and release steps, but also provided us with new information that could be missed in these steps when using only a HuH-7 assay system. However, increasing the size of the viral genome by introducing exogenous genes [RL and the encephalomyocarditis virus internal ribosomal site (EMCV-IRES)] reduced the efficiency of HCV RNA replication. To overcome this issue, we tried to improve the efficiency of HCV RNA replication by introducing adaptive mutations and by subcloning the parental cells.

Here, we developed JFH-1 HCV production reporter-assay systems in HuH-7- and Li23-derived cells using adaptive mutations and subcloned cells, which monitor the life cycle of HCV with luciferase activity. We also tested the effect of the mutations in NS5B from the JFH-1 strain on RNA replication of the specific genotype 1b O strain.

RESULTS

HCV mutations caused by long-term cell culture

The efficiency of HCV RNA replication depends on viral genetic mutations, host cells and viral genome size. For development of the HCV reporter-assay system, use of a longer viral genome reduced the efficiency of virus replication. To compensate for this issue, we tried to introduce adaptive mutations into the JFH-1 genome. We examined the viral sequences of JFH-1 130 days after infection of HuH-7-derived RSc cells. We performed RT-PCR for three parts of the viral genome: Core to NS2, NS3 to NS5A, and NS5B to 3′X. These three parts were separated by the *Age*I, *Spe*I, *Bsr*GI and *Xba*I sites on the viral genome. We introduced PCR products into the cloning vector and three independent clones were subjected to sequencing analysis.

In the Core to NS2 region between the *Age*I and *Spe*I sites (designated AS), there were eight common mutations with amino acid substitutions: lysine to glutamate at aa 78 (K78E) in Core, P251L and A351D in E1, V402A, I414T and K715N in E2, Y771C in p7, and D962G in NS2 (Fig. 1a). In the NS3 to NS5A region between *Spe*I and *Bsr*GI sites (designated SB), there were eight common mutations with amino acid substitutions: V1460I and M1611T in NS3, and I2270T, Q2307R, S2363L, M2392T, S2426A and C2441S in NS5A (Fig. 1b). In the NS5B to 3′X region between the *Bsr*GI and *Xba*I sites (designated BX), there was only one common mutation with an amino acid substitution, V2995L in NS5B (Fig. 1c). The determined sequences were studied further to enhance HCV RNA replication in the JFH-1 reporter assay.

Effect of genetic mutations on HCV RNA replication

To monitor the virus life cycle more easily, we constructed dicistronic JFH-1 with a reporter gene, pJR/C-5B. The first cistron contained the RL gene and was translated by the HCV-IRES. The second cistron contained the JFH-1 ORF and was translated by the EMCV-IRES. This construct facilitated monitoring of all steps of the virus life cycle by quantification of RL activity. However, the use of a longer viral genome resulted in lower replication efficiency. We tested the effect on HCV RNA replication of amino acid substitution caused during long-term cell culture.

The amino acid substitution clusters from three independent clones in Core to NS2 (AS-1, AS-2, AS-3) were introduced into pJR/C-5B. *In vitro*-transcribed HCV RNA was introduced into HuH-7-derived RSc cells, and RL activities were monitored 24, 48 and 72 h after electroporation (Fig. 2a). AS-3 exhibited higher replication efficiency than the wild type (WT). However, the replication efficiency of AS-2 was almost equal to that of the WT, and AS-1 exhibited lower replication efficiency than the WT. AS-3 possessed the highest replication efficiency among the tested JFH-1 mutants: at 72 h, the luciferase value of this clone was approximately 100 times that at 24 h.

The three pJR/C-5B constructs with mutations in NS3 to NS5A (SB-2, SB-3 and SB-4) were transcribed and introduced into RSc cells to compare the efficiency of HCV RNA replication (Fig. 2b). Unexpectedly, RL activity was not increased over 72 h after electroporation and exhibited a pattern similar to that of JFH-1 without the GDD motif. This result indicates that the mutation in NS3 to NS5A exhibited a negative effect on HCV RNA replication.

Finally, we tested the effect of the mutations in the NS5B region on HCV RNA replication. BX-2 contains two mutations with amino acid substitution (H2505Q and V2995L) and BX-7 contains only V2995L (Fig. 2c). JFH-1 with mutation(s) of BX-2 or BX-7 exhibited strong enhancement of HCV RNA replication. These results indicate that V2995L works as a strong replication-enhancing mutation (REM) in JFH-1 HCV RNA replication.

†Present address: Center for AIDS Research, Kumamoto University, Kumamoto 860-0811, Japan.

Three supplementary figures are available with the online version of this paper.

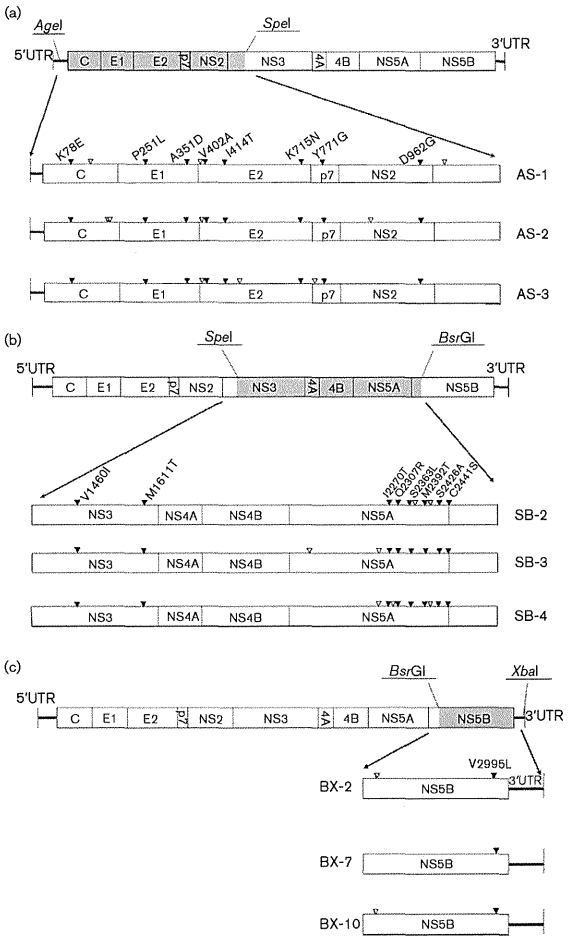

Fig. 1. Genetic mutations causing amino acid substitutions during long-term HCV infection. RT-PCR was performed for HCV RNAs from HuH-7 cells 130 days after JFH-1 infection. PCR products were subcloned into the pBluescript II plasmid. Three clones of (a) the Core to NS2 region between the *Age*I and *Spe*I sites (AS), (b) the NS3 to NS5A region between the *Spe*I and *Bsr*GI sites (SB) and (c) the NS5B to 3′X region between the *Bsr*GI and *Xba*I sites (BX) were subjected to sequencing analysis. ▼ and ▽ represent conservative and non-conservative amino acid substitutions, respectively.

Mutations in NS5B enhanced HCV RNA replication differently in genotypes 1b and 2a

V2995L in NS5B is a common substitution, occurring in three clones, and H2505Q is conserved in two clones (BX-2 and BX-10). We examined the corresponding amino acids at positions 2995 and 2505 in genotype 1b replication-competent HCV strains O, 1B-4 and KAH5 (Fig. 3a) (Nishimura *et al.*, 2009). The histidine at aa 2505 in JFH-1 is conserved in O, 1B-4 and KAH5 at the corresponding position, aa 2482. The valine at aa 2995 in JFH-1 is an alanine in O, 1B-4 and KAH5 at the corresponding position, aa 2972 (Fig. 3a). It is not clear whether the adaptive mutation found in genotype 2a is effective in genotype 1b HCV. Therefore, we investigated the effect of V2995L and/or H2505Q substitution on genotype 1b HCV RNA replication. We introduced substitutions V2995L and/or H2505Q into the subgenomic replicon, pOR/3-5B (HCV-O). In contrast to the case of JFH-1, H2505Q but not V2995L enhanced HCV-O RNA replication (Fig. 3b). These results indicate that the mutations in NS5B derived from JFH-1 functioned differently in genotype 1b HCV-O RNA replication.

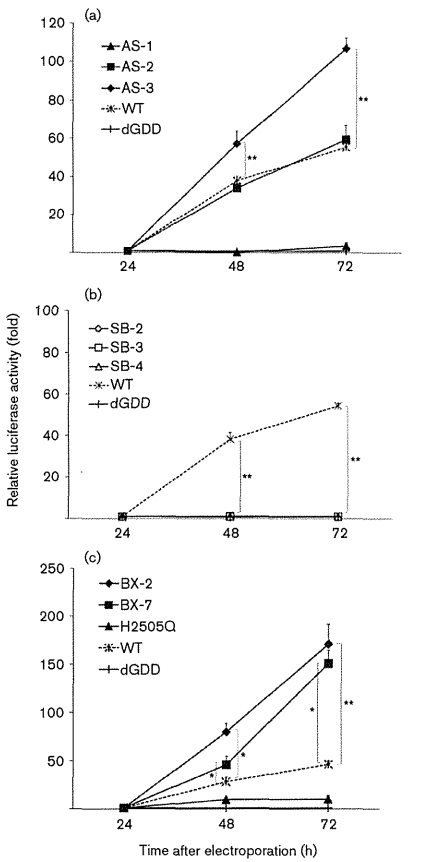

Fig. 2. Effect of amino acid substitutions on HCV RNA replication. (a) The Core to NS2 region; (b) the NS3 to NS5A region; (c) the NS5B to 3′X region. Amino acid substitutions were introduced into p*JR/C5B* and *in vitro*-synthesized RNAs were electroporated into HuH-7-derived RSc cells. RL activity was determined 24, 48 and 72 h after electroporation. dGDD, Negative control without the GDD motif; WT, wild type. *$P<0.05$; **$P<0.01$.

HCV infection in HuH-7- and Li23-derived cell lines

As well as viral genetic mutations, the choice of host cells is important for the efficiency of HCV RNA replication. Cured cells in which HCV RNAs were eliminated by IFN-α, such as HuH-7.5, HuH-7.5.1 and our RSc cells, exhibit higher replication efficiency than their parental HuH-7 cells (Ariumi *et al.*, 2007; Blight *et al.*, 2002; Zhong *et al.*, 2005). Therefore, we examined whether subcloned Li23 cells might enhance HCV RNA replication. We performed serial subcloning of Li23 cells from Li23-derived ORL8c cells by the limiting-dilution method (Fig. 4a). ORL8c cells are a cured cell line in which genome-length HCV RNAs were eliminated by interferon (IFN) treatment (Kato *et al.*, 2009). The subclonal Li23-derived cell lines were selected from among 50–100 independent single cells in 96-well plates by three-round limiting dilution from ORL8c cells (Fig. S1a, available in JGV Online). First, L8c15 cells were selected from their parental ORL8c cells by limiting dilution. Then, C22 cells were selected from their parental L8c15 cells by limiting dilution. Finally, D7 cells were selected from C22 cells by limiting dilution (Fig. S1b). Together, these steps resulted in the

(a)

Consensus		TFDRLQVLDDHYRDVLKE	
JFH-1	2495	TFDRTQVLDAHYDSVLKD	2512
O	2472	TFDRLQVLDDHYRDVLKE	2489
KAH-5	2472	TFDRLQVLDDHYRDVLKE	2489
1B-4	2472	TFDRLQVLDDHYRDVLKE	2489
Consensus		PAASRLDLSGWFVAGYSGGDIYHS	
JFH-1	2982	PEARLLDLSSWFTVGAGGGDIFHS	3005
O	2959	PAASRLDLSGWFVAGYSGGDIYHS	2982
KAH-5	2959	PAASRLDLSGWFVAGYSGGDIYHS	2982
1B-4	2959	PAASRLDLSGWFVAGYSGGDIYHS	2982

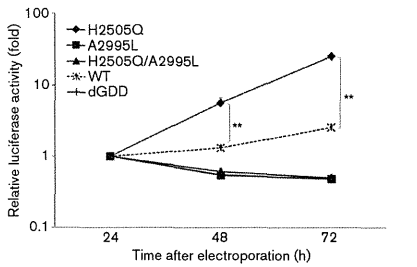

Fig. 3. Effect of amino acid substitutions in NS5B on genotype 1b and 2a HCV RNA replication. (a) Alignment of amino acids at positions 2505 (JFH-1) and 2482 (genotype 1b) and around the adjacent region (upper panel). Alignment of amino acids at positions 2995 (JFH-1) and 2972 (genotype 1b) and around the adjacent region (lower panel). The HCV strains O, KAH5 and 1B-4 belong to genotype 1b. (b) H2505Q and/or V2995L were introduced into the HCV-O subgenomic replicon (pOR/3-5B), and transcribed RNAs were electroporated into RSc cells. RL activities were tested 24, 48 and 72 h after infection. dGDD, Negative control without the GDD motif; WT, wild type. **$P<0.01$.

selection of three subclonal cell lines that respectively exhibited the strongest replication efficiency in each round of selection. The lineages of the selected cell lines after three rounds of subcloning were designated L8c15, C22 and D7 cells, respectively.

We tested the subcloned cells for their HCV infectivities in comparison with those of HuH-7 and HuH-7-derived RSc cells. We reported previously that RSc cells could strongly support HCV replication and production (Kato *et al.*, 2009). Li23 and its derived ORL8c, L8c15, C22 and D7 cell lines were infected using the supernatant from RSc cells replicating JR/C-5B with BX-2 mutations at an m.o.i. of 0.2 (Fig. 4b, c). RL activities were determined 24, 48, 72 and 96 h after infection and f.f.u. ml^{-1} were determined 48 h after infection. The efficiency of HCV infectivity was highest in D7 cells, followed in order by C22, L8c15 and Li23 cells. HCV RNA replication in D7 cells was almost equal to that in RSc cells. These results suggest that the subcloned cell lines exhibit higher susceptibility to HCV infection than their parental cells.

Next, we further characterized the susceptibility of D7 cells to HCV infection in comparison with RSc cells, because D7 cells exhibited the highest susceptibility to HCV infection among the Li23-derived cell lines. D7 cells also exhibited the highest production and release of Core into the supernatant among the parental C22-derived subclonal

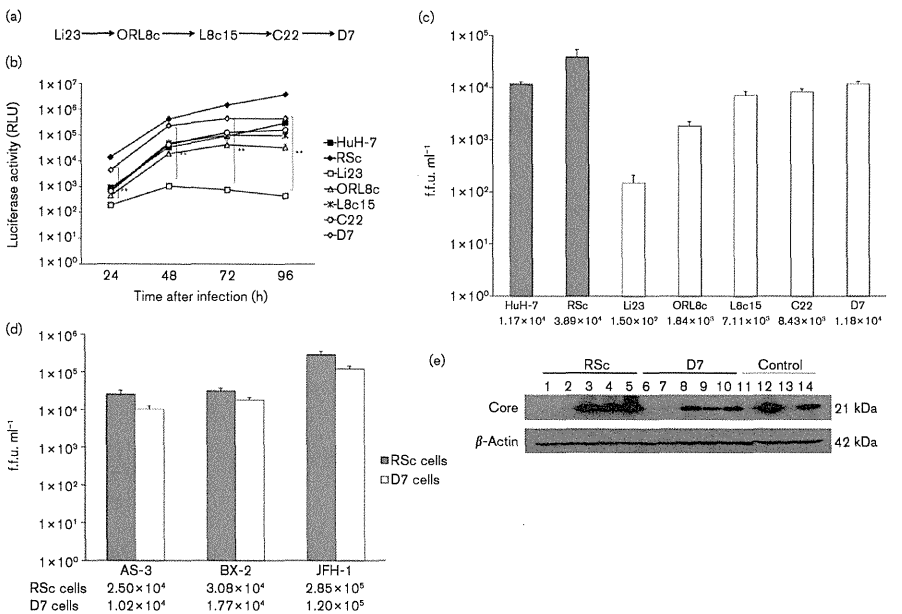

Fig. 4. HCV infection in HuH-7- and Li23-derived cell lines. (a) History of the selection of subclonal Li23-derived cell lines. (b) HuH-7, HuH-7-derived RSc, and Li23-derived ORL8c, L8c15, C22 and D7 cells were inoculated with supernatant from RSc cells replicating JR/C5B/BX-2. $^{**}P<0.01$. (c) f.f.u. ml^{-1} values were determined 48 h after infection of HuH-7- and Li23-derived cells with HCV using the supernatant from RSc cells replicating JR/C5B/BX-2 . (d) f.f.u. ml^{-1} values were determined 48 h after infection of RSc or D7 cells with HCV using the supernatant from RSc cells replicating JR/C5B/AS-3 or JR/C5B/BX-2. Supernatant from authentic JFH-1-replicating RSc cells was used as a positive control. (e) Core expression levels in RSc or D7 cells were determined 1, 2, 3 and 4 days after infection with JFH-1 with BX-2 mutations. Lanes: 1 and 6, mock-infected cells; 2 and 7, cells 1 day after infection; 3 and 8, cells 2 days after infection; 4 and 9, cells 3 days after infection; 5 and 10, cells 4 days after infection; 11 and 12, OR6c and OR6 cells, respectively; 13 and 14, ORL8c and ORL8 cells, respectively. OR6 and ORL8 were used as positive controls; OR6c and OR8c were used as negative controls. β-Actin was used as a control for the amount of protein loaded per lane.

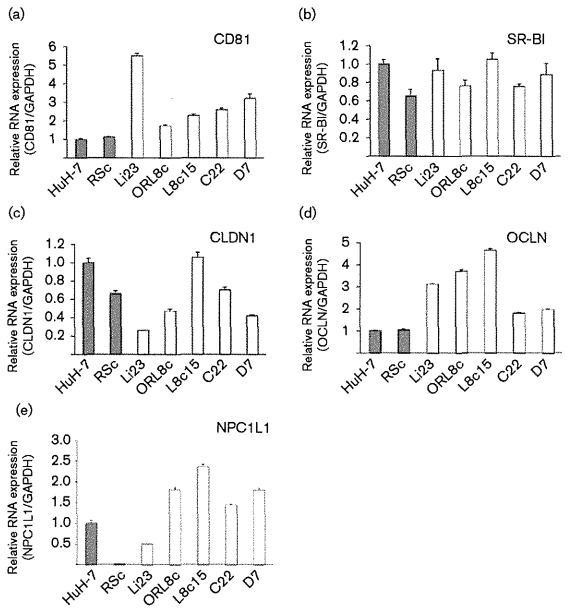

Fig. 5. Expression levels of HCV receptors in HuH-7- and Li23-derived cells. Quantitative RT-PCR was performed for CD81, SR-BI, CLDN1, OCLN and NPC1L1 as described in Methods. Relative expression levels of mRNA are shown, when the expression level of each receptor in HuH-7 was assigned to be 1. GAPDH was used as an internal control. Experiments were done in triplicate.

cells (Fig. S1b). The susceptibility of the HCV reporter-assay system to HCV infection was examined using HuH-7- and Li23-derived cells. Supernatants from RSc cells replicating JR/C-5B with AS-3 or BX-2 mutations were used as inocula. The supernatant from authentic JFH-1-replicating RSc cells was used as a positive control. RSc and D7 cells were inoculated with each HCV-containing supernatant and f.f.u. ml^{-1} were determined 48 h after infection. As shown in Fig. 4(d), the values of f.f.u. ml^{-1} for AS-3 were 2.5×10^4 and 1.0×10^4 in RSc and D7 cells, respectively; those for BX-2 were 3.1×10^4 and 1.8×10^4 in RSc and D7 cells, respectively; and those for authentic JFH-1 were 2.9×10^5 and 1.2×10^5 in RSc and D7 cells, respectively. These results indicate that the infectivities of these three inocula were almost equal in RSc and D7 cells.

Next we examined Core expression after infection of RSc and D7 cells with HCV, as D7 cells exhibited the highest infectivity among the Li23-derived cell lines (Fig. 4e). Core was detected 2, 3 and 4 days after infection of the supernatant from RSc cells infected by JR/C-5B with BX-2. Although Core expression in D7 cells was slightly weaker than that in RSc cells, the signal of Core in HCV-infected D7 cells was equal to that in stable ORL8 cells. These results suggest that the JFH-1 reporter-assay system in Li23 cells is useful not only for the RL assay, but also for Core expression.

Expression of HCV receptors in parental and subclonal hepatoma cell lines

We tested expression of the HCV receptors CD81, scavenger receptor class B member I (SR-BI), claudin-1 (CLDN1) and occludin (OCLN). We also examined the expression of the recently reported HCV entry factor Niemann–Pick C1-like 1 (NPC1L1) (Sainz *et al.*, 2012). Expression levels of CD81 in Li23 and its subclonal cells were higher than those in HuH-7 and RSc cells (Fig. 5a). Although expression of CD81 in Li23-derived cell lines was lower than that in parental Li23 cells, interestingly the expression levels of CD81 increased during the rounds of selection. There is no difference in the expression of SR-BI among the cell lines tested (Fig. 5b). The expression of CLDN1 in Li23-derived cells was higher than that in parental Li23 cells (Fig. 5c). Expression levels of OCLN in Li23 and its subclonal cells were higher than those in HuH-7 and RSc cells (Fig. 5d). Finally, the expression of NPC1L1 in Li23-derived cell lines was higher than that in parental Li23 cells (Fig. 5e). It is noteworthy that the expression level of NPC1L1 in RSc cells was approximately 2 $\log_{10}$ lower than that in parental HuH-7 cells. Taken together, these results indicate that the expression levels of CLDN1 and NPC1L1 in Li23-derived cells were higher than those in parental Li23 cells.